Wire Arc Additive Manufacturing (WAAM) Process Analysis on Stainless Steel Built Samples

Master degree in Mechanical Engineering – Industrial Production

Ricardo Jorge da Silva Viola

Leiria, January 2020

Wire Arc Additive Manufacturing (WAAM) Process Analysis on Stainless Steel Built Samples

Master degree in Mechanical Engineering – Industrial Production

Ricardo Jorge da Silva Viola

Project Report under the supervision of Doctor Mário António Simões Correia, Doctor Maria Leopoldina Mendes Ribeiro de Sousa Alves, both Professors from Polytechnic of Leiria and Doctor Pierre Michaud, Responsible of Additive Manufacturing in Addimadour, France.

Leiria, January of 2020

Originality and Copyright

This project report is original, made only for this purpose, and all authors whose studies and publications were used to complete it are duly acknowledged.

Acknowledgments

I would like to express my truly acknowledgments to my family and friends, for their constructive contribute, their support and for always believing in me.

I would also like to thank to all my Professors that contributed so much for my training throughout the master, specially to Doctor Mário Correia and Doctor Leopoldina Alves, for all the motivation, their knowledge, dedication ad contribution for my academic, professional and personal growth.

A special thanks to Doctor Pierre Michaud and his great team at Addimadour, for hosting me warmly, for their availability and knowledge provided throughout the entire time.

Abstract

The increasing developed complexity parts geometry demanded by the industry nowadays, represents a challenge itself, not only for the standard production processes that do not have an answer for it, but also to repair these and other parts in a more cost effectively process with a short delivery period. A technological response to these needs is relying on the Wire Arc Additive Manufacturing (WAAM) process development.

This thesis was developed in Addimadour, an additive manufacturing research platform, located in Bayonne France, that has as objective the development of the Laser Metal Deposition Powder (LMD-P), Laser Metal Deposition Wire (LMD-W), Selective Laser Melting (SLM), ColdSpray – ArcSpray, Fused Deposition Modelling Robotized (FDMR) and Wire Arc Additive Manufacturing (WAAM) technologic processes, procedures, and providing consistent production parameters to industrial partners.

The starting point for this thesis was an extensive research, regarding the chosen material that was a duplex stainless-steel ER2209 applied by WAAM technology. This process consists in deposing layer by layer material through an electric arc with the help of a robot that runs the paths to generate the defined geometry. Relying on an innovator process with lower process temperatures named Cold Metal Transfer (CMT) technology, different experiments were done with the aim to understand the relations between process parameters and results obtained.

Firstly, three experiments were done to establish direct links between input parameters and the shape of depositions achieved. Secondly, other two experiments were done, with the aim of understand the existing dynamic between two or more cords produced together, but also to achieve the best shape possible to ensure the finishing of the surface quality. At last, two walls were produced as a result of all the knowledge collected.

All the experiments done, were followed by analysis and observation of all macroscopic and microscopic specifications. Regarding the microscopic observations and measurements, it was used a microscope and software, specially designed for this type of analysis.

Two different mechanical tests were done to the samples with the objective of characterize the material produced by this production process. One was the microhardness test that were carried out in all samples, using a Vickers testing machine. The results of these tests were a pattern and a range of values. For the second test, a three-point flexural test was made on samples, regarding the values of flexural force-displacement to evaluate flexural behaviour of the built samples.

Keywords: WAAM, CMT, ER2209 duplex stainless-steel, Built deposition, HAZ, Microhardness

Resumo

Na indústria dos dias de hoje existe uma crescente necessidade de produzir peças de geometrias cada vez mais complexas, geometrias estas que, por si só, são um desafio à produção através dos processos convencionais, uma vez que estes processos não têm capacidade de resposta para esta necessidade, assim como para a reparação das mesmas e outras passíveis de reparar por este processo, de uma forma rentável e com períodos de entrega mais curtos. A resposta tecnológica para estas necessidades pode estar associada ao desenvolvimento do processo de Wire Arc Additive Manufacturing (WAAM).

Esta tese foi desenvolvida no Addimadour, uma plataforma de pesquisa dedicada ao fabrico aditivo, localizada em Bayonne, França, que tem como objetivo o desenvolvimento dos processos tecnológicos e seus respetivos procedimentos das tecnologias de Laser Metal Deposition Powder (LMD-P), Laser Metal Deposition Wire (LMD-W), Selective Laser Melting (SLM), ColdSpray – ArcSpray, Fused Deposition Modeling Robotized (FDMR) and Wire Arc Additive Manufacturing (WAAM), e o fornecimento de parâmetros de produção consistentes, aos seus parceiros industriais.

O ponto de partida desta tese foi uma extensa pesquisa de acordo com o material escolhido, aço inox duplex ER2209, utilizado pela tecnologia WAAM. Este processo consiste em depositar material camada a camada, através dum arco elétrico com a ajuda de um robot que, percorre os trajetos que realizará a geometria definida. Baseado num processo tecnológico inovador, com temperaturas de processo baixas, denominado Cold Metal Transfer (CMT), foram feitas diferentes experiências com o objetivo de relacionar parâmetros de processo introduzidos com os resultados obtidos.

Inicialmente, foram feitas três experiências para estabelecer relações entre os parâmetros introduzidos e a forma das deposições que foram atingidas. De seguida, outras duas experiências foram realizadas, com o objetivo de entender a dinâmica existente entre dois ou mais cordões, produzidos juntos, mas também para atingir o melhor formato e superfície possível, para cada deposição. Por fim, duas paredes foram produzidas como resultado de todo o conhecimento adquirido.

Todas as experiências feitas foram seguidas de uma análise e observação de todas as especificações macroscópicas e microscópicas. Referente às observações e medições microscópicas, foi usado um microscópio, e um software especialmente desenvolvido para este tipo de análise.

Foram realizados dois testes mecânicos diferentes às amostras, com o objetivo de caracterizar o material produzido por este processo de produção. Um deles é o teste de dureza, que foi levado a cabo em todas as amostras com recurso a uma máquina que realiza o teste de Vickers. Destes testes, resultaram um padrão na disposição de valores, assim como um intervalo de valores consistente em todas as amostras.
No segundo teste, o teste de flexão em três pontos, foi feito em amostras tendo em atenção os valores de força-deslocamento para avaliar o comportamento à flexão das amostras construídas.

Contents

List of Figures

List of Tables

List of Abbreviations and Acronyms

ALC	Arc Length Correction
AM	Additive Manufacturing
ASTM	American Society for Testing and Materials
CMT	Cold Metal Transfer
DMLS	Direct Metal Laser Sintering
EBM	Electron Beam Melting
ESTG	School of Technology and Management
FDMR	Fused Deposition Modelling Robotized
DC	Dynamic Correction
GMAW	Gas Metal Arc Welding
HAZ	Heat Affected Zone
HV	Vickers Hardness
LMD-P	Laser Metal Deposition Powder
LMD-W	Laser Metal Deposition Wire
MAG	Metal Active Gas
MIG	Metal Inert Gas
SLM	Selective Laser Melting
WAAM	Wire Arc Additive Manufacturing

1. Introduction

This thesis is focused on analysis of the process of building parts on stainless-steel by Wire Arc Additive Manufacturing (WAAM). These types of technologies and variants are increasing weight in our society. Sometimes due to the need for repair of damaged components, in other situations to produce geometrically complex components and on the other hand to reduce the environmental impact on the production and repair of these components. With the rising of the environmental concerns, and the need for a better resources' management associated to the production, the use of the additive manufacturing might be the solution required. The simplicity and adaptability of the WAAM process made it the optimal choice for this development.

In terms of materials, stainless-steel is one of the most important used industrially. The mechanical, thermic and chemical behaviour is already largely studied. It is also known for its added-value or for its expensive cost production due to the pouring process. For it to be cost-effective, it has to be used to produce large parts with limited geometries. Having this in mind, duplex stainless-steel is the optimal material to be studied in the development of this thesis.

1.1. Additive Manufacturing Process

Additive manufacturing processes are usually designated by 3D printing. It is possible to use different types of technology to produce a 3D metal part by these processes such as Wire Arc Additive Manufacturing (WAAM), Selective Laser Melting (SLM), Electron Beam Melting (EBM), Direct Metal Laser Sintering (DMLS), among others. (Compositadour, 2018)

This type of processes has the main characteristic of being produced layer by layer, on top of a substrate or without it depending on the used technology. Every single one of them consists in adding material with approximately parts geometry.

The process starts with a CAD 3D model of the part. Then, it is used a software to create a mesh and to slice it in order to be constructed layer by layer. The number of layers depends on the surface finish required (Figure 1.1).

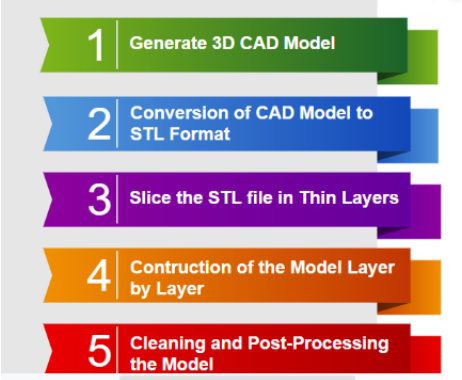

Figure 1.1 – Steps of Additive Manufacturing production

1.2. The Investigation Centre

The experimental part of the thesis took place in Bayonne, France, in Addimadour, which is a new platform for innovation and technology transfer focused on metal additive manufacturing. It is one of the first centre in France to offer manufacturers solutions in this field (Figure 1.2).

Figure 1.2 – Addimadour Infrastructures (Compositadour, 2018)

Addimadour was co-conceived with a group of manufacturers, due to the efforts and the financings of the "Communauté d'Agglomération Pays Basque" and the "Nouvelle Aquitaine Region".

This platform is managed by ESTIA – École Supérieure Des Technologies Industrielles Avancées (also located in Bayonne), and is part of Compositadour which is specialized in Robotics and Composites.

The Investigation Centre focus on the development of the following research themes:

"Mechanical characteristics' improvement of parts obtained by additive manufacturing.

- Development of optimal process parameter ensuring good material properties;
- Real time instrumentation development for monitoring and feedback;
- Development of deposition strategies adapted to additive manufacturing processes.

Numerical modelling of multi-physics additive manufacturing processes:

- Thermal, mechanical and metallurgical simulation for behaviour prediction (residual stresses and deformation);
- Topological optimization (finite elements sizing for improving the performance / mass ratio of high value-added parts)." (Compositadour, 2018)

1.3. Thesis Objectives

The analysis of the additive manufacturing cords produced by WAAM technology were performed according two different aspects:

- The Material Properties: in this approach, generally, it is done an initial study to understand what the predicted microstructures and the type of internal structures should be. The experimental procedure produces the structures to be analysed using different parameters to obtain the cords;
- The Geometry of the cords: in this approach an ideal shape of the exterior and the interior of the cord is analysed.

The present work and analysis were done following the geometry of the cords approach. In this type of approach, the external shape of the cord is analysed according to its height, width, geometry, length, colour and eventually some defects that might appear on surface, like spatter. It is also very important to do a correct analysis of cords interior to identify porosity, inclusions, dimensions of the cords and the magnitude of the penetration.

To develop the stainless-steel process production of components through WAAM, it is necessary to increase the knowledge of the following key-points:

1. To understand the main characteristics of the deposited material with the WAAM process;
2. The optimization of the process parameters as amperage, voltage, robot speed and wire feed speed aiming to optimal cord geometry;
3. The correlation between input parameters and defects;
4. Development of a correlation between the obtained microstructures with the parameters used on the experiments;
5. Find the microhardness pattern values inside the cords.

A microscopic analysis is done to all cords produced, all the different parameters, to fully understand the implications of each parameter in its construction. This analysis allows to compare the main results with those available on the bibliography.

To complete the analysis of each cord, microhardness tests are performed in the middle cut of cord. This test has the purpose to understand if there is a pattern in the microhardness values regarding start and end of deposition. The same evaluation was made concerning down and top of the cord.

The final goal of this thesis is to build two walls by WAAM using the parameters defined/optimized by the first experiments. Three-point flexural tests were performed on samples withdraw from those walls in order to achieve flexural mechanical properties such as young modulus and the maximum strength that allows to understand how the process influences the material properties.

1.4. Thesis Structure

In Chapter 1 (this Chapter) it is made the introduction of technology, materials, investigation centre, main objectives and thesis structure description.

Chapter 2, gives a brief explanation about WAAM process, the materials used by this technology, the process parameters that influences the outcome products made by this technology. On its last topic, it is explained how the complex technology of CMT works and the parameters and the limitations associated with this equipment.

The Chapter 3 introduces the experimental methodology and gives a brief presentation of all the equipment and material used in all the experiments.

Chapter 4 details all the experimental procedures, such as general procedure, the defined parameters and tests.

In the Chapter 5 the main results obtained are presented, where is provided all the collected data, the chosen cords and depositions from the experiments, the comparison between cords and walls, and all the analysis (macroscopic, microscopic, microstructure, microhardness and three-point flexural test).

The last chapter, Chapter 6, summarizes the main conclusions obtained from the experiments and their analysis and future developments are suggested.

2. State of the Art of the WAAM Processes

2.1. WAAM Classification

The American Society for Testing and Materials (ASTM) developed a standard ASTM F42 with several guidelines that classifies the Additive Manufacturing processes in seven categories:

- Vat Photopolymerization
- Material Jetting
- Binder Jetting
- Material Extrusion
- Power Bed Fusion
- Sheet Lamination
- Directed Energy Deposition

The process used in this thesis (WAAM) could be included on the Direct Energy Deposition processes.

2.2. WAAM Processes

The WAAM process has the meaning of Wire Arc Additive Manufacturing. This process consists in an electric arc, as a heat source, that melts the wire and the substrate where the material is being deposited. WAAM builds parts, with the required geometry, by adding material, layer by layer. Currently, the CMT process is equipped with a complex equipment that controls the wire feeding, the electric arc and the gas volume added. The trajectory of the layers is the only parameter that is controlled by the robot software.

This production process consists in designing CAD model, slicing into layers, tool-path generating, choosing welding parameters, material deposition and post-processing.

According to Posch, Chladil & Chladil (2017), to produce wings, turbine blades and valves, and many other big components by AM, “economic considerations are more dominant and it is necessary to reduce the additive manufactured component costs”.

2.3.Materials

The materials used in the WAAM process (processes that are being currently in development) are the Titanium (TiAl6V4B) used in the aeronautic and chemical industries; the Inconel 7718 (NiFe19Cr19Nb5Mo3) used in aeronautic industry and on the manufacturing of tools dedicated to work with high temperatures; Steel (ER316LSi, SMV3S, ER2209 duplex) used on the assembly and repair of stainless-steel parts, boilers and tubes, in under pressure equipment, in metallic constructions that do not exceed the work temperature of 400 ºC, in constructions near the sea, in moulds for glass, dies and insert for stamping, and in the naval industry; and Aluminium (AlSi5, AlSi5GrY, AlMg5Cr, AlSi7Mg0,5Ti, AlCu6MnZrTi) used on extruded aluminium parts and repair of foundries parts, naval construction, on railroads, on roads and in aerospace and aeronautic industries. The materials to this process come in wire spools in which the wire can have different thicknesses according to their final purpose, mainly provided by the supplier Selectarc Welding.

2.4.Process Parameters

The process parameters usually depend on the material to be used and the geometry of the parts to be produced (Figure 2.1).

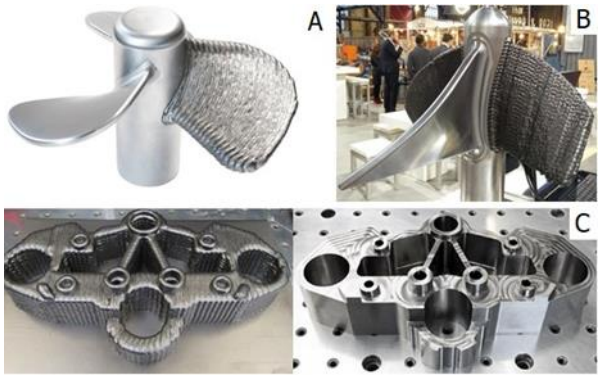

Figure 2.1 – Examples of parts produced by WAAM technology (Huntingdon Fusion Techniques (A); Material district (B); Avianik (C))

Developing parts for different markets have different challenges. The starting point is always the basic understanding and the number of parameters that are directly linked or that restraint the final product achieved. Developing the basis of a production technology requires a deep understanding of the key parameters that correctly tune and allow to achieve a good result.

Simple precautions with the material, like keeping the filler wire "clean and dry, and stored in a covered container until use" are assured while handling it (TMR Stainless, 2014). Vignesh (2017) states that "a deposition strategy limitation, required in additive manufacturing, is that the processing tool should be always normal to the working plane; thus the inclination is chosen to be constant at 90 degrees", and also "to minimize aspiration of air into the shielding gas" (TMR Stainless, 2014) the angle is kept constant in all the experiments.

Using the correct procedures like maintaining the width of the root gap carefully, "to ensure consistent heat input and dilution in the root pass", or initiating the gas flow "several seconds ahead of striking the arc, and it should be maintained for several seconds after the arc is extinguished, ideally long enough for the weld and HAZ to cool below the oxidation range of the stainless steel" must be followed carefully. Respecting these procedures suggested by the TMR Stainless (2014) as well as the flow rates of 12-18 l/min would help to protect "from atmospheric oxidation and contamination" and to achieve a good result and, as according to Vignesh (2017), the flow rate gas and the gas itself used during WAAM, "influences many factors such as surface appearance".

Vignesh (2017) stated that the parameters of amperage, voltage, wire feed speed and welding speed "are very crucial to obtain the desired weld bead geometry and properties for WAAM deposition"; and that when they have a "properly calculated combination" the weld shows the best quality "in terms of geometrical aspects such as Bead Width (W), Height (H) and Depth of Penetration (P) and metallurgical aspects such as defect free weld beads, less spatter and inclusions".

According to Posch *et.al.* (2017) "the wire feed rate was set to 4.2 m/min, the welding speed was 36 cm/min" related with the amperage that "was 145 A" and "the voltage 11.9 V" that shown good results in a blade production. The wire manufacturers also indicate, for 1.2 diameter of wire, similar values regarding the amperage and voltage but there are other parameters to consider and explore, like paths' strategies as Vignesh (2017) states. These values are going to be the basis for the search for the right law in the Fronius equipment.

The influence of the parameters, stated by Vignesh (2017) are "the current (amps) produces the heat and penetration, the voltage produces the arc that carries this heat and the travel

speed supports this heat and the resulting molten metal to be deposited on the substrate." These are the parameters with the most importance and where the focus of the thesis would be.

2.5. Technology

2.5.1. CMT – Cold Metal Transfer

The Cold Metal Transfer (CMT) was the process chosen for this thesis development as it is "a highly developed version of Metal Inert Gas / Metal Active Gas (MIG/MAG) arc welding process with a precise process control and low heat input to the base material." (Imoudu, 2017).

The CMT equipment was developed by an Austrian company called Fronius, to help the user to achieve better depositions through setting some parameters inside each law. Fronius developed "synergic laws" that have instructions to be used regarding the material chosen. Inside each "synergic law" it is possible to adjust only some parameters like the wire's feeding speed or the arc's hardness, while others are unaltered by the user but changed automatically by the processes controller Fronius, adjusting them to the changes introduced by the user (Figure 2.2 and Figure 2.3).

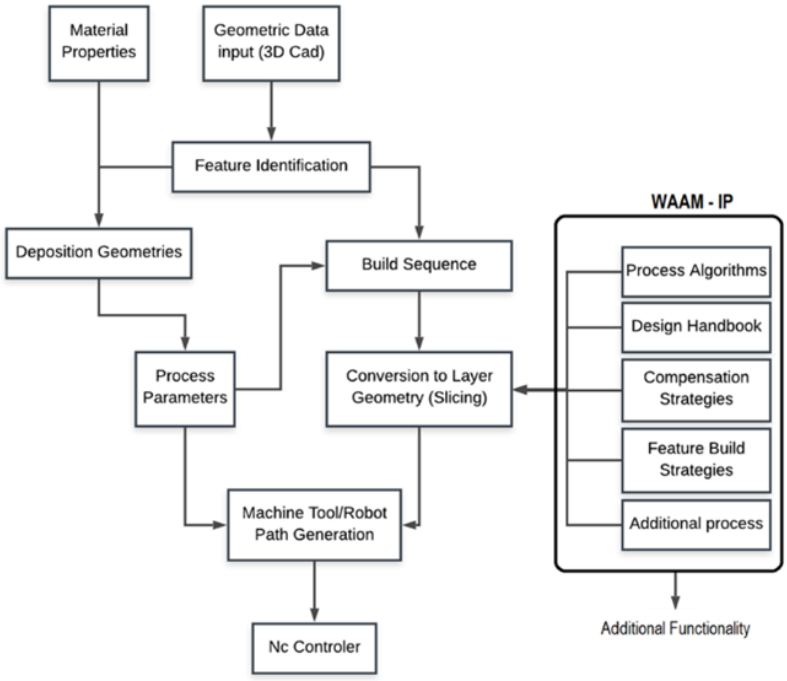

Figure 2.2 – Scheme of Fronius steps and interaction in WAAM equipment

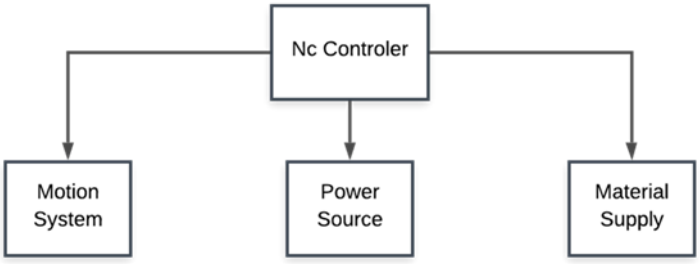

Figure 2.3 – Distribution of the information introduced in Fronius

2.5.2. Synergic Laws

According to Imoudu (2017), Fronius developed a concept designated by synergic law "for different filler materials and filler diameters". There is a major importance of this synergic laws "in the CMT welding process because they provide the basic parameters automatically to each filler material" and each filler diameters. A good choice of this law, together with good adjustment of the welding parameters, controlled by the CMT, should provide quality welds. Because the amount of data in each law, there is a need to choose the right one using the tables supplied by Fronius, where it is referred the indicated laws for each type of material and upload them to the CMT equipment, through the remote control.

The creation of a synergic law has, as a fixed parameter, a low value of wire feed speed and, with the help of an oscilloscope and a high-speed camera, a process of detailed examination of the different characteristics and optimization is developed, achieving an ideal value of voltage. This optimization process is developed for all the wire feeding speed values, presented in each law.

The gathered voltage values, collected by the arc length correction, are in a range of 60%, being 30% above the ideal and 30% below it, defining an ideal value, for each wire feeding speed. This range is shown, in yellow defining the working area, in the Figure 2.4.

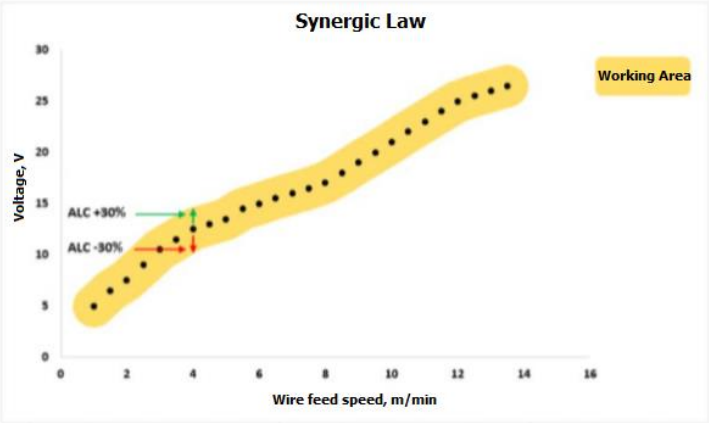

Figure 2.4 – Illustration of a Synergic Law (Adapted from Fronius, 2014)

The wire feed speed has a direct link with the power, controlling it in agreement with the synergic law used but other links, with the wire feed speed are referred by Selvi, Vishvaksenan & Rajasekar (2018): "the wire feed rate and the cycle arcing phase are controlled to realise sufficient energy to melt both the base material and a globule of filler wire" that have a great importance for the CMT process.

The correction parameters also have a major influence in the process as stated in Imoudu (2017), ALC (Arc Length Correction) and DC (Dynamic Correction) "also have effect on the wire feed rate", this relation is also to take into account.

As referred before, the wire feed speed parameter has a direct influence on the CMT process in different aspects. According to Almeida (2010), it was possible to observe that the real wire feed speed actually was different from the defined on Fronius control. Not being the wire feed speed constant, knowing that the direction of the wire (forward and backward) changes with high-frequency, according to the signal controller, it is possible to have to introduce some changes to achieve a good balance between parameters.

2.5.3. CMT Innovation

The innovation on the CMT process is the movement associated to the wire tip. The equipment relies in two electric engines to control the wire (one in the wire feeder and one in the torch). The combination of wire movements done by these engines and the existence of a buffer, allow the wire tip to do high frequency movements, forward and backward, achieving this way a perfect cadence of droplets accurately defined (Figure 2.5). Supplying limited energy, suitable just to melt the wire and the surface of the base metal, results in

minimum arc burning time. This characteristic results in a process with low energy inputs that combined with “an accurate robotic movement of the CMT welding torch, geometries with minimum thicknesses in the range of 2–4 mm can be built up layer by layer” (Posch, *et.al.*, 2017).

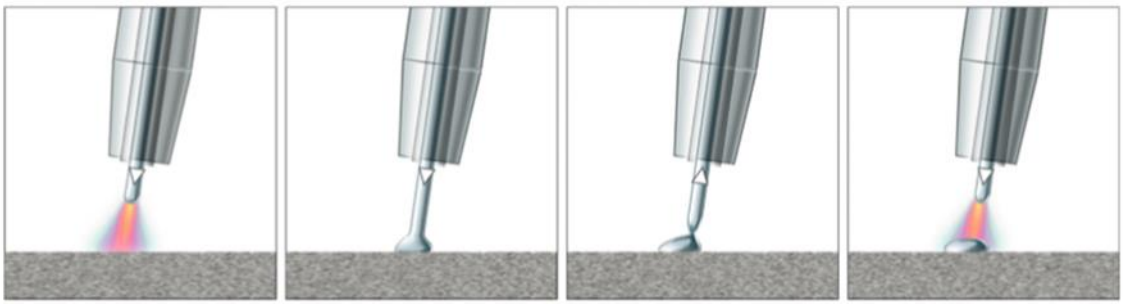

Figure 2.5 – “Basic CMT process, one cycle” (Fronius, 2014)

The minimum wall thickness that is possible to achieve depend on the type of material, the diameter of the filler wire, the wire feed speed and heat supplied to the process, Posch, *et.al.* (2017) “the lower the heat input, the smaller the minimum achievable wall thickness.”

According to Posch *et.al.* (2017) if the need is to build thicker walls, they can be achieved by using different strategies of path generated. These strategies could also be assisted with different settings in the CMT machine.

Concerning the finishing surface left by this process, Posch *et.al.* (2017) that it is quite smooth and “Surface roughness measurements of the CMT blade showed a comparable roughness as achieved by sand casting, hot rolling, or flame cutting” which left (if achievable) only minor post processing requirements needed (depending on the type of part produced).

There are, in the CMT processes, some variants of the process that make it more adaptable for other material requirements and uses. These variants are the CMT Pulse, CMT Advance, CMT Pulse Advance, CMT Dynamic, CMT Pin and CMT Synchro Pulse. Each one of these variants have their own specification regarding an extra cycle, or a different cycle, done by the wire movements and its speed, the amperage and the voltage input.

The Figure 2.6 shows, as an example, a representation of the CMT and pulse cycles. The cycle done in the normal CMT is referred as CMT phase, and the cycle associated to the CMT pulse is the conjugation of the CMT phase with the referred pulse phases.

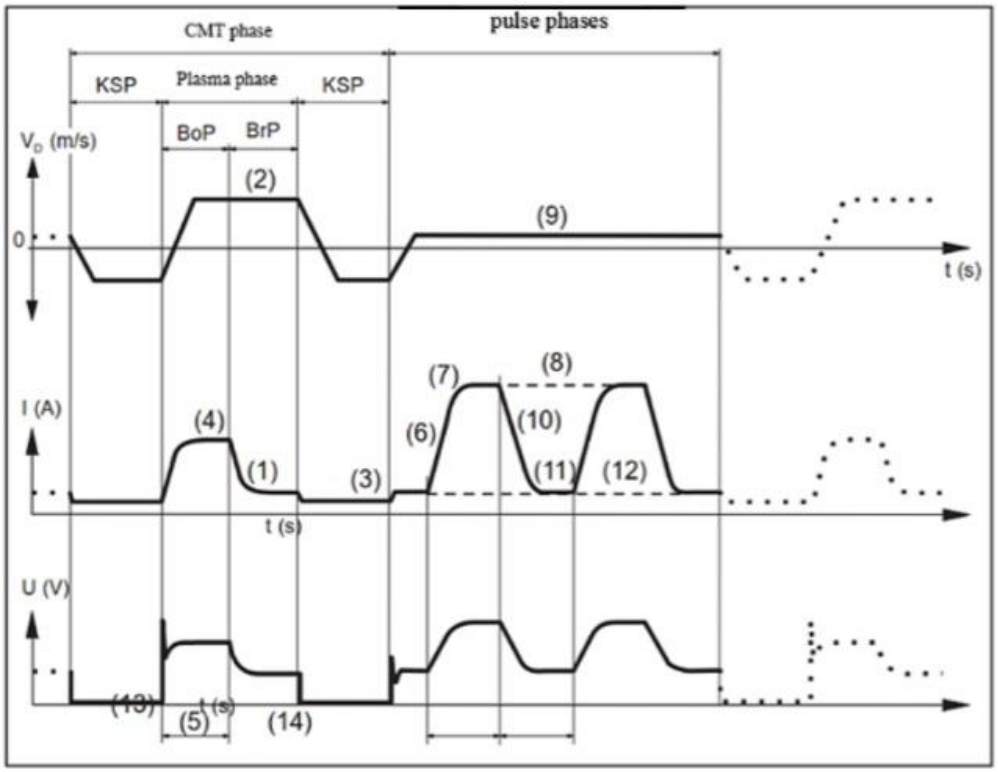

Figure 2.6 – "Wire speed rate, current and voltage curves during a CMT Pulse cycle" (Tapiola, 2017)

2.5.4. Advantages and Disadvantages of CMT

The CMT process is easily automated achieving a better control of the process, that is reflected in the management of the electric arc length done by the system. The great advantage of this process is its reduced heat input during the deposition, comparing to other conventional processes. As Posch, *et.al.* (2017) said "The realizable wall thicknesses are mainly determined by the welding heat input: the lower the heat input, the smaller the minimum achievable wall thickness".

The disadvantages of CMT are the spatter formation during the construction process of the thin walls as stated in Posch, *et.al.* (2017), "a significant reduction of the process energy is required which increases the risk of process instabilities and spatter formation". On the other hand, as reported by Imoudu (2017) "the short arc process no longer exists for higher currents meaning the CMT can't be used" limiting its application to lower amperage inputs.

2.5.5. Correction Parameters

The achievement of a perfect deposition relies not only in the choice of the right synergic law for the material chosen, but also in the optimization of the process parameters.

The CMT developed what is called by Correction Parameters, to help this optimization. There are two: Arc Length Correction (ALC) and Dynamic Correction (DC). The "ALC, is used to set the spatial elongation of the arc plasma column. Shorter arc has a favourable effect on welding speed and against undercuts, and a long arc has positive effects in terms of formation of wide weld seam and edge formation". Regarding the DC influence, this "correction simulates inductance and it is used to adjust the duration and property of the short-circuit break. In other words, DC controls the arc pressure by adjusting the reignition current" (Tapiola, 2017).

2.5.6. Welding Power

The power (Watt) supplied to the CMT process has a big influence in the process. This influence is inputted in the process in the form of two parameters separately: the amperage in ampers and the voltage that comes in volts.

The formula that describes this relation is:

$$Arc\ Power = Average\ Amperage\ x\ Average\ Voltage \quad (1)$$

In the CMT it is possible to have the same power value supplied to the system at the same time that the both parameters (amperage and voltage) could have various combinations possible, with very different values.

The theoretical heat input for this process could also be calculated in kJ/mm, according to the European standards (EN ISO 1011), by the formula:

$$Heat\ input = Thermal\ Efficiency\ \frac{Voltage\ x\ Amperage\ x\ 60}{Travel\ Speed} \quad (2)$$

This formula transcribes "the amount of electrical energy that is supplied to a weld during the welding process" according to Anand (2019).

Also, by the standards of ASME under the European system the heat input is referred as Arc energy. With this difference, the formula is:

$$Heat\ input = Thermal\ Efficiency\ x\ Arc\ energy \quad (3)$$

The appearance of the thermal efficiency parameter in the formula, is explained by the heat lost by the process in various forms, like radiation, among others, and that in reality do not contribute effectively for heating and melting the wire in the base metal. Due to this loss, there was the necessity to introduce a compensation factor (thermal efficiency) to correct the result value achieved with this formula. By default, according to Anand (2019), the value used could be the 0.8, that it is normally correlated to the conventional process of MIG/MAG, once these processes have more heat input, they generally also have more losses.

The CMT equipment records, in its memory drive, the average, amperage and voltage used during the welding. An analysis of this data, collected by the software Fronius Xplorer can provide the values for these formulas. There are also others software in the market, that associated to the CMT equipment, collect more detailed and accurate data for analysis, regarding more parameters.

2.5.7. Welding Geometries

In consonance with Imoudu (2017) and Tapiola (2017), the welding geometries and shape have a greater importance for deposition process. The cord dimensions, its exterior and interior shape reveals the influence that the input parameters have.

The physical properties that are analysed for this understanding are the cord height, width, penetration depth, as well as the geometry shown in terms of centration. The alignment of the penetration with the cords higher point, the symmetry of the external shape as the internal are also evaluated.

From the external point of view, the consistency of the weld geometry, concavity and colour is also analysed to understand the stability of the process. There is the need to observe the existence of non-programmed curbs (or S) that are linked to instability of the process or to the wire tip.

2.5.8. Shielding Gas

The shielding gases can be divided in two categories: the inert or semi-inert, based on their properties in accordance with EN ISO 14175. The first ones are cost effective, compared with the semi-inert, used in welding; and the second ones when used in small controlled quantities, can improve weld characteristics.

Argon is an inert shielding gas that does not react with the work piece. The benefits for its use are the improvement in wetting, and flow characteristics of the weld metal.

The characteristics of the gas CO_2 is that it provides a deep penetration and, mixed with argon in low percentage (1-2%), it reduces the surface tension of the molten area, at the same time being the least expensive shielding gas. The disadvantage of it is that it affects negatively the arc stability, enabling the appearance of spatter or creating droplets and leaving a highly oxidized surface.

The contribution of the Nitric oxide has an environmental objective to reduce the ozone production and at the same time to stabilize the electric arc during the process. The presence of nitrogen reduces the distortion of the weld part, having a positive influence in the arc stability, penetration, weld shape and colour at the same time that contributes to maintain a proper nitrogen content in the duplex stainless steels and to increase the welding speed. (in https://www.aga.se/en/products_ren/cutting_welding_gases/shielding_gases/mison_shielding_gases/index.html)

2.5.9. Weld Imperfections and Defects

The CMT process is not free of flaws and defects, which could have several sources like the shielding gas used, the parameters combination, the material used, the geometry adopted among others. These flaws have a great importance regarding the process, once they contribute actively for the final result in terms of geometry and quality of the final product in its microstructure and surface finishing.

The flaws more common in the process are the porosity, inclusions, bead humping, cracking and excessive convexity as reported by Mendez (2003), and could affect the integrity of the part produced as the post process costs.

The origin of the flaws has to be analysed in each deposition to understand which are the parameters contributing for it.

Being subject of several studies, welding has already some correlation between the flaws and its probable origin, like porosity, “generally associated with gas for the period of the solidification of a weld bead and generally recognised as cavity-type discontinuity” (Imoudu, 2017), but the porosity could have more origins like the strategy for the deposition.

Another big source of flaws is the wrong combination of parameters chosen for the deposition regarding the material used. It is very important to use the right combination of the Law in CMT, the wire feed speed, the robot speed, the shielding gas chosen and the flow rate of the shielding gas. There are also other parameters contributing for the flaw’s appearance and they are the surrounding conditions like temperature, humidity, wind, among others.

3. Equipment and materials

3.1. Equipment used

3.1.1. Equipment used in the production

CMT Welding Equipment

The Figure 3.1 describes all the equipment used by the CMT. As it can be seen, it is a quite complex system where all the parameters regarding the production of the parts are controlled by the TP 3200, except the robot's speed that is controlled by KRC2.

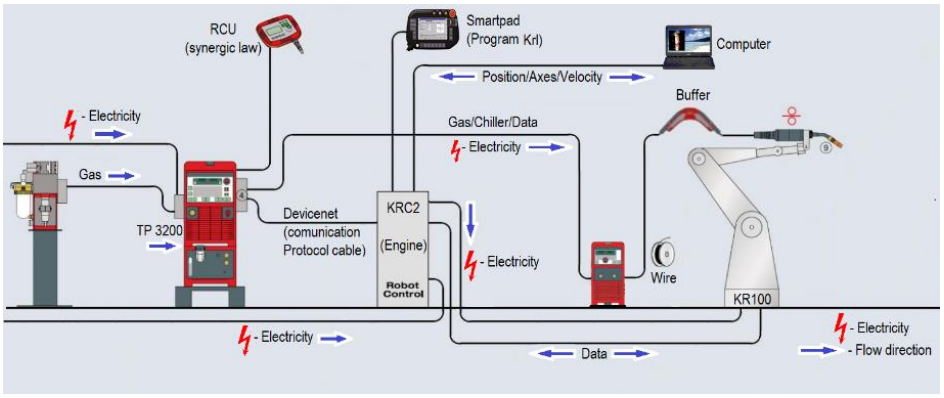

Figure 3.1 - CMT Scheme of all the equipment and flux of data (adapted from Alcaraz, 2015)

Robot KUKA KR 100-2 HA 2000

The robot KUKA is a KR 100-2 HA 2000 model (Figure 3.2) and is used to handle the CMT torch. It is made of cast light alloy which leads to a high resistance to vibration. This robot has the important function to perform all the defined strategies for depositions.

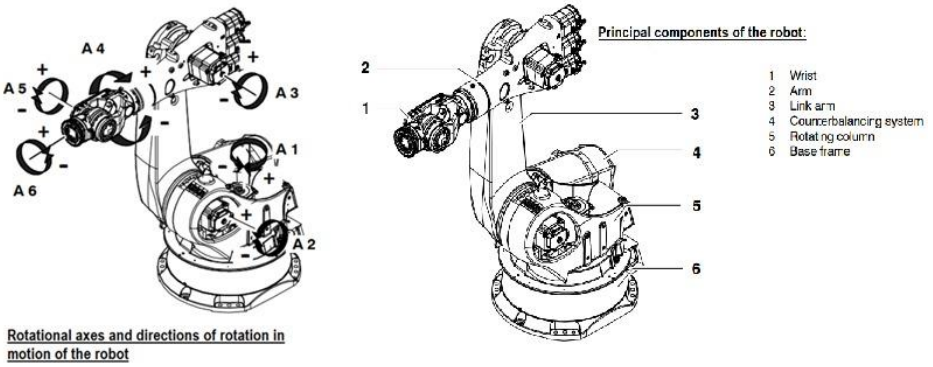

Figure 3.2 – Robot KUKA's angles and main components (Spez KR 100 HA, 2006 Datasheet)

3.1.2. Equipment used in the samples construction

Cutting machine

In order to cut and prepare the samples for analysis it was used a cutting machine Labotom-5 from Struers. It is a machine without cut velocity regulation and with forward speed manually controlled. The cut is made with liquid cooling and lubrification. The work table has a dimension of 316 x 225 mm allowing to make all the cuts necessary to the samples construction (Struers Labotom 5 Datasheet).

Polishing machine

The pre-polishing / polishing machine is a Struers LaboPol30 and is located at the laboratory of metallography.

The equipment includes a "software" Struers LaboForce100 that has already pre-programmed all the procedures regarding each material to be polished. In these programs are also used the LaboDoser100, that includes chemicals used during the polishing procedure, leaving for the users the simple task of changing the polishing discs (LaboPol30 Datasheet).

Chemical Vapours Hood

The Chemcap Clearview Fume Hood BC 8004 is used to do the samples construction that are going to be polished and analysed afterwards. The main function is to protect the users from the toxic vapours released from the chemicals used during the construction in order to protect them from the vapours produced during the chemical attack (in Clearview Fume Hood Datasheet).

3.1.3. Equipment used to analyse materials

Microscope

The microscope used is a Leica DM 1750 M (Figure 3.3). This equipment allows to analyse the microstructure of the samples produced with four lenses (x5, x20, x50 and x100). This microscope has an integrated module that allows the microscope to send and work the images, in real time, to a computer. This computer uses the LEICA software that allows the

user to see and correctly tune the images and their properties (with a clear vision on a screen), with several options to work the images collected (LEICA DM 1750 M Datasheet).

Figure 3.3 – Leica DM 1750 M

Microhardness machine

The Presi Vickers Microtech MX7 (Figure 3.4) is a microhardness analysis equipment with automatic load application that was used for measuring the microhardness of all the samples.

The precision of this equipment is 0.1 µm (x200 - x1000) and the load range is from 5 to 1000gf of load application. The time and the load applied can be adjusted (Presi catalog, 2020).

Figure 3.4 – Vickers Microtech MX7 (Presi catalog, 2020)

Turret Milling Machine

The HOLKE F-10-V machine is a three axes manual surface milling and it was used to mill the final walls produced to construct samples for the three-point flexural test, assuring that all have the same dimensions. The main purpose of this millings was to prepare the samples for some additional superficial finish made in the surface grinder Chevalier.

The HOLKE F-10-V has a work table with 1220 x 255 mm, the spindle power is of 1.5 kW and the axle rotation goes from 57 rpm/min to 2275 rpm/min (Holke F-10-V Datasheet).

Surface Grinder machine

The Hesse Chevalier FSG-3A818 is a three axes automatic surface grinder and it was used to finish the surface of all the samples, coming from the same wall. This surface grinder has a magnetic work table with dimensions of 457 x 203 mm, with a grinding area of 457 x 203 x 450 mm, which allows to finish more than one sample at the same time (Hesse Chevalier FSG-3A818 Datasheet).

Three-point Flexural machine

The Roell Zwick Z100 (Figure 3.5) is the equipment that was used to perform the three-point flexural tests in the wall samples. These tests were performed in a controlled laboratorial environment in order to assure similar conditions for every test.

Figure 3.5 – Roell Zwick Z100

3.2.Material used for these experiments

The material used in the substrates, as to perform all the experiments described above, was the Stainless-steel ER2209, a duplex stainless-steel. It was chosen the Ø1.2-mm classified as G 22 9 3 N L by EN ISO 14343-A, SS2209 according to EN ISO 14343-B and ER2209 according to AWS A5.9.

By definition, duplex stainless-steel is a two-phase steel: with ferrite and austenite. This type of material has in its composition, ideally, 50% of ferrite and 50% of austenite microstructure. According to Padilla, Plaut & Rios (2007) duplex stainless-steel has "an interesting combination of properties: a yield strength (YS) twicer higher than the one for the austenitic and ferritic common types, greater plasticity and toughness".

The choice of this material takes into account various and important factors in the production industry nowadays. The cost of the material was considered such as the production costs of parts with it. Having in mind that AM has, as a target market, short runs of parts for specific industries that are growing and have the need to build more complex parts, faster. To fulfil the production requirements of the industries, this material needs to have its parameters properly developed to find the right tune for each parameter. However, it plays an important role, its tonnage only represents 2.2% of the whole steel production, being austenitic stainless steels representing 60% and ferritic steels 30% of the whole stainless-steel productions (Padilla *et.al*., 2007)

The chemical composition of this material is described in Table 3.1.

Table 3.1 – Chemical composition of Duplex Stainless-steel (Aircraft Materials)

Weight %	C	Mn	Si	Cr	Ni	S	P	Mo	Cu	N
ER2209	0.03 max	0.50 - 2.0	0.90 max	21.5 - 23.5	7.5 - 9.5	0.03 max	0.03 max	2.5 - 3.5	0.75 max	0.08 - 0.20

The typical mechanical properties of this material are described in Table 3.2.

Table 3.2 – Typical Mechanical Properties of Duplex Stainless-steel (Aircraft Materials)

Material	Ultimate Tensile Strength	Yield Strength (0.2 %)	Elongation (%)
	MPa	MPa	
ER 2209	720	560	26

According to the FSH Welding Group, this stainless steel has some advantages. It has high resistance to corrosion, to fatigue, to erosion and to chloride stress corrosion cracking. It also has good properties in strength, toughness, sulphide stress corrosion resistance and good characteristics in terms of welding and workability. Among other austenitic stainless steels, it is the one with higher thermal conductivity and lower thermal expansion. (FS

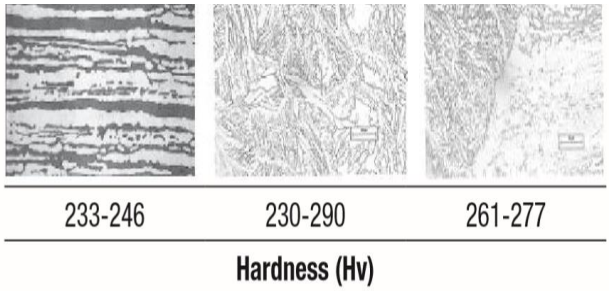

Figure 3.6 – Microstructures and values of microhardness of Duplex Stainless-steel (FSH Welding Group)

In the Figure 3.6, it is shown the microstructures and the values of microhardness (HV) typical of this material.

The advice given by the material supplier is that the temperature of the substrate, before welding, should be about 20ºC, without any pre-heating treatment for this material (Duplex Stainless Steel), so the parameter of heat input and range temperature can be respected.

3.2.1. Microstructures

The Duplex Stainless-steel quality, in the weld area, requires a good ratio balance of austenite and ferrite deposits (Figure 3.7B). A phase balance is very important in the material. For example, if there is too much ferrite (more than 70%), it will have less ductility, less toughness and less corrosion resistance; if there is too much austenite (more than 80%), it will have less mechanical strength and less stress corrosion cracking resistance. The ideal percentage of ferrite is 30-55% (FSH Welding Group).

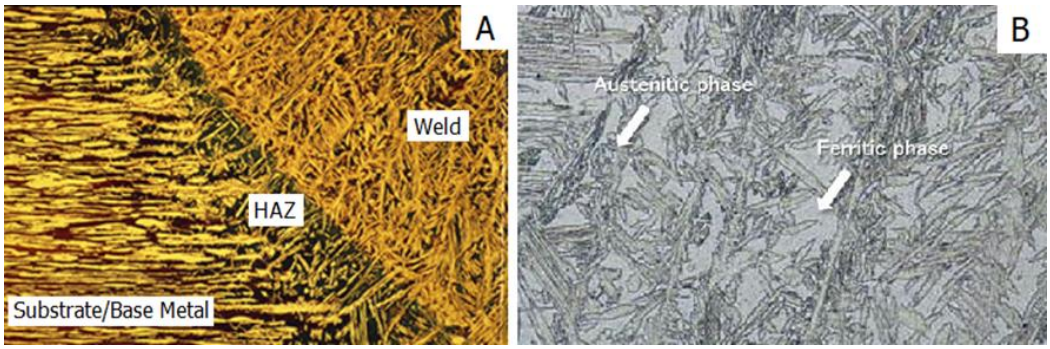

Figure 3.7 – Representation of A-the transition between the weld/deposited material and the substrate/base metal (adapted from Nilsson, 2016) and B –"the duplex stainless steel weld metal" (Kobelco)

As referred by Taban & Kaluç (2013) "Duplex stainless steels in general solidify as δ-ferrite, and the austenite phase forms by nucleation at ferrite grain boundaries during cooling to room temperature. Consequently, the amount of austenite resulting at room temperature in welded joints becomes a function of the thermal history experienced during welding." This function of the thermal history is the reason to do cuts in each cord or wall to have access and understand the development of the deposition (Figure 3.7A).

The statement of Taban & Kaluç (2013) "The higher the cooling rate, the higher the ferrite content occurs in the duplex structure", is going to be explained during the analysis of the cuts of the cords or walls, if the structure reveals where it had a faster or slower cooling rate.

4. Experimental Methodology

4.1. General Procedure

Each experiment followed a common procedure, regardless the changes that can be done in the different parameters:

1. This procedure starts with substrate preparation (in case it is needed). It can be grinded, polished and cleaned, or just the last two ones. The polish phase is made with the elliptical polisher with a polish disc P60;
2. The second step is to fix the substrate in the work table to prevent it from moving in any direction and to prevent the bending factor that is associated to this type of depositions;
3. The pre-deposition step includes to polish the substrate again and clean it with alcohol and paper and assure the equipment is prepared for depositions (Appendices B);
4. Next step the cord and wall deposition, according to the parameters specifications previously defined theoretically, following the safety procedures (Appendices C);
5. After the deposition, it is needed to catalogue all the cords and analyse them through a macroscopic analysis;
6. After a thorough macroscopic analysis of the cords and walls deposition, cuts are made in three points: 1) immediately after the beginning of the cord (more or less 10 mm), 2) at the middle 3) and at the end (more or less 10 mm before end). The aim of this cuts is to fit in the moulds for the samples for microscope analysis;
7. After the cuts, it is time to make the samples for the microscopic analysis (protocol described in 4.5.1. Protocol);
8. When the samples are prepared, they are polished in the Labopol 30, following the procedure previously described (protocol described in 4.6. Polishing);
9. The chemical attack is done after the polishing phase (protocol described in 4.7. Chemical Attack);
10. After the chemical attack the samples are positioned in the microscope LEICA DM 1750M to observe and describe all the internal microstructures and cords shapes (in profile); to measure the contact angles with the substrate; and to understand if there are irregularities or defects, like pores or inclusions. Photographs are taken to document the analysis with the help of the LEICA software;
11. In the end it is time to do the microhardness analysis and record data.

4.2. Defined parameters

In the first three experiments the main purpose is to find the best parameters (law, robot speed and wire feed speed) that will allow to have the cord with the best shape.

In the first experiment, with the aim to understand the influence of the automatically defined and occulted (by Fronius) deposition parameters of each law, five different laws were used, different laws that have different amperages and voltages. These laws were selected in the CMT Fronius and the criteria was the values of amperage and voltage, despite being different, they were close to the ones referred in the literature as the ideal ones for this material, setting the robot speed and the wire feed speed, with values described in Posch *et.al.* (2017). The Law CMT 875 had the values of voltage, robot speed and wire feed speed close to the reference values but a low value of amperage. This Law was chosen with the aim of trying to identify the contribution of amperage for the ensemble, keeping all the other parameters (voltage, robot speed and wire feed speed) unaltered.

After finding the right Law, different values for the robot (KUKA) speed were used in the second experiment in order to understand the influence of this parameter in the cord shapes obtained. With the right Law and the right robot speed already chosen, it was time to try different wire feeding speeds. On the CMT there is a correlation between the wire feeding speed, the amperage and the voltage. Due to this correlation, when the wire feeding speed changes, the values of the amperage and the voltage are also changed automatically by the CMT (Table 4.1).

In all these experiments there are some parameters that are going to remain the same, like the gas and the gas flow. The gas used was always the Mison 2, composed of Argon + 2.0% CO_2 + NO, and the gas flow was always 17.5 l/min. Other fixed parameters are the Arc's Height and the Arc's Hardness, that were always zero, and the torch mode was always 2 strokes.

In all this experiments the existing cooling system (Appendices D) was not used, the wire thickness was 1.2 mm for all the experiments, the nozzle was in a 90-degree angle and the path in these experiments was linear and with only one cord.

Table 4.1 – Defined parameters (Law; Robot and Wire Speed Experiments)

		Cord	Synergic Law	Type of Gas	Gas charge (l/min)	Amperage (A)	Voltage (V)	Robot Speed (m/min)	Wire Speed (m/min)	Path's Direction
Law Experiment	1st substrate	1.0	**CMT1093**	Mison 2	17.5	**136**	**13.7**	0.36	4.2	Longitudinal
		1.1	**CMT1164**	Mison 2	17.5	**140**	**13.4**	0.36	4.2	Longitudinal
		1.2	**CMT1093**	Mison 2	17.5	**151**	**13.1**	0.36	4.2	Longitudinal
	2nd substrate	1.3	**CMT875**	Mison 2	17.5	**66**	**12.5**	0.36	4.2	Longitudinal
		1.4	**CMT1098**	Mison 2	17.5	**150**	**16.1**	0.36	4.2	Longitudinal
Robot Speed Experiment	3rd substrate	1.5	CMT1093	Mison 2	17.5	151	13.1	**0.54**	4.2	Longitudinal
		1.6	CMT1093	Mison 2	17.5	151	13.1	**0.72**	4.2	Longitudinal
		1.7	CMT1093	Mison 2	17.5	151	13.1	**0.9**	4.2	Longitudinal
		1.8	CMT1093	Mison 2	17.5	151	13.1	**1.08**	4.2	Longitudinal
Wire Speed Experiment	4th substrate	1.9	CMT1093	Mison 2	17.5	**118**	**11.8**	0.72	**3.2**	Longitudinal
		2.0	CMT1093	Mison 2	17.5	**167**	**16.3**	0.72	**5.2**	Longitudinal
		2.1	CMT1093	Mison 2	17.5	**185**	**19.1**	0.72	**6.2**	Longitudinal
		2.2	CMT1093	Mison 2	17.5	**210**	**20.5**	0.72	**7.2**	Longitudinal
		2.3	CMT1093	Mison 2	17.5	**136**	**12.2**	0.72	**3.7**	Longitudinal

For the microscopic analysis of the cords deposition it was used some diminutive to help locating the areas that are going to be described. The Figure 4.1 is a scheme of the WAAM deposition cord with a perfect shape that is aimed to achieve. It is also to introduce some of the concept used in the measures and analysis.

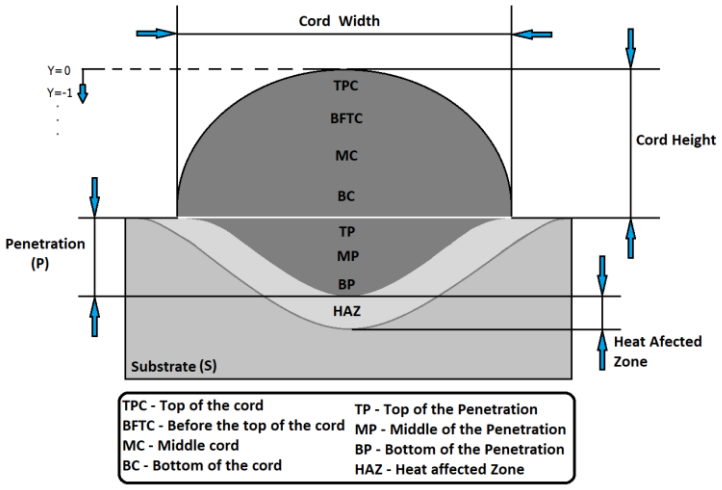

Figure 4.1 – Description of the diminutive and names used in this analysis

In the second part of the work, after achieving a good set of parameters to produce the cords with the best shape, it is time to understand the behaviour in the interaction between multiple cords depositions (Table 4.2). To start in the Multi-cord experiments it was done four deposition cords in sequence, side by side, but with different overlaps between them. In the

next five deposition cords it was deposited two cords in the substrate and two on the top of that. The overlap between the pair of cords were changed from 70% to 30%, and this experiment had the purpose to confirm the fulfilment of the gap between cords and to see if the material that overlap the cords do not influence the geometry of the wall to tend to one side, leading it to grow crooked.

Table 4.2– Defined parameters (Multi-cord and Walls Try-out Experiment; Wall Construction)

		Deposition	Synergic Law	Type of Gas	Gas charge (l/min)	Wire Speed (m/min)	Robot Speed (m/min)	Amperage (A)	Voltage (V)	Path's Direction	Overlap (%)
Multi-cord Experiment	5th Substrate	2.4	CMT1093	Mison 2	17.5	5.2	0.72	167	16.3	Longitudinal	**70/60/50**
		2.5	CMT1093	Mison 2	17.5	5.2	0.72	167	16.3	Longitudinal	**70**
		2.6	CMT1093	Mison 2	17.5	5.2	0.72	167	16.3	Longitudinal	**60**
		2.7	CMT1093	Mison 2	17.5	5.2	0.72	167	16.3	Longitudinal	**50**
		2.8	CMT1093	Mison 2	17.5	5.2	0.72	167	16.3	Longitudinal	**40**
		2.9	CMT1093	Mison 2	17.5	5.2	0.72	167	16.3	Longitudinal	**30**
Walls Try-out Experiment	6th substrate	3.0	CMT1093	Mison 2	17.5	5.2	0.72	167	16.3	**Longitudinal bi-directional**	**40**
		3.1	CMT1093	Mison 2	17.5	5.2	0.72	167	16.3	**Longitudinal unidirectional**	**40**
		3.2	CMT1093	Mison 2	17.5	5.2	0.72	167	16.3	**Longitudinal unidirectional**	**50**
		3.3	CMT1093	Mison 2	17.5	5.2	**0.72 2.4**	167	16.3	**Transversal**	**40**
Wall Construction	7th substrate	3.4	CMT1093	Mison 2	17.5	5.2	0.72	167	16.3	Longitudinal Bi-directional	50
		3.5	CMT1093	Mison 2	17.5	5.2	0.72	167	16.3	Longitudinal Bi-directional	50

The deposition 2.4 had the aim of understanding the behaviour of four cords, overlapping themselves with different percentage of overlap: 70% between first and second cords; 60% between the second and third cords; and 50% between the third and fourth cords (all made in sequence and with unidirectional path). In the Figure 4.2 it is possible to see the different overlaps used between the cords, being the first cord 2.4.1 and the last 2.4.4.

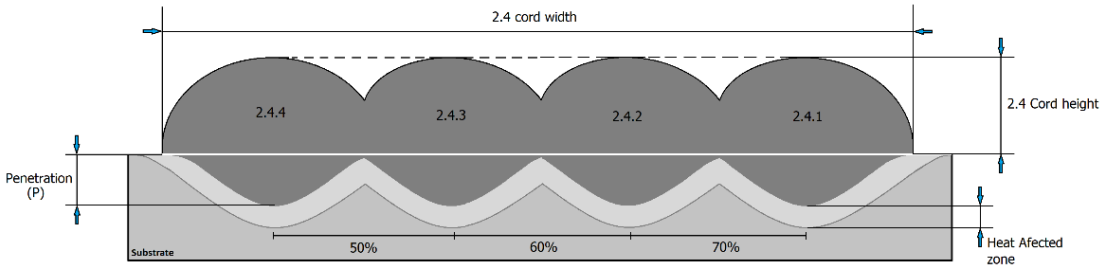

Figure 4.2 – Deposition 2.4 scheme

The Figure 4.3 is a scheme that represents the ideal shape of the four cords deposited (two on top of other two), experimented from the 2.5 to 2.9 samples.

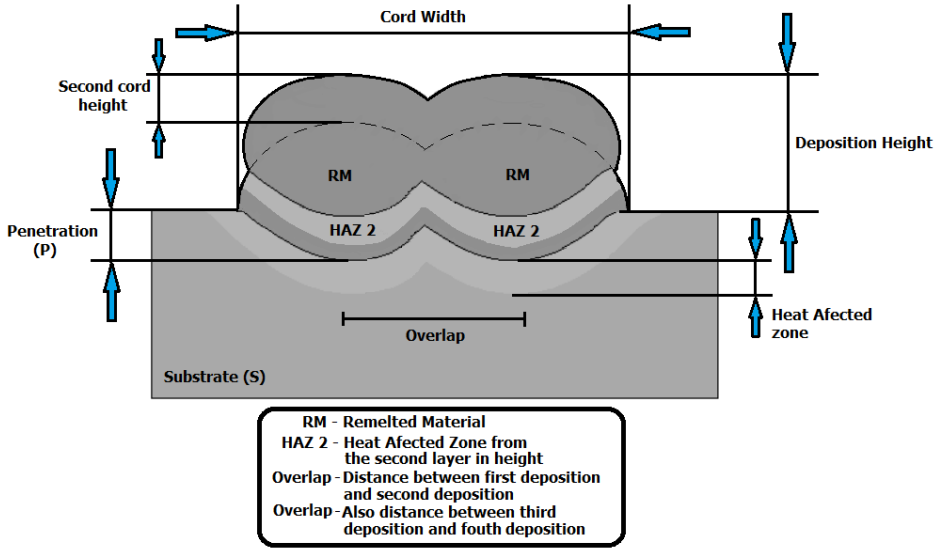

Figure 4.3 – Deposition 2.5 to 2.9 scheme

In the fifth experiment, called Walls Try out it was tested four cords side by side, and eight layers of them. This shown the dynamic between layers as between cords. This experiment also tested different strategies of deposition, so it was possible to choose the most consistent one, that shown the best results in terms of wall quality, superficial finishing and lack of flaws.

The Figure 4.4 represents a scheme of the ideal shape of the wall and cords distribution inside the wall. The percentage of overlap could be altered accordingly to the flaws or lack of quality of the wall produced.

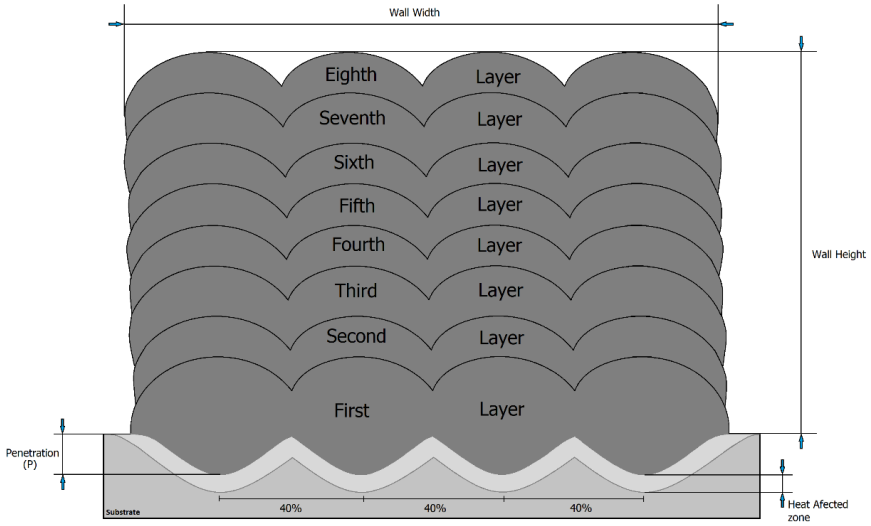

Figure 4.4 – Deposition 3.0 to 3.3 scheme

The programming of the 3.0 deposition wall was to do the four cords side by side, using a bi-directional and continuous deposition, where the robot only stopped during the transition from one direction to the other. The overlap between cords, for this experiment, was 40% (4.43mm) of the cord chosen on the previous experiment. The length chosen was 150 mm, to allow the process to stabilize between transitions (Figure 4.5A).

In the 3.1 deposition wall the path is the linear one (Figure 4.5B) with the cords being done always in the same direction with 150 mm of length and with an overlap of 40% between the cords. After the fourth cord of each layer is done, the robot returns to the starting point of the first cord. This process was repeated for eight layers.

For the 3.2 deposition wall (Figure 4.5C) it was tried the deposition of four cords side by side as in the 3.1 wall, but this time with the overlap of 50% between them. The aim of this deposition wall was also to achieve the eight layers' height.

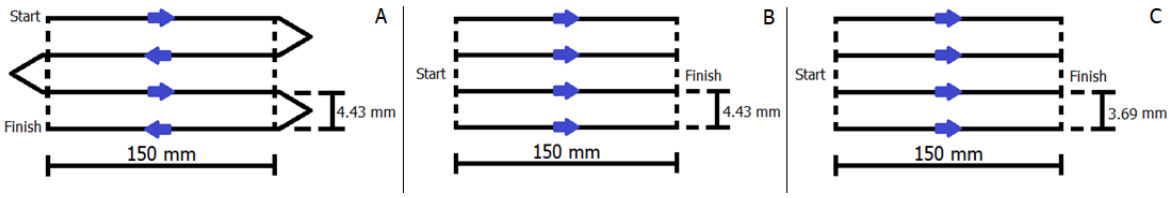

Figure 4.5 – Depositions wall trajectory: A-3.0; B-3.1; C-3.2

In the 3.3 deposition wall, the overlap used was 40% (4.43mm of the chosen cord) and the strategy adopted (Figure 4.6) was the same as in the 3.0 deposition wall, but this time with

the aim of testing different orientation (transversal instead of longitudinal). This deposition was divided in two different sub-depositions, the 3.3A where it was tested the same parameters used before, but with a different strategy; and in the 3.3B it was tested a formula developed in Addimadour that has the objective of giving back an increased robot speed as a compensation for the slower movements that the robot does due to winding paths. The robot speed developed by the formula, with the compensation factor, was 2.4 m/min.

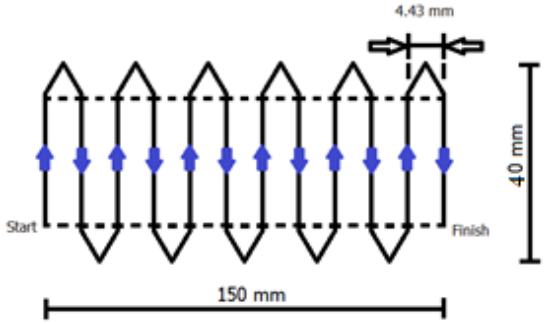

Figure 4.6 – 3.3 deposition wall trajectory

After all the deposition walls done, a final wall with larger dimensions, was made using the parameters and strategy that presented the best results. From this final wall, some samples were taken to do some laboratorial tests.

4.3.Defined tests

During the experiments, microhardness tests are performed in all cords, with a charge of 500gf, to understand how the values are influenced by the parameters tested. This is one way to understand how the material behaves itself accordingly to the changes made.

The Microhardness test was performed by the Vickers Microtech MX7 that allows to do the indentation in every part of the cord. For a standardization and a better comprehension of the results, indentations were done, always at the minimum distance between them, as recommended by the manufacturer and according to the ISO 6507-1:2018. Measurements were taken in vertical line crossing, in all the extension of the cords and walls (Figure 4.7) until it reaches the deep substrate. This procedure had the aim to reach a vertical range pattern of values, the influence of the cooling rate on the top of the cords and walls, and the differences between the substrate affected thermally and the penetration.

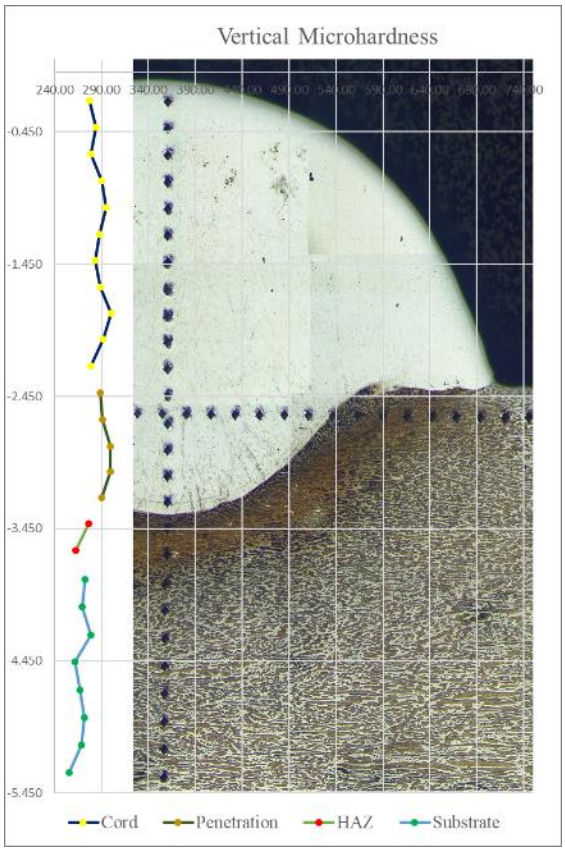

Figure 4.7 – Vertical microhardness reference image

The other type of approach, to measure the microhardness, was the horizontal at a constant distance of the surface of the material (Figure 4.8). The aim of this measurement was to start in the substrate non affected thermally and cross all the material that could be affected thermally, cross the transition between heat affected and penetration zone in a horizontal line to understand if the material properties across the cord are the same in the various points of the penetration. Finally, this line of indentations crossed again the transition zone between the penetration and the heat affected zone as the area under the cord until it reaches again the substrate, virtually non-affected. The comparisons of all this data provided a good hardness pattern existing in the cords.

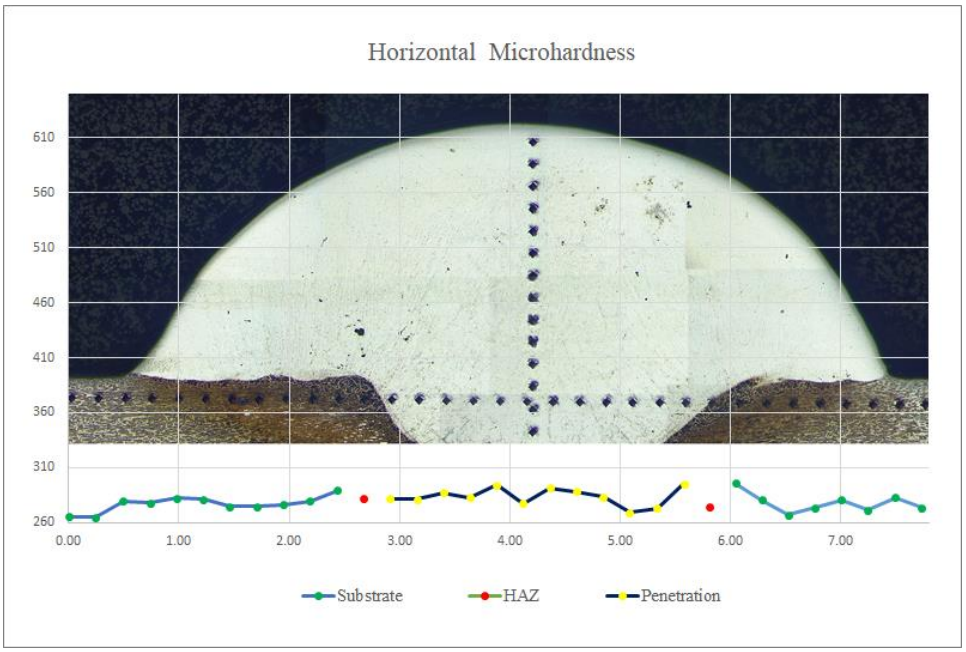

Figure 4.8 – Horizontal microhardness reference image

On the Roell Zwick Z100, three-point flexural tests, with a distance of 50 mm (Figure 4.9A), between two support points were performed to determine the Young Flexural Module value for this type of process production of stainless-steel cords, the limits of elasticity, maximum strength and fracture strength. This tests also provided the graphic with the distribution force vs. displacement.

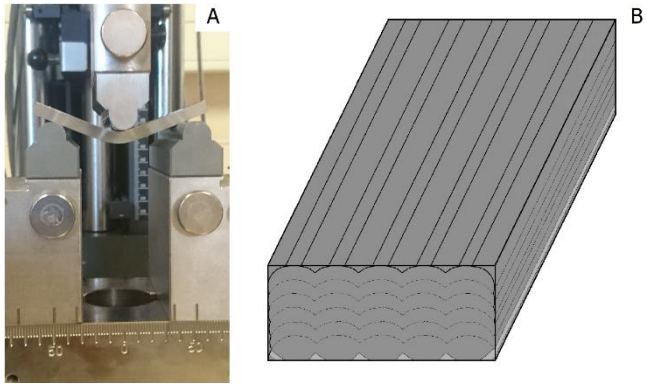

Figure 4.9 – A-Three-point flexural test example; B-Cords orientation in the sample

The Figure 4.9B is a schematic representation of the cords disposition in the sample for the three-point flexural test. The samples were withdrawn from the bottom of the walls, without reaching the first layer.

4.4.Marks and cuts

There was the need to make some cuts in the depositions, in order to analyse the cords. A total of three transversal cuts were marked as exemplified in the Figure 4.10A, and some additional cuts as seen in Figure 4.10B to allow to make samples to analyse, separately, the beginning, middle and end of each deposition.

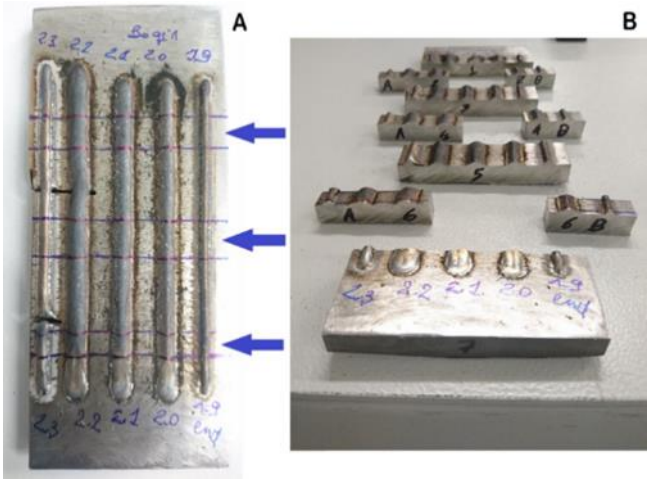

Figure 4.10 – A-marks and B-cuts, made, reference image

The cuts were made with Struers Labotom-5 using a proper disc for this material. According to Carou, Rubio and Benedicto (2017) the use of the Presi cutting fluid (in this case with Labotom) provides increase tool life, requires lower cutting forces and power, higher cutting speeds and feed rates, and allows a better workpiece quality.

4.5.Microstructure samples preparation

In order to construct the samples properly and following the same procedure for all of them, a protocol for the construction of the samples has been drawn up and will be presented below.

4.5.1. Microstructure samples Protocol preparation

1. Put the cut parts of the cords inside the moulds (Figure 4.11);
2. Take photos of the parts catalogued inside the mould;
3. Put the moulds with the metal parts inside the chamber to collect the chemical vapours;
4. In one paper cup, join 2 spoons of Peroxide de Dibenzoyl powder and one spoon of Flacon liquid catalysator (Acrylic catalyst) (Figure 4.12A). Other resins may be

used, in which case the preparation instructions suggested by the manufacturer shall be followed;

5. Mix everything very well with a stick until there is no powder (Figure 4.12B);
6. Dump all the liquid (while it is still enough liquid) in the moulds around the metal parts;
7. Wait between 1 to 2 hours for it to solidify, inside the chamber;
8. Remove the samples from the mould, usually produced manually (Figure 4.13B and C);
9. According to the photos mentioned in the point 2 of the protocol, catalogue the samples.

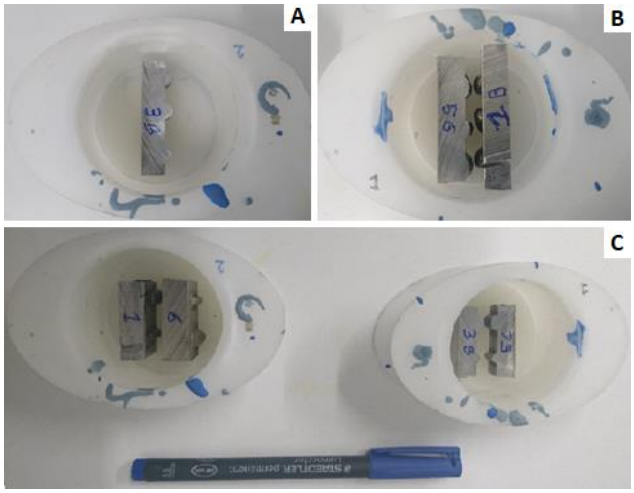

Figure 4.11 – Displacement of the cut cord parts in the mould shaper

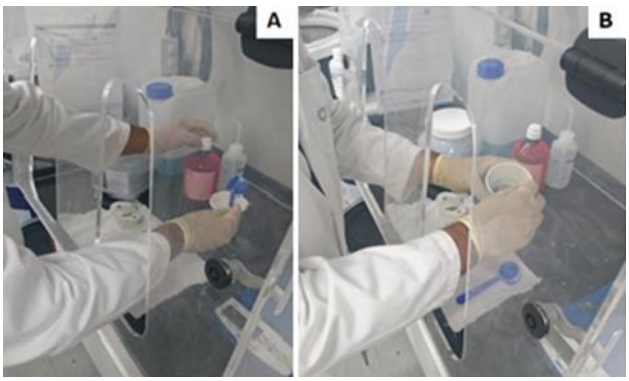

Figure 4.12 – A-One spoon of the liquid catalyst; B-Mixing both reagents

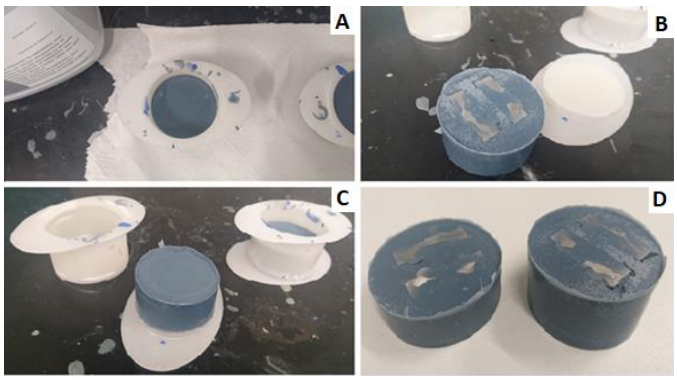

Figure 4.13 – A-Sample after liquid placement; B and C-View from the top of the sample; D-Both samples for analysis

4.5.2. Polishing microstructure samples

After the cuts were made it was time to do the polishing. It was used the Struers Labo Force 100 (Figure 4.14) which already has a protocol to polish this type of samples. The protocol referred to, is set out below.

4.5.3. Polishing Protocol

Pre-Polishing:

1. Using a polishing disc Md Piano 80, with water as lubricant, at the speed of 300 rpm and 25N of pressing force. This pre-defined programme lasts 10 minutes;
2. Using the polishing disc Md Piano 220 (granulometry of 68 µm), with water as lubricant, at the speed of 300 rpm and 25N of pressing force. This pre-defined programme lasts 10 minutes;
3. Using the polishing disc MD Largo (granulometry of 9 µm), with DiaPro Largo as lubricant, at the speed of 150 rpm and 40N of pressing force. This programme lasts 4 minutes.

Polishing:

1. With the polishing disc MD-Mol (granulometry of 3 µm), with DiaProMol as lubricant, at the speed of 150 rpm and 20N of pressing force. This programme lasts 3 minutes;
2. With the polishing disc MD-Chem (granulometry of 1 µm), with OP-S as a lubricant, at the speed of 150 rpm and 15N of pressing force. This programme lasts 1 minute.

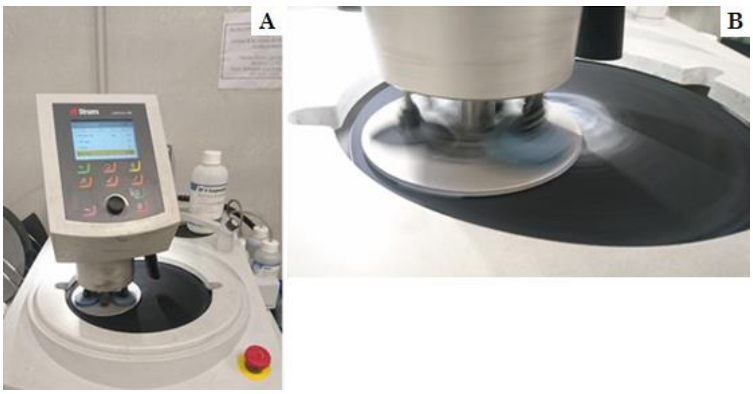

Figure 4.14 – A-Pre-polishing; B-Polishing the samples

Due to the excess of material in the bottom of the samples (Figure 4.13, B and D), the first step of the pre-polishing had to be repeated for 3 times.

The second was repeated twice due to the deep scratches made in the first step.
The third step was repeated twice to provide a better finished surface for the polishing.
The polishing first step was repeated twice because of the deterioration of the disc.
In order to get a perfect finished surface (Figure 4.15) the last step was repeated twice.

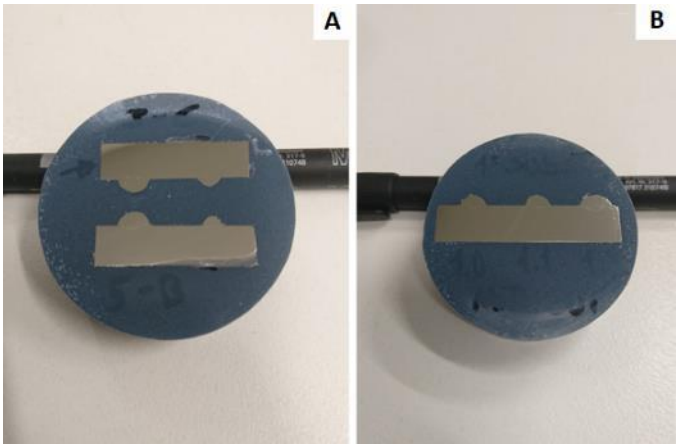

Figure 4.15 – Samples after all the polishing procedure

4.5.4. Chemical Attack

After the samples were polished, as it is shown in Figure 4.15, it was made the chemical attack which consisted in exposing the samples to a chemical attack during a specific period of time (Figure 4.16).

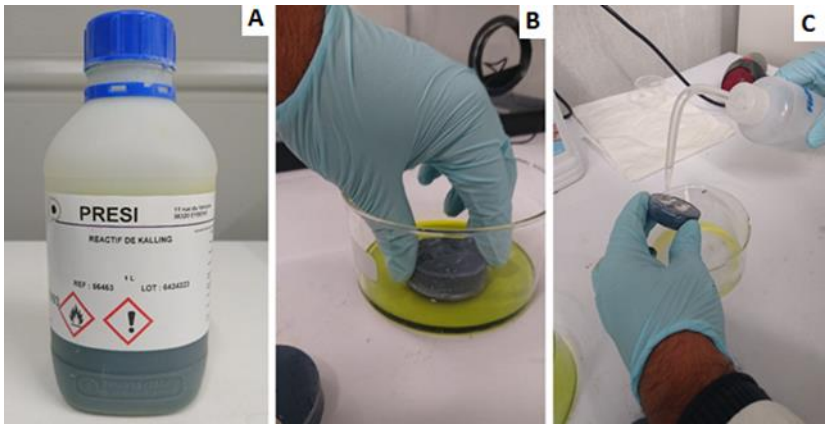

Figure 4.16 – A-Reagent Kalling; B-Procedure of exposure the sample and C-washing it with alcohol

During this procedure the samples were exposed for a period of 5 seconds to Kalling reagent and then washed with alcohol and checked the surface. It was necessary to repeat the exposure for another 5 seconds until the difference between layers were clearly observable.

5. Results and discussion

5.1. Laws Experiment

5.1.1. Cords deposition Macroscopic Analysis

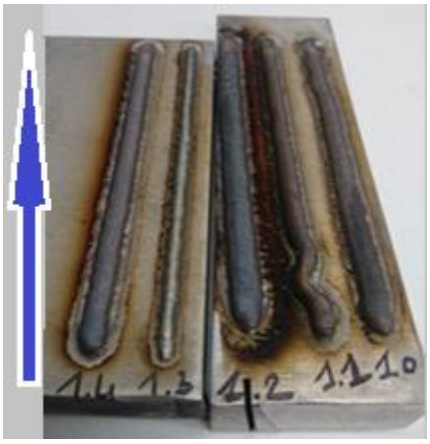

Figure 5.1 – Law Experiments five cords

The cord identified as 1.0 presented a stable start, as shown on the right side of the Figure 5.1. It stays stable until 100 mm and after that, it turns unstable and makes the S curb before stopping. The colour of the cord is homogeneous, despite the burns seen in some places that could mean that the process here was too slow, or unstable, having oscillations in the power provided to the process. The resulted contact angles are reasonable what could mean a good penetration, but on the other way, it can be observed that the side wall is not 100% consistent.

It is also noticeable that it does not show signs of superficial porosity, inclusions or bead humping, which indicates that the robot speed used and the wire feed speed were correctly tuned.

The cord 1.1 presented a very unstable start, as seen by the S curb in the Figure 5.1, on the beginning of the cord, and stabilizes after 15 mm remaining stable until the end. The colour of the cord is too dark and the contact angle it has is consistent, but it can be observed that the cord is not wide enough which could indicate a poor penetration in the substrate.

Before the process stabilizes, aside from not showing signs of superficial porosity or inclusions, it can be observed a fickle melting, which could lead to those defects. It is not identifiable bead humping even in the unstable zone.

The cord 1.2 revealed a very stable process, as seen in the Figure 5.1, from the beginning until the end of the cord. The colour of the cord is not darker and the contact angle is wider which could indicate a bad penetration. A wider cord could also mean that too much energy was used for this speed and that lead to a too wider melt pool and poor superficial quality, with oxides and porosity. Bead humping is not identifiable but it can be seen that this process has a bad surface finishing and a lot of spatter around the cords deposition. It is possible to identify the heat penetration on the side wall of the substrate.

The cord 1.3 resulted from a consistent process but it can't be said if it is stable or not. A small bead humping was identifiable during the process as shown at the Figure 5.1. The colour of the cord is lighter, the best of all the processes, but the contact angle value it has is low. There is a too sharp concavity that could indicate it has a poor penetration in the substrate. It is also noticeable absence of superficial porosity or inclusions during all the process.

The cord 1.4 is the most homogeneous of all the cords done in this first experiment, as shown in the Figure 5.1**Figure 5.1**. The colour of the cord is dark and it can be seen the burns all around the cord. The contact angle is the best of all the deposited cords, which could indicate a good penetration. As observed in the side wall, it is the most consistent of all depositions. It is also noticeable that it does not show signs of superficial porosity, inclusions or bead humping which indicates that the robot speed used and the wire feed speed were the corrected ones.

5.1.2. Process temperatures

The Table 5.1 describes all the temperatures measured in these experiments.

Table 5.1 – Laws Experimental process temperatures

	Cord	Medium Humidity (%)	Medium room Temperature (ºC)	Initial substrate Temperature (ºC)	Final substrate Temperature (ºC)
1st substrate	1.0	58.5	27.0	25.0	61.0
	1.1	59.0	27.6	28.6	64.0
	1.2	58.0	27.9	27.6	54.0
2nd Substrate	1.3	57.3	28.0	28.2	41.5
	1.4	58.3	28.1	28.5	46.2

The humidity and the room temperature, for all the experiments, were measured by a static equipment in the room wall, and all the substrates measurements were done in the same place, before and immediately after the deposition, with a portable equipment.

5.1.3. Comparison between all cords

The Table 5.2 presents the interaction between amperage and voltage used in each deposition and the samples values measured regarding the height and the width of the cords.

Table 5.2 – Laws Experimental macroscopic measurements

Sample	Amperage (A)	Voltage (V)	Width min (mm)	Width max (mm)	Height min (mm)	Height max (mm)
1.0	136	13.7	5.8	6.2	2.6	2.9
1.1	140	13.4	5.6	5.9	2.7	2.95
1.2	151	13.1	7.5	7.8	2.7	2.9
1.3	66	12.5	3.4	3.8	1.8	2
1.4	150	16.1	5.8	6.1	2.85	3.1

According to Table 5.2, the amperage has a big influence in the cord width. Has it can be seen, the 1.3 cord, produced with an amperage of 66 A, corresponds to the smallest value of width (between 3.4 and 3.8 mm) but, on the contrary, the cord 1.2 that is the one with the highest value of Amperage (151 A), corresponds to the biggest value of width (between 7.5 and 7.8 mm). This means that, for the same parameters, the use of higher amperages leads to higher values of width.

When comparing the cords 1.2 and 1.4 (both have the highest values of amperage) it is noticeable that there are other different parameters that influence the final result. The voltage could also influence the cord but, to be sure of, it is necessary to confirm if all the other parameters are the same, or if there are other changes inside the law that could justify these differences.

5.1.4. Cords Deposition Microscopic Analysis

The Figure 5.2 represents all the Laws Experiments cords deposition. This set can give a better idea of the shapes by comparing each other. As it can be seen in the figure, the cords 1.0, 1.1 and 1.4 have the penetration a little dislocated to the right side. It is also clear that the cord 1.3 has the smallest dimension cord of all in terms of penetration and width. All the cords 1.0, 1.1 and 1.4 present a non-homogeneous geometry of the cord.

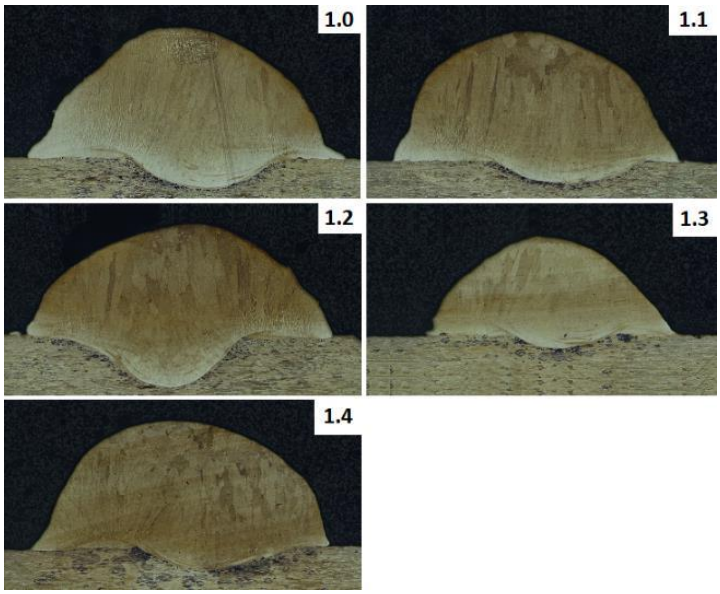

Figure 5.2 – Image of all the Laws Experiment cords' deposition

It can be concluded that the cord 1.2 revealed the best geometry and the best penetration on the substrate (Table 5.3) and is also the more centred. This cord, despite the small external irregularities in the shape on the right side, is also the most homogeneous.

Table 5.3 – Laws Experiment microscopic measurements

Sample	Amperage (A)	Voltage (V)	Cords Height (µm)	Penetration (µm)	Left Contact Angle (º)	Right Contact Angle (º)
1.0	136	13,7	2746	632	137	149
1.1	140	13.4	2800	453	118	123
1.2	151	13.1	2772	1273	119	114
1.3	66	12.5	1801	216	114	129
1.4	150	16.1	2767	465	130	105

5.1.5. Detailed analysis of cord 1.2

The cord deposition that revealed the best quality was the 1.2, made by using the CMT Law 1093. That is the reason why it was used for the following experiments, despite of the presence of spatter and the appearance of burn on the top of the cord (Figure 5.3). However, these defects are manageable.

Figure 5.3 – Overview of the cord 1.2

The side contact angles have some defects as can be observed in Figure 5.4 , originated due to a large amount of heat input that is mainly centred on the middle of the cord, leaving on the sides a big difference between temperatures of the substrate and the melted material that lead to this sharp contact angles. These defects are manageable by adapting parameters like robot and wire speeds.

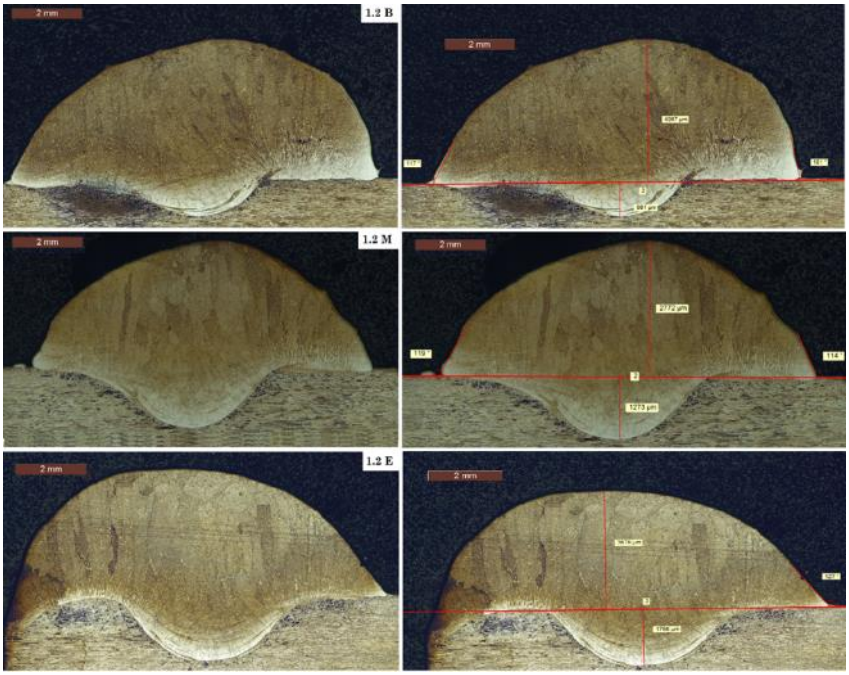

Figure 5.4 – Complete analysis of the cord 1.2 and its measurements

In this comparison it is possible to see that the size of the penetration, from the beginning (1.2B), through (the 1.2M) to the end (1.2E) is always growing. The measurements seen in the Figure 5.4 are represented on the Table 5.4 for a better comparison:

Table 5.4 –Microscopic measurements of the cord 1.2

Placement	Height (µm)	Depth (µm)	Left Contact Angle (º)	Right Contact Angle (º)
Beginning	4067	981	117	101
Middle	2772	1273	119	114
End	3679	1756	--	127

It is clear that the deposition starts with a low depth (even if it is a good value for depth), and improves with the elapse of the process. The beginning and the middle of the cord present height discrepancies between them which reveals that the process was not completely stable. As the initial height value measured might induce to an error, the evaluation should be done after the process and the cords height are more stable, as it can be achieved at the middle of the cord and at the end. The end height value of the cord is also

bigger than the middle cord's value due to the slowdown of the robot speed, as the wire feed speed was the same. Observing the result contact angles, it is possible to realize that the shape of the cord is getting wider along the process, improving the contact angles.

A closer look to the middle cut from the cord 1.2 (Figure 5.5) is necessary to obtain a more adequate understanding of the process.

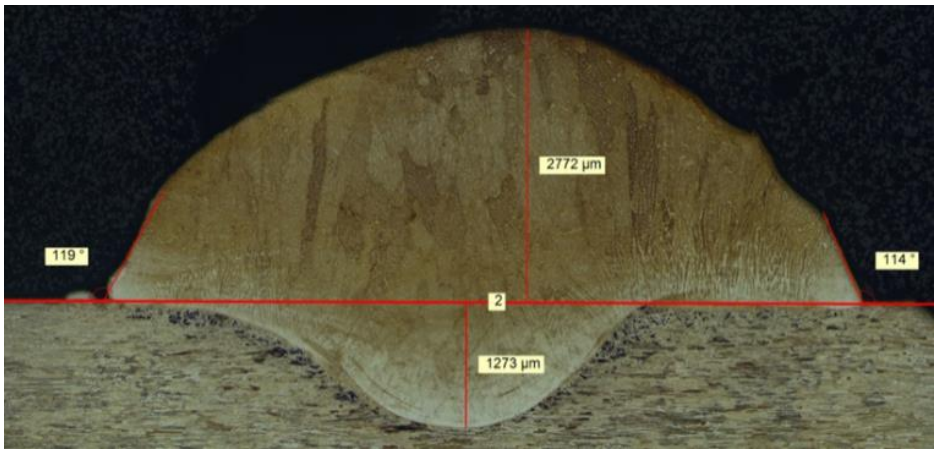

Figure 5.5 – Measurements of the cord 1.2 (middle cut)

This cord is the second higher of all and the one with deeper penetration. It is noticeable that there is a difference of more than half of the magnitude between the value of this penetration and those of all the other cords. The contact angle on the right side is too sharp and could indicate some porosity between the melted material and the substrate due to a fast cooldown of the material in this side of the cord. As it can be seen, there are no porosity and the layer is not glued, but fused. The contact angle on the left side is good and the cord on this side presents a good shape. Also, on the left side there is a drop of melted material that might have been projected due to a high input of energy.

It is noticeable that this cord resulted in a better fusion of the substrate on the left side than on the right side, where it can be seen a shaper curb between the penetration of the addition material and the substrate. This cord apparently has no porosity and is a good candidate for the following experiment.

Flaws on 1.2 cord

In the Figure 5.6 it can be seen all the flaws in this cord. The red circle shows the melted material deposited on the side of the cord (maybe a projection) and it can be seen on the extremity of the cord that it shows a beginning of dripping.

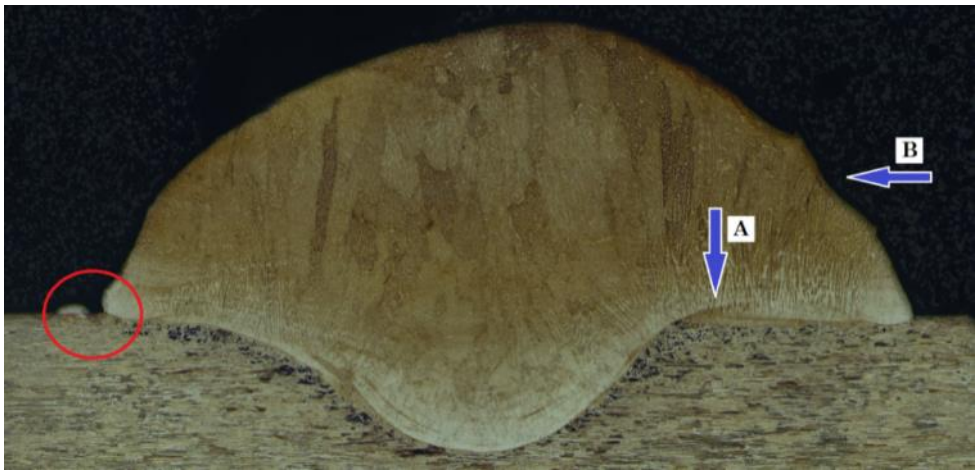

Figure 5.6 – Flaws of the 1.2 cord

The A arrow shows the flux of melted material comping from the centre of the penetration zone due to the flux currents. The B arrow shows an irregularity on shape on the side of the wall maybe due to a different cooling rate between layers. This is the cord with less defects of all and with a good external despite the small defect above mentioned.

Microstructures of 1.2 cord

The Figure 5.7 represents the microstructure images associated to the place where they were obtained. It is possible to understand that the microstructure is different according to the place on the deposition.

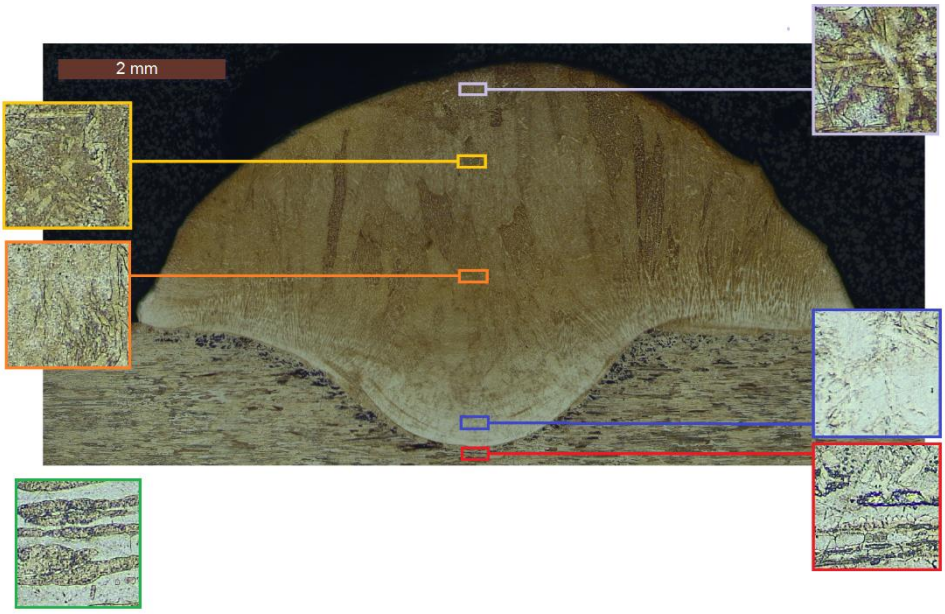

Figure 5.7 – Cut of the chosen cord 1.2 with microstructures and their localization

In the green square, it is possible to see the substrate microstructure and it is clear the rolling process production of the stainless-steel effect. The white zones correspond to the ferrite and the darker zones are the austenite.

In the red square it is shown the heat affected zone where the substrate structure is clearly affected by the heat of the material deposition. It is not clearly identifiable in this figure but the austenitic microstructure is combined with some parts of the substrate microstructure, indicating a good fusion between them. This is also the start of the austenite presence in a small percentage.

In the blue square it is possible to identify a very small percentage of tenuous austenite (light colour) which can be due to the lack of effect of the chemical attack on this part of the structure.

The austenite grain structure, seen in the orange square, has considerably bigger length and width to the one seen in the blue square. The grain shown seems to be increasing size from the bottom of the penetration into this point.

In the yellow square it is possible to see that the bigger and thicker grains saw in the orange square are getting smaller but in larger percentage. The length is shorter but the width is the same and more spread.

The purple square shows the biggest percentage of austenitic grain structures with medium size comparing to the rest of the cord. The largest percentage is reached in this area possibly due to the slow cooling.

5.2.Robot Speed Experiments

5.2.1. Cords Deposition Macroscopic Analysis

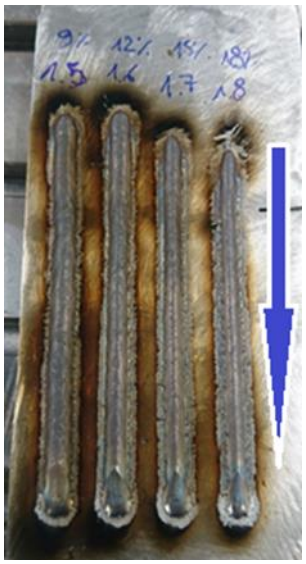

Figure 5.8 – Robot Speed Experiment's four cords

According to the Figure 5.8, the cord 1.5 presents a good shape and, comparing to the one that was done previously with the same law in the first experiment, it has a lighter colour, and does not show signs of burnt layer on the top of the cord. The colour on the surrounding of the cord is still a "burn colour" due to the heat input and some small spatter. In the beginning of the cord it can be seen that there are some instability and the volume of materials deposited is larger due to the increase of the robot speed, starting from 0 to 0.54 m/min, although the wire feed speed was still the same.

The cord 1.6 presented the best shape of all depositions that were done (Figure 5.8). It has a light colour and does not show signs of burnt layer on the top of the cord, signs of porosity or of inclusions. The colour of the surrounding of the cord is still a "burn colour", especially at the beginning and at the end of the cord. With the speed increasing, the induced heat at the middle cord is lower so the cord does not have the burn marks. Besides, it can't be seen spatter but, during the process, it was visible. With respect to the end position, this cord revealed to be the most stable process of all cords, from the beginning to the end. The material volume deposited is also larger in the beginning due to the same reasons mentioned for the cord 1.5.

The cord 1.7 has a good shape and lighter colour, not showing signs of porosity or inclusions. The colour of the surrounding of the cord is still just a little “burn colour” but only in the beginning and in the end of the cord (Figure 5.8). With the speed increasing, the induced heat at the middle cord is lower due to the lower volume of material. There are no signs of spatter in the substrate but during the process it was visible. The material’s volume is also smaller in the beginning in comparison with the previous cords, so this appears to be a more homogeneous cord.

The cord 1.8 has the smallest width of all and it also has the lightest colour. There are no signs of porosity or inclusions. The colour of the cord is a “burn colour” only at the beginning. It is possible to see (Figure 5.8) that the process started unstable, doing just a small cord and a spatter, as shown on the right side of the cord. During this deposition it was possible to see less amount of spatter, although bigger than all the other depositions. The material volume deposition during all the cord appears to be the most homogeneous of all.

5.2.2. Process Temperatures

The Table 5.5 describes all the temperatures registered in this experiment.

Table 5.5 – Robot Speed Experimental process temperatures

	Cord	Medium Humidity (%)	Medium room's Temperature (ºC)	Initial substrate Temperature (ºC)	Final substrate Temperature (Cº)
3th substrate	1.5	60.9	26.3	26.9	29.7
	1.6	61.0	26.3	30.2	31.8
	1.7	61.1	26.3	32.3	32.9
	1.8	61.2	26.3	33.2	33.9

5.2.3. Comparison between all cords

The Table 5.6 shows the correlation between the robot speed used in each deposition and the values measured at the samples regarding the height and the width of the cords.

Table 5.6 – Robot speed experiment macroscopic measurements

Sample	Robot Speed (m/min)	Length (mm)	Height min (mm)	Height max (mm)	Width min (mm)	Width max (mm)
1.2	**0.36**	**110**	**2.7**	**2.9**	**7.5**	**7.8**
1.5	0.54	105.6	2.15	2.7	6.9	7.6
1.6	0.72	107.6	1.9	2.45	6.0	7.25
1.7	0.90	100.15	1.5	2.3	5.3	6.5
1.8	1.08	94.1	1.6	2.1	4.8	6.0

According to the Table 5.6 it is possible to observe that, besides the pre-defined length was 110 mm, none of the cords reached this value, being the best cords the 1.5 and 1.6. Those cords also revealed a more stable process which means that, for the wire feed speed in this law, the values of the robot speed should be around 0.54 m/min and 0.72 m/min. Those two cords also shown the higher values in terms of height and width, which indicates a well-compensated cord deposition process.

The cords 1.7 and 1.8 (with faster robot speed) shown lower values when comparing height and width, which could mean that this robot speed is too fast for the wire feed speed that were used.

5.2.4. Cords Deposition Microscopic Analysis

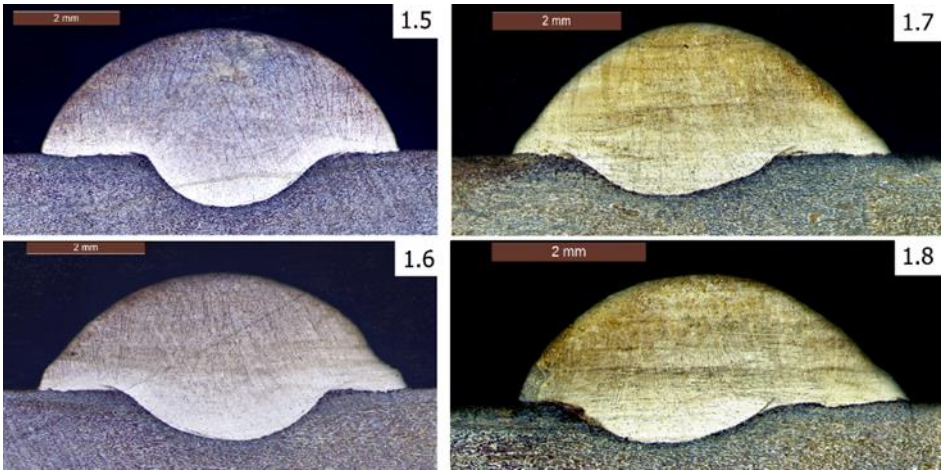

Figure 5.9 – Image of all the Robot Speed Experiment cords deposition

The Figure 5.9 illustrates all the robot speed experiment cords deposition. Through this figure it is possible to understand that the shape of these cords is very close to each other in terms of general dimensions and contact angles.
The cord 1.5 has the best external shape, highly homogeneous and a good penetration value, although is not symmetric. This penetration is considered too concentrated.

The cord 1.6 has also a very good external shape and has an improvement on the penetration, being wider and with a good penetration height.

The cord 1.7 revealed a low value of penetration and is dislocated to the left side. The external shape of this cord is not as symmetric as the ones presented before and it is also significantly lower.

The cord 1.8 resulted in the most non-uniform shape of this experiment. It is clear that the increment of the robot speed reduced largely the penetration depth. It also has the penetration dislocated to the left side, even more than the observed in the cord 1.7. It is possible to identify a pattern shown in the Figure 5.9 and with the help of the Table 5.7. It is clear that the best shapes of the cord were reached for values around 0.54 m/min e 0.72 m/min of robot speed. From values of 0.90 m/min and 1.08 m/min (cord 1.7 and 1.8, respectively) the performed measurements presented lower values and the shape is more irregular which could mean that for these robot speeds the wire feed speed should have a higher value.

Table 5.7 – Robot Speed microscopic measurements

Sample	Robot Speed (m/min)	Cords' Height (µm)	Penetration (µm)	Left Contact Angle (º)	Right Contact Angle (º)
1.2	**0.36**	**2772**	**1273**	**119**	**114**
1.5	0.54	2349	1016	112	114
1.6	0.72	2002	871	121	134
1.7	0.90	1829	507	131	134
1.8	1.08	1669	541	116	134

5.2.5. Detailed analysis of cord 1.6

The chosen cord from this experiment that shows the best shape's qualities is the cord 1.6. The value of 0.72 m/min is the robot speed that demonstrates the best results and is going to be used in the following experiment.

Figure 5.10 – Overview of the cord 1.6

This cord presents a good colour despite the burning all around it. It also seems consistent in most part of it and it resulted from a very stable process. The defects shown in the Figure 5.10 is an accumulation of deposited material on the beginning of this cord, which stabilizes after approximately 10mm, and it has a more uniform height on all the cord.

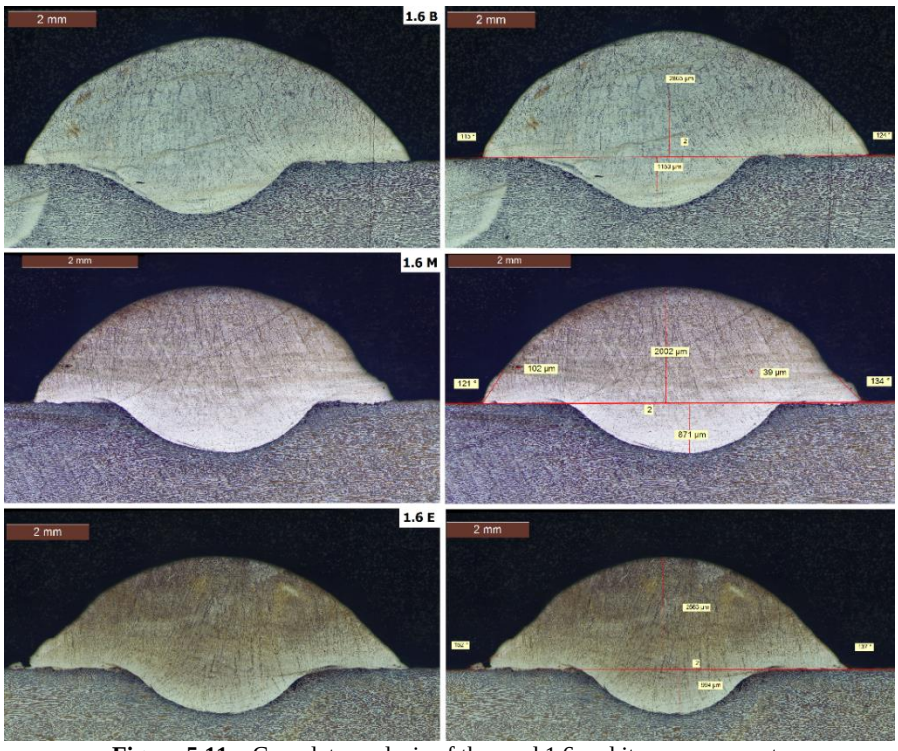

Figure 5.11 – Complete analysis of the cord 1.6 and its measurements

In this comparison of the beginning, middle and end of the cord 1.6 (Figure 5.11) it is possible to see that this cord does not have the best start, although it has a very good penetration value, but not centred, as it can be seen in 1.6B. It can also be seen that the contact angles, on the right and left side of the penetration, are quite different. This means that, at the distance that the first cut (1.6B) of this analysis was made, the process wasn't still very stable.

In the middle (1.6M) and in the end (1.6E) cuts, it is possible to see that the penetration is a more centred with the contact angles more homogeneous between each other. It is also visible that the external shape of the cord is more homogeneous which ends up being one of

the best shape cords that was achieved. According to these results it can be stated that the parameters used could provide a good candidate cord to build the wall.

The measurements presented in the Figure 5.11 are represented on the Table 5.8 for a better comparison:

Table 5.8 –Microscopic measurements of the cord 1.6

Placement	Height (µm)	Depth (µm)	Left Contact Angle (º)	Right Contact Angle (º)
Beginning	2865	1153	115	124
Middle	2002	871	121	134
End	2563	994	152	137

The measures of height and depth (Table 5.8) show an evolution from the beginning to the end of the cord that could evidence that the middle values resulted, actually, from the process still in stabilization. The final values demonstrate the potential of this parameters once they are the best values leading the best shape cord.

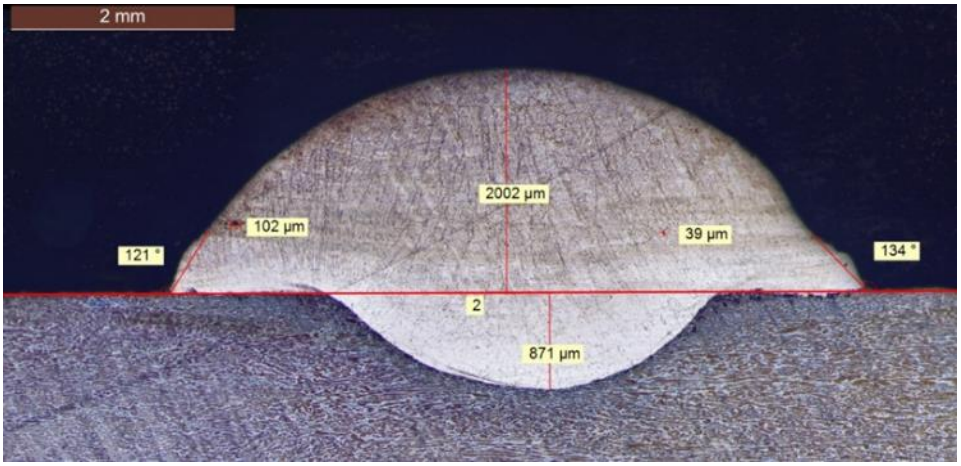

Figure 5.12 – Measurements of the 1.6 cord (middle cut)

This cord has the second highest value of cord height (2002µm) and also the second-best value for the penetration (871µm) (Figure 5.12). Besides the referred values, the shape of the cord is good and just have a small anomaly on the right side. The strongest points of this cord are the cord external shape despite the small anomaly and the shape of the penetration in the substrate. On both sides of the cord it is possible to see that the melted material is correctly welded to the substrate. Despite not being so homogeneous on the external shape this has better side contact angles and the shape of the penetration is much better than the one in the cord 1.5 and it also presents a dilution value slightly better.

The two points measured in the Figure 5.12, with 102 μm and 39 μm, could be porosity or it could be due to the chemical attack. It turned out to be (after another polishing and chemical attack) black spots resulting from the chemical reagent Kalling.

Flaws on 1.6 cord

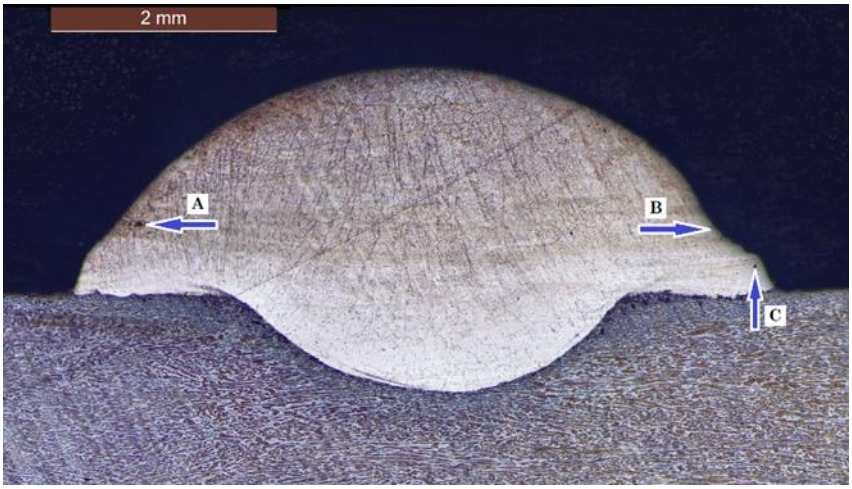

Figure 5.13 – Flaws of the cord 1.6

The flaws pointed out, in the Figure 5.13 with the A arrow is a porosity in the cord. The B arrow indicates shape flaws that might had occurred due to a difference on the cooling rate, that lead to a wider layer in the base of the cord and an inverted parable on top of it. Although these cords have a good shape, the C arrow indicates a small porosity on the side of the cord (the part that usually is milled).

Microstructures of 1.6 cord

In the Figure 5.14 it can be seen the microscopic images of microstructures associated to the place where they were taken. It is possible to understand that the microstructure is different according to its place on the deposition.

Due problems during chemical attack the result was different from that was expected. All microstructures images are almost white, grey and darker grey.

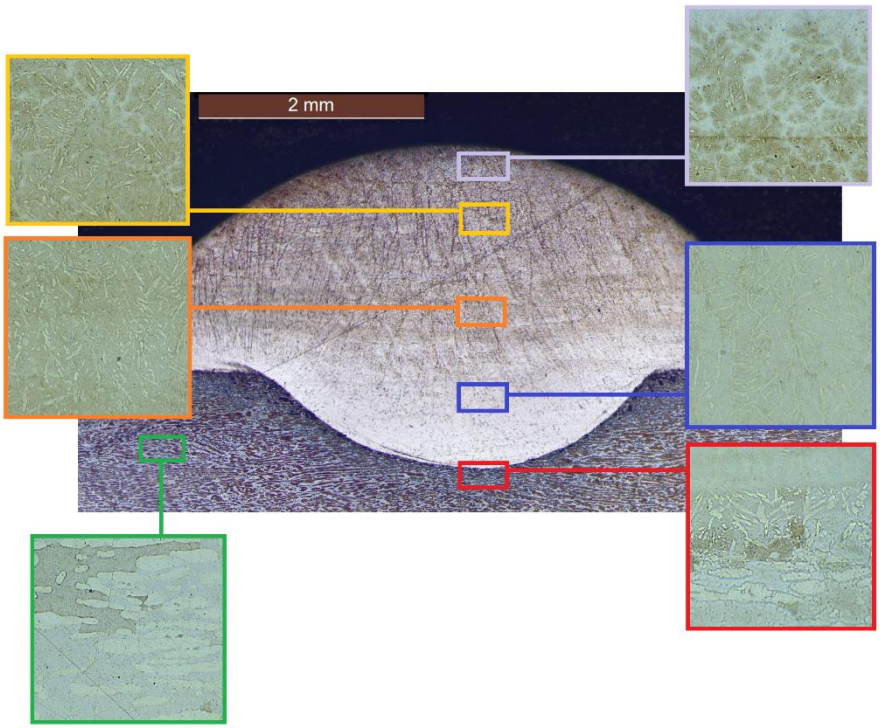

Figure 5.14 – Cut of the chosen cord 1.6 with microstructures and their localization

In the green square is shown the microstructures of the substrate used for this experiment. This is a two-phase microstructure (as the two previous substrates) where is possible to visualize, in the grey and darker grey zones, the austenite and in the white zones, the ferrite, with an orientation coherent to the rolling process production.

The red square shows the junction between the substrate and the penetration. This area designated by heat affected zone, has both (substrate and penetration) microstructures and it is also possible to see the microstructures of substrate affected thermally due to the deposition.

In the blue square it can be seen ferrite and the first appearance of austenite in very small quantities coming from the bottom of the penetration. This grain is still small and in a low percentage.

The orange square shows a higher percentage of ferrite phase but is also noticeable that the austenite grains that appeared in the red square, are increasing size and the percentage is slightly bigger.

The yellow square shows ferrite and austenite, this last in a higher percentage when comparing with the orange square. Although the higher percentage, the grain is different, getting smaller but a lot spreader in this area of the cord.

In the purple square, despite the action of the chemical attack it is clear the austenitic structure in the ferrite, as this grain has a considerable size and percentage, leaving the perception that the austenite percentage is bigger than ferrite, maybe due to the slower cooling rate.

5.3. Wire Feed Speed Experiment

5.3.1. Cords Deposition Macroscopic Analysis

Figure 5.15 – Wire Feed Speed Experiment five cords

The cord 1.9 made in this experiment resulted in the smallest and the thinnest of all. During this first deposition it was possible to see that the process did not have spatter. The shape does not seem to be good because the side contact angles are too sharp. That might indicate a weak penetration. This cord was stable during the process but as it can be seen in Figure 5.15, it has some bead humping at the beginning and at the end (maybe due to the acceleration and the de-acceleration of the robot).

The cord 2.0 presented a better shape than the 1.9 cord (the difference in wire feed speed is from 3.2 m/min to 5.2 m/min). It is wider and the deposition is more stable, as it can be seen in the Figure 5.15. This deposition had a lot of spatter during the process, which might result from the increase values of amperage to 167A and voltage to 16.3V. The increment of the amperage and voltage values are related to the CMT machine (Fronius) in a way that, when

the wire feed speed is increased it also increases the values of the amperage and voltage for values defined by each law. This deposition appears to have a good penetration and no bead humping, and it can also be seen that, at the beginning of the cord it is higher, but after the process stabilizes it is more homogeneous, and it has a higher heat input as there is burn marks all around it.

From the point of view of the process parameters, the cord 2.1 was stable. It had even more heat input than the 2.0, as it can be seen by the burn marks all around the cord (Figure 5.15). This cord seems less high and wider, which might indicate a better penetration. The process was full of thick spatter and in high percentage. This might also be related to the increased values of the amperage and voltage. It also seems to have a very wider contact angle with the substrate. However, on the profile of the cord it is possible to see the welded layer with no glued zones varying with welded ones.

The cord 2.2 (Figure 5.15) presented a burn colour on the cord and all around it. This process, besides from being stable (the middle curb is due to the cut in the substrate), had a major percentage of spatter, that deposited itself on every metal around the cord, gluing themselves to the place where they fall. The contact angle with the substrate is too wide open on both sides, giving the cord a poor shape, but apparently with a good penetration.

The cord 2.3 wasn’t originally planned but it was made by taking the advantage of the free space in the substrate (Figure 5.15). The choice to make this last cord had, as a criteria, the understanding of the behaviour during the process (if it had spatter or not) so as the understanding of the shape achieved with the values of wire feed speed, amperage and voltage between the ones associated with the deposition of the cord 1.2 and the cord 1.9. The cord 1.2 was made with the values of 4.2 m/min, 151A and 13.1V and the cord 1.9 had a wire feed speed of 3.2 m/min, 118A and 11.8V. This new deposition was made with a value of 3.7 m/min for the wire feed speed, 136A for the amperage and 12.2V for the voltage. As it is possible to see in Figure 5.15, the contact angle between the cord and the substrate is better than the one in the 1.9 cord, the colour of the cord is good and apparently has a good penetration. The height value of the cord locates between the cords 1.2 and 1.9. During the process there wasn´t spatter at all and the process was very stable. It also does not show burn marks (the defects it has were induced by the cuts that the substrate had).

5.3.2. Process temperatures

The Table 5.9 describes all the temperatures measured in this experiment.

Table 5.9 – Wire speed experimental process temperatures

	Cord	Medium Humidity (%)	Medium room's Temperature (ºC)	Initial substrate Temperature (ºC)	Final substrate Temperature (ºC)
4th substrate	1.9	58.3	25.0	24.4	28.0
	2.0	59.2	25.0	27.5	37.2
	2.1	59.6	25.0	34.0	49.0
	2.2	60.5	25.1	39.0	59.0
	2.3	61.0	25.1	38.0	45.6

5.3.3. Comparison between all cords

The Table 5.10 shows the correlation between the wire feed speed, amperage and voltage (automatically defined by CMT, according to the Wire Feed Speed) and the values measured at the samples, regarding the length, height and width.

Table 5.10 – Wire's Speed Experiment macroscopic measurements

Sample	Wire Feed Speed (m/min)	Amperage (A)	Voltage (V)	Length (mm)	Height min (mm)	Height max (mm)	Width min (mm)	Width max (mm)
1.2	**4.2**	**151**	**13.1**	**110**	**2.7**	**2.9**	**7.5**	**7.8**
1.9	3.2	118	11.8	103.25	2.05	2.75	2.65	3.85
2.0	5.2	167	16.3	106.45	1.7	2.55	6.5	7.7
2.1	6.2	185	19.1	106.10	1.85	2.85	7.5	8.5
2.2	7.2	210	20.5	110.45	1.7	2.8	7.4	8.4
2.3	3.7	136	12.2	108.07	1.85	2.7	3.6	5.4

The Table 5.10 has highlighted in bold and grey, the values of the cord 1.2, done in the first experiment, comparing with all the other cords measurements from this wire feed speed experiment. As it can be seen, the length only reaches the programmed 110mm in the 2.2 sample, produced with a 7.2 m/min wire speed.

All the other cords are shorter in length than the programmed. The cords 2.0 and 2.1 have a similar length and a very close gap between the minimum and maximum values of height and width. In the height values, the higher comes from the cord 1.2 in the first experiment and, in the present experiment, the higher value was obtained from the cord 1.9 that is also the one with less gap between the maximum and minimum height. All the other cords presented gaps between 0.7 mm and 1.1 mm, which is quite irregular. The cords height could

be influenced for some minimal unevenness during the grinding made on the preparation of the substrate.

The lower variability of width (0.3 mm) was obtained in the cord 1.2. From the cords made in this experiment, the 2.1 and 2.2 reached a maximum width with variability of 1 mm, the major gap between values. This gap could indicate lack of stability in the junction between substrate and deposited material.

5.3.4. Cord Deposition Microscopic Analysis

The cords 1.9 and 2.3 hardly has penetration, as the Figure 5.16 shows. The concavity shown on the external shape, the very sharp contact angles and the almost none penetration, represents that the material could be glued to the surface of the substrate, instead of being welded. This shape could be a result of a lack of input energy during the process.

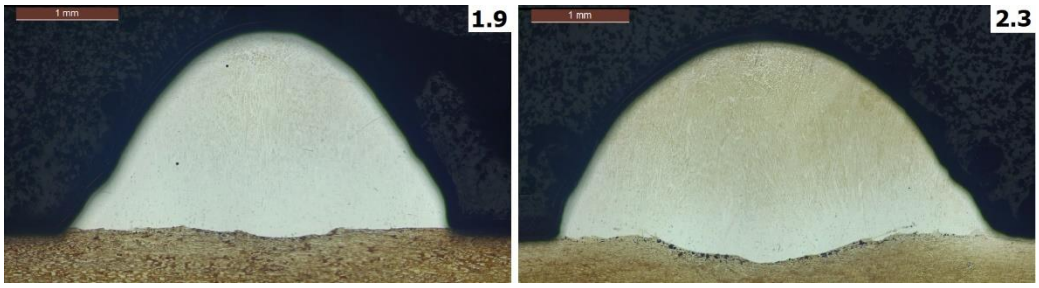

Figure 5.16 – Comparison between cord 1.9 and cord 2.3

From this experiment it is possible to understand that the cord contact angles with the substrate decrease with the increment of the wire feed speed and there is an optimum wire feed speed, for the 0.72 m/min robot speed (and possibly to each robot speed). Although the cord deposition appears to be stable in the 2.0, 2.1 and 2.2, the process is not, which led to a lot of spatter. This spatter could not only lead to a bad superficial aspect, but it could also influence the depositions microstructure if some spatter fall in the path of the deposition. The height of the cords, shown in the Figure 5.17, was supposed to decrease with speed increment (and by consequence the increment of amperage and voltage) but as the **Table 5.11** reveals the theorical pattern is not necessarily true. The start always has a major deposition compared with the rest of the cord, this characteristic has a big influence in a maximum value of the height, once it is always achieved in the beginning, resulting in an extension of the gap between the lower and the higher value of each cord.

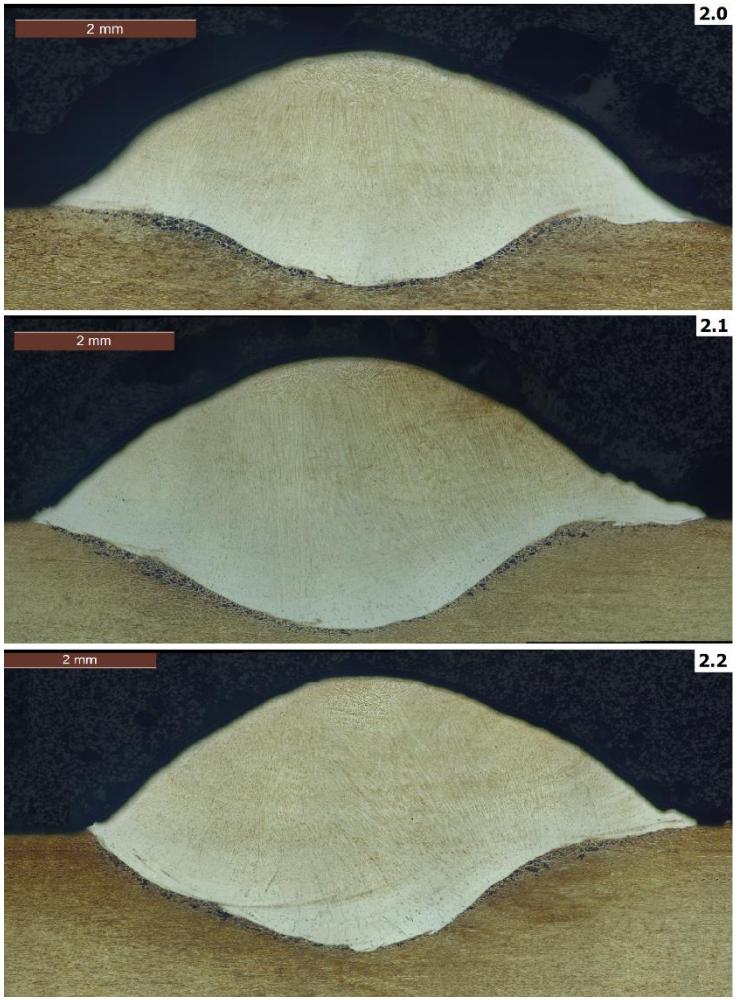

Figure 5.17 – Comparison between cords 2.0, 2.1 and 2.2

The cords 2.0, 2.1 and 2.2 show that with more heat input, the shape of the cord's penetration is going to change reaching more area and melting more substrate's material, which means that they have higher values of dilution. These higher values of dilution don't mean, by themselves, that the cord is better as the shape of the penetration and the external shape of the cord are also very important.

Table 5.11 – Wire speed experiment microscopic measurements

Sample	Wire's Speed (m/min)	Cords' Height (µm)	Penetration (µm)	Left Contact Angle (º)	Right Contact Angle (º)
1.2	**4.2**	**2772**	**1273**	**119**	**114**
1.9	3.2	1973	53	125	108
2.0	5.2	2075	870	142	147
2.1	6.2	2066	1346	141	158
2.2	7.2	2314	1813	139	135
2.3	3.7	1984	219	111	121

5.3.5. Detailed analysis of cord 2.0

The chosen cord of this experiment is the 2.0 because it congregates the best shape with the good colour and good values for height, width and penetration.

Figure 5.18 – Overview of the cord 2.0

As seen in the Figure 5.18, the cord 2.0 is characterized by a good colour of the material in all the extension of the cord. It is possible to see that the contact angles are consistent and that the process, during the deposition, was very stable despite having some spatters. It can be seen some differences between the beginning and, 10 mm to 20 mm after, where the cord seems more stable in terms of height, which is a normal behaviour, having in mind the increasing robot's speed in the start of the deposition.

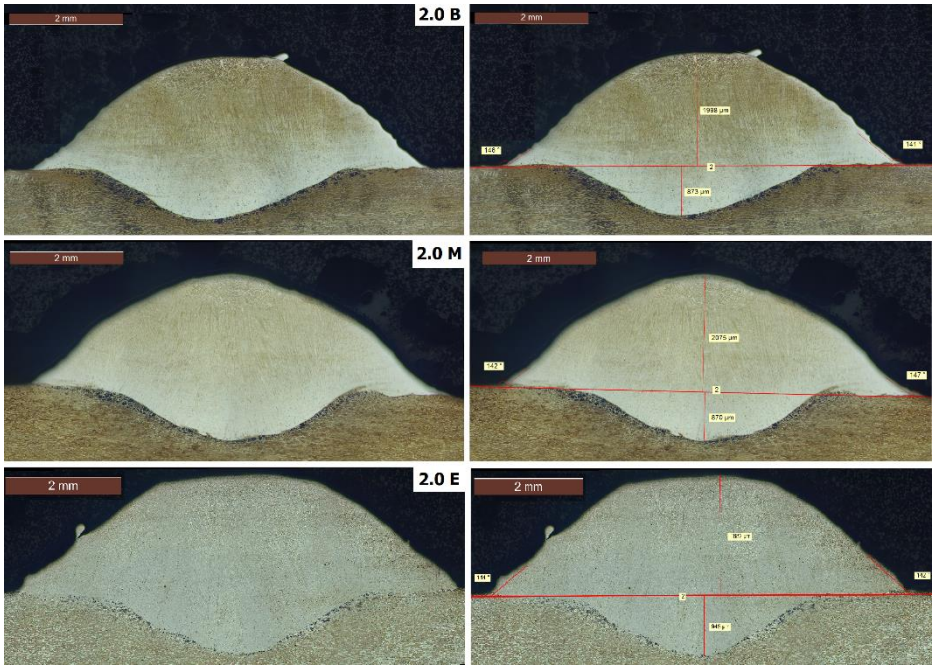

Figure 5.19 – Complete analysis of the cord 2.0 and its measurements

In this comparison of the beginning, middle and end of the cord (Figure 5.19) it is possible to see that this cord is very consistent regarding the height and depth. The contact angles described on Table 5.12 are very similar in all the cuts. The Figure 5.19 - 2.0B shows a slight dislocated penetration to the left side. This small defect is corrected throughout the cord development, as it can be seen in the Figure 5.19 - 2.0M cut where the depth is already perfectly aligned with the highest point of the cord, and keeps it until the end. The Figure

5.19 - 2.0E shows a flatten surface on top of the cord, typical of the end of all deposition cords. This is not a defect but a characteristic regarding the point where the cut was made.

Table 5.12 – Microscopic measurements of the cord 2.0

Placement	Height (µm)	Depth (µm)	Left Contact Angle (º)	Right Contact Angle (º)
Beginning	1998	873	146	141
Middle	2075	870	142	147
End	1882	945	144	142

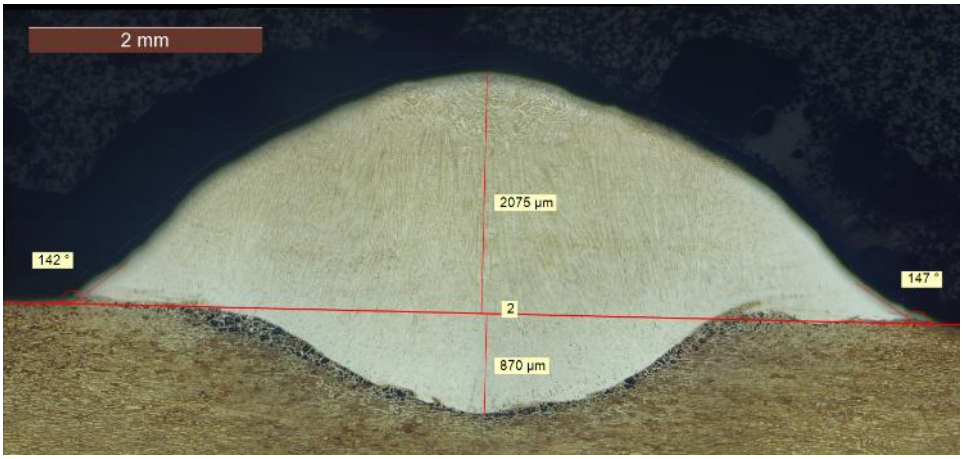

Figure 5.20 – Measurements of the cord 2.0 (middle cut)

This cord is very homogeneous and, as it can be seen, it appears to have a normal distribution graphic shape (Figure 5.20). A good penetration value of 870 µm (the third-best value), a height of 2075 µm (the second-best value) and with the best shape format of penetration (top of penetration aligned with the top of the cord height) of all. These two measurements allow to achieve a dilution percentage of 29.50, which is considered a very good value according to the bibliography.

The contact angles are also very good, with values of 142º on the left and 147º on the right side.

This cut also shows that the process parameters were well chosen (from the cord's shape point of view) and that it hasn't porosities, inclusions and bead humping.

Flaws on 2.0 cord

As it is possible to see in the Figure 5.4, the cord 2.0 shows some small imperfections comparing the left with the right side of the penetration. The right side has some small waves

between the substrate and the deposited material. This type of small defects is very common and normal, even in a good cord like this one. There are no visible flaws in this cut, meaning that the process was stable and performed with the adequate parameters.

Microstructures of 2.0 cord

In the Figure 5.21 it can be seen the microscopic images of microstructures associated to the place where they were taken.

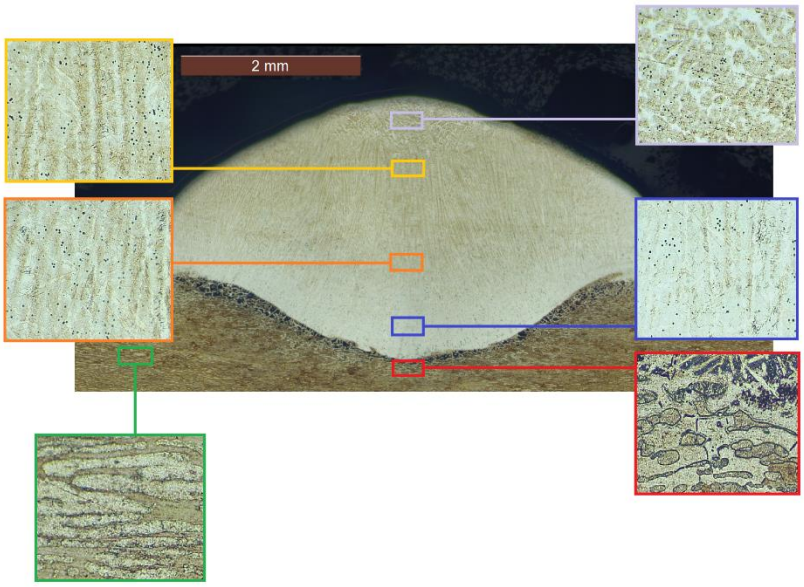

Figure 5.21 – Cut of the chosen cord 2.0 with microstructures and their localization

In the green square it is shown the same microstructure observed in all the other substrates, which is austenite and ferrite elongated grains in the disposition provided by the rolling process.

In the red square, it is possible to see the heat affected zone in the substrate microstructure and where it is also possible to see small ferrite grains growing in a sort of perpendicular orientation, in the transition between the substrate and the deposited material.

The blue square shows the thin austenitic microstructures growing with vertical orientation in the cord.

On the orange square it is possible to understand that the austenitic microstructures observed in the blue square are growing in width and length, consistent with the cooling rate that is lower as it goes away from the penetration zone.

The yellow square shows the same microstructure that the orange square but, in this case, it is possible to spot grain frontiers between austenite and ferrite very well. It also shows some smaller austenitic microstructures but in higher quantity.

The purple square shows strange formations on the top of the cord with different disposition, maybe due to the chemical attack. Underneath these strange formations, it is possible to see small austenite grains in a less percentage, smaller size and width, which is consistent with a slow cooling rate, also seen in the yellow square.

5.4.Multi-cord Experiment

5.4.1. Deposition Macroscopic Analysis

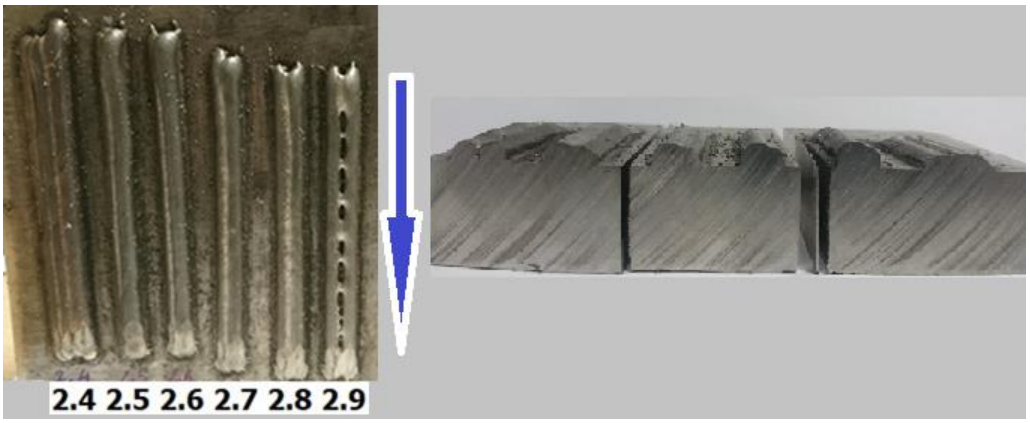

Figure 5.22 – Multi-cord Experiment six depositions

The deposition 2.4 shown in the Figure 5.22 is the result of all the better parameters used in the previous experiments, except the overlap that is going to be analysed in this experiment. This deposition obtained with four cords presented a characteristic colour of the stainless steel, but the overlap is not very regular between the first and the second cords (overlap of 70%) in all their extension. During this process, it had spatter that can be seen deposited on the side of the cord. The first three cords, with 70%, 60% and 50% of overlap respectively, shown a consistent cord with small differences in height due to the different overlaps used. The last cord, that had 40% of overlap between it and the third cord, revealed a considerable different length on comparison to the others. Due to the 40% overlap this cord shows a more visible contour than the others, being possible to see it well defined, even in the overlap part.

As it can be seen on Figure 5.22, the deposition 2.5 done with four cords (two with overlap between them of 70% and two, on top of them, with the same overlap), doesn’t show a very

regular overlap between the last two cords (third and fourth). In some places, there are more overlap than in others and it has an accumulation of material in the beginning of the cords, where it makes a little S curb and shows some process instability.

The deposition 2.6 was also performed with four cords (two with overlap between them of 60% and two, on top of them, with the same overlap) and, as it can be seen on Figure 5.22, on the first 1/3 of the cord's length approximately, it is visible an accumulation of material and a small instability (less than seen on 2.5). However, on the last 2/3 of the length, it is visible a very regular deposition overlap, although still showing a big difference between the third and fourth cord height which could lead to lean the future layers.

The deposition 2.7 shows (Figure 5.22) a very stable process and overlap of 50% during all the four cords, but it still has a difference between the third and the fourth cord height that, with an increasing on the number of layers on top of each other, might lean the final wall to one side.

The deposition 2.8 is the flattest one of all this experiment. It also shows (Figure 5.22) a very stable process and overlap of 40%. This cord doesn't show instability on the start or in any other place of the deposition. The colour of the cords is also good. The only sign that could indicate a future flaw is a small tenue concavity between the two top cords. With the increasing number of layers this deformation might grow reaching a size that creates holes leading to lack of material between the cords or between the layers.

The deposition 2.9, with an overlap of 30% shows lack of metal between cords. The value of 30% overlap is clearly not enough for these parameters. It is also possible to see in the Figure 5.22 that the process is not very stable, due to having only some junctions in common between the two last cords, fact that was also visible between the first two cords.

5.4.2. Process Temperatures

The Table 5.13 describes all the temperatures measured in this experiment.

Table 5.13 – Multi-cord Experiment process temperatures

	Deposition	Medium Humidity (%)	Medium room's Temperature (ºC)	Initial substrate Temperature (ºC)	Final substrate Temperature (ºC)
5th substrate	2.4	45.9	20.6	21.3	35.4
	2.5	46	20.5	24.3	44.2
	2.6	45.8	20.5	26.7	42.7
	2.7	45.8	20.7	25.2	45.3
	2.8	45.6	20.6	24.9	52.6
	2.9	45.6	20.6	28.7	56.3

5.4.3. Comparison between all depositions

The Table 5.14 and the Table 5.15 show the interaction between the overlap used in each deposition, and the values measured at the samples regarding the length, height and the width.

Table 5.14 – Multi-cord Experiment macroscopic measurements (deposition 2.4)

Cord	Sub-Cord	Overlap (%)	Length (mm)	Height min (mm)	Height max (mm)	Width min (mm)	Width max (mm)
2.4	2.4.1	0	106	3	3.3	13.5	14.1
	2.4.2	70	105				
	2.4.3	60	106				
	2.4.4	50	110				

The Table 5.14 shows the values of height that only reflects the minimum and the maximum height. It was not easy to measure all the cords height since the overlap between them doesn't allow it. Even though, it can be seen that the height increases from the first to the third cord, leaving the first cord (a little far) having the lower height. The variation of the width results from the process start, where there is a larger accumulation of material. With four cords side by side, starting all of them on the same side, it will increase the width of the deposition in this area when comparing with the end, where the process is more stable and have less accumulation of material.

Table 5.15 – Multi-cord experiment macroscopic measurements (depositions 2.5 to 2.9)

Cord	Overlap (%)	Length (mm)	First layer average Height (mm)	Deposition Height min (mm)	Deposition Height max (mm)	Width min (mm)	Width max (mm)
2.5	70	110	2.75	4.4	6.10	7.95	8.80
2.6	60	110	2.70	4.4	6.20	8.15	8.85
2.7	50	110	2.45	4	5.65	9.00	9.35
2.8	40	110	2.35	4	5.30	9.75	10.25
2.9	30	110	2.20	3.1	4.70	10.40	10.90

It is possible to see in the Table 5.15 that all the depositions (from 2.5 to 2.9) reached the programmed length. Examining the table, a pattern is recognizable in the first layer average height, decreasing from the cord with 70% overlap to 30% overlap. This is coherent once it is going to have less material deposited overlapping. The final height of each deposition is a reflex of the whole four cords together. The table shows that, with the exception of the cord 2.6 with 60% overlap (and not being an abnormal value), all the others are decreasing their sizes, with the decreasing of the overlap value, which means that a pattern can be identified. The width measurements clearly show the increasing distance between cords while the overlap decreases.

5.4.4. Deposition Microscopic Analysis

The Figure 5.23 shows the result of an experiment that consisted in the deposition of four cords with different overlaps. It can be seen that the first cord (on the right side) has a considerable smaller size comparing with the three others. This reduced size occurs because part of its material was re-melted, contributing to the volume of the second cord. This second cord was deposited with a 70% of overlap and it is higher and with more area than the first one. The third cord is higher but has less area, and is possible to see that the overlap of 60% is making the top of the cord flat in a small part of it. It is clearly understandable that there are two penetrations with the same depth (the second and third), and at the same time the first and the last are the ones with higher penetration value.

Figure 5.23 – Image of the deposition 2.4

It is clear that the last cord (on the left side, with 50% overlap) has a better penetration than the cords before because the heat input is split between the substrate area and the previous deposited cord. This distribution resulted in a lower depth penetration and the shape on the top of the cord can be seen not like a stair growing as in the previous three cords, but as an almost flat surface.

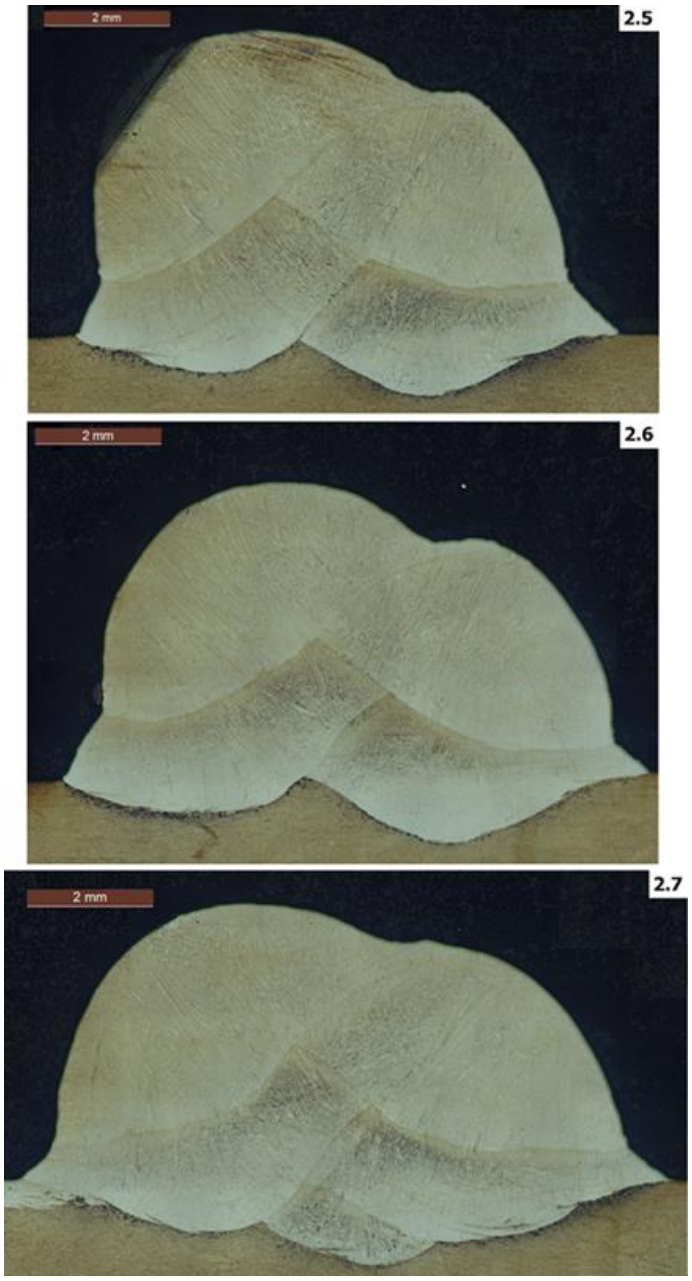

Figure 5.24 – Image of the depositions from 2.5 to 2.7

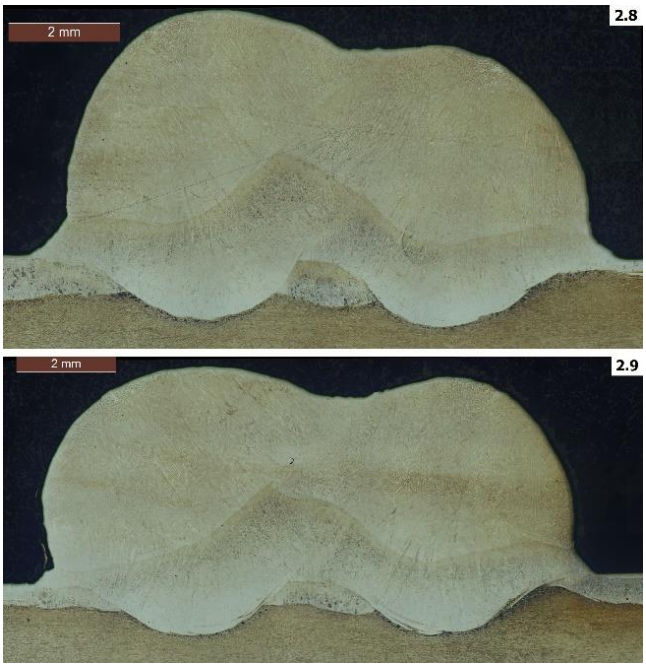

Figure 5.25 – Image of the depositions from 2.8 to 2.9

The microscopic figure of the cuts shows, with clarity, the disposition of the four cords that form each deposition. It is clear that the overlap is decreasing from the depositions 2.5 to 2.9. As shown in the Figure 5.24 and Figure 5.25, there are material deposited in the first two cords that are partially re-melted. The first two cords are always wider than the two deposited on top of them. With this analysis it can be identifiable that, between the penetrations of the first two cords (depositions 2.7, 2.8 and 2.9) and on both sides of the penetration near substrate's surface there are some deposited material from previous experiments since this was a reused substrate. This material has a similar tone to the depositions 2.7, 2.8 and 2.9. Despite this reuse of substrate material, it is visually identifiable the cords' placement and the overlap material after doing the chemical attack.

From the first deposition to the 2.8 there is a favourable evolution of the cords surface quality, coming from bumping surface in the 2.5 to a nearly flat surface on the 2.8. This evolution observed between the top of the cords in all depositions is directly linked to the decreasing percentage of overlap.

In the deposition 2.9, the overlap percentage is considered too low once it can already be observed two cords separate, showing a depression between them.

Table 5.16 – Multi-cord Experiment microscopic measurements (deposition 2.4)

Cord	Sub-Cord	Overlap (%)	Cords Height (µm)	Penetration (µm)	Area (µm^2)	Total Width (µm)
2.4	2.4.1	0	--	833	5790564	14156
	2.4.2	70	2818	552	10258665	
	2.4.3	60	3176	355	9762911	
	2.4.4	50	2847	792	11846962	

As a result of the used overlaps (Table 5.16) until the 2.4.3, the height deposition is increasing which means that the overlap used was excessive. The 2.4.4 shows that with 50% of overlap the height value is not the highest; however, this last cord shows a better penetration when comparing to the cords that are also overlapping. Is also possible to understand that the value of 50% overlap results in a larger area of the cord, reflecting a better distribution of the deposited material. This better distribution leads to a better width and not so higher cord.

Table 5.17 – Multi-cord experiment microscopic measurements (depositions from 2.5 to 2.9)

Cord	Sub-Cord	Overlap (%)	Cords Height (µm)	Penetration (µm)	Area (µm^2)	Total Width (µm)
2.5	2.5.1	0	3891	918	6333197	8591
	2.5.3			--	9409797	
	2.5.2	70	4880	564	7036454	
	2.5.4			--	11900173	
2.6	2.6.1	0	3789	1031	6291760	9309
	2.6.3			--	9947185	
	2.6.2	60	4692	491	7461773	
	2.6.4			--	12155054	
2.7	2.7.1	0	3803	954	6427923	10236
	2.7.3			--	10931251	
	2.7.2	50	4386	795	7458180	
	2.7.4			--	12743654	
2.8	2.8.1	0	3516	1122	5755417	10463
	2.8.3			--	11925626	
	2.8.2	40	4077	1052	7576895	
	2.8.4			--	12440563	
2.9	2.9.1	0	4053	1130	6442353	11178
	2.9.3			--	14832079	
	2.9.2	30	4321	1075	8420367	
	2.9.4			--	16284907	

Besides it is possible to identify that the set of cords, on the left side of the depositions always have a higher value (Figure 5.26). The cords height does not present a clear pattern between the used overlap and the height reached by them so the correlation between overlap and cords height is not linear. However, it is clear that the set of the second and fourth cords (left cords) are always higher than the first and third. This occurs because it was stopped after four cords. If it was made a fifth cord, it would be higher than the fourth because of the accumulation of material in the overlap area.

The Table 5.17 shows that a better penetration always occur in the first cord and after that in the second. This occurs because the heat input distribution between substrate and the first cord already deposited.

Regarding to the areas of each cord inside each deposition, it can be seen they have approximate values but, in general, with the decreasing overlap from 70% to 30%, the total areas (the four cords summed up) are increasing (Figure 5.27).
The width shown in the Table 5.17 reflects the decreasing in overlap values.

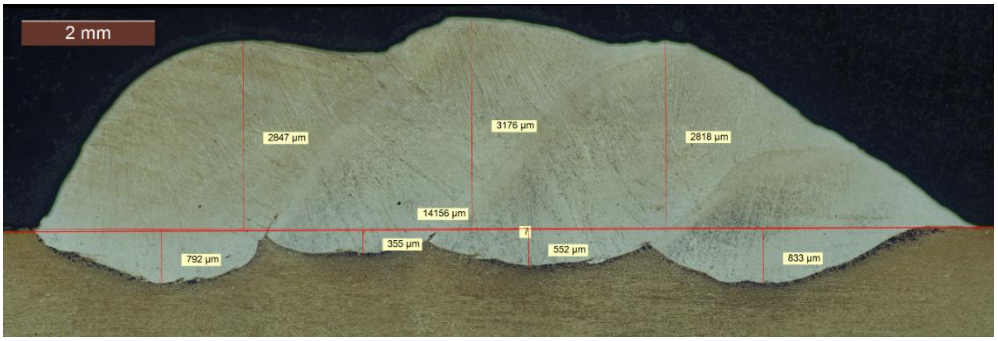

Figure 5.26 – Measurements of the deposition 2.4

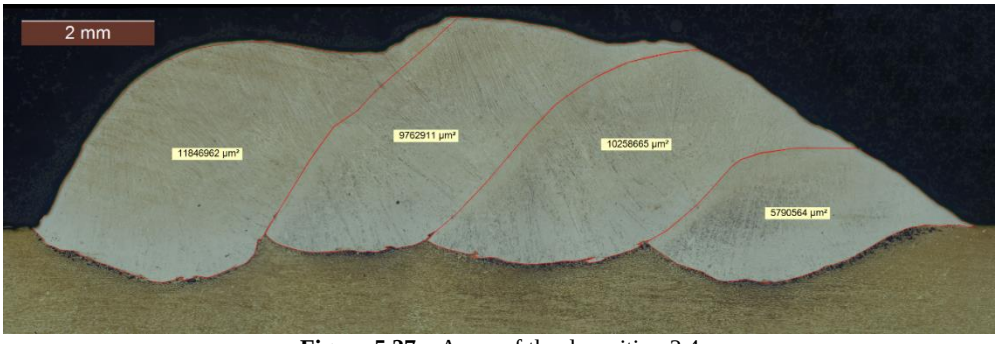

Figure 5.27 – Areas of the deposition 2.4

5.4.5. Detailed analysis of 2.7 and 2.8 depositions

The chosen depositions, regarding the overlaps, are going to be: the one with 50% overlap (2.7 deposition) and the one with 40% overlap (2.8 deposition).

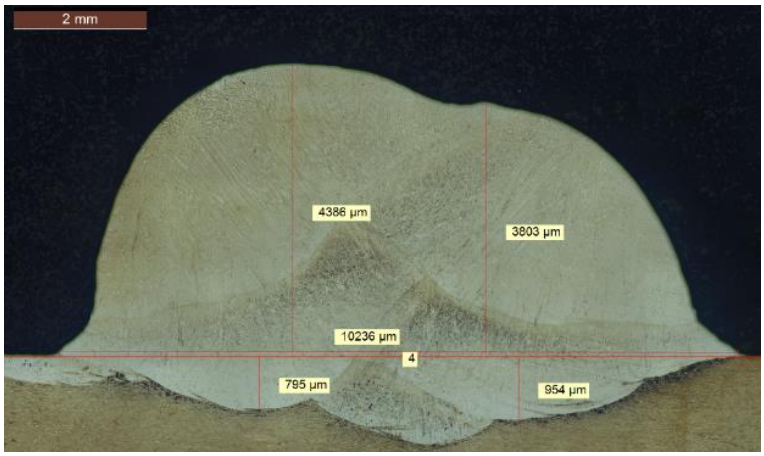

Figure 5.28 – Measurements of the deposition 2.7 (middle cut**)**

The deposition 2.7 presented on the Figure 5.28 shows good measurements results regarding the height, width and penetration when comparing to the other cords. This deposition was very stable, reaching the programmed length and the side of the cords didn't show major flaws. The Figure 5.28 shows that both penetrations have closer values meaning that they are both made in similar conditions. A good colour and a good distribution of the areas (Figure 5.29) with a clearly direction of growing, perpendicular to the surface, are other characteristics that lead to this choice.

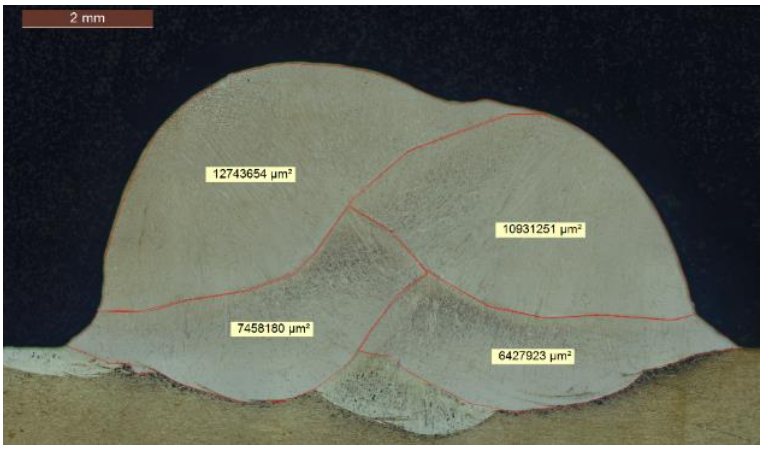

Figure 5.29 – Areas measurements of the deposition 2.7 (middle cut)

The Figure 5.30 represents the deposition 2.8. The reasons for this choice are the similar penetration depth; the good deposition of the cords on top of each other; and by being the one with the highest value of width (without having lack of material between the cords or the layers). Another reason to choose this deposition was because of the flatten surface on top of the junction cords. Despite the differences on height on the top of the cord, this flat surface could mean that if it was added more layers, the growth would be perpendicular to the substrate, which is the main purpose.

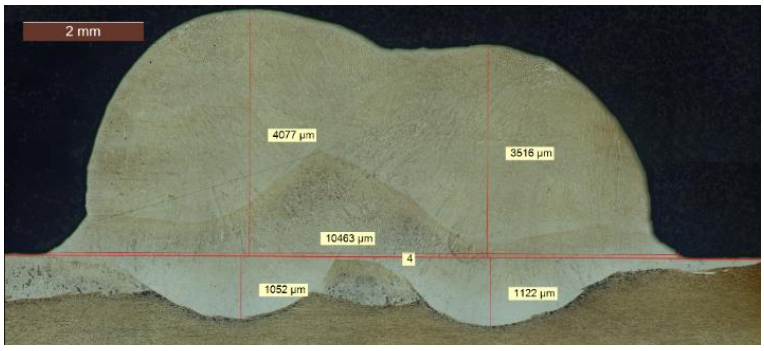

Figure 5.30 – Measurements of the deposition 2.8 (middle cut)

This deposition, as it can be seen in Figure 5.31, has a very good and consistent material distribution by the areas of each cord, reflecting no flaws between cords or layers. Another good characteristic in this deposition is that the material is not spreading too much which could mean that adding more layers it would accomplish a larger but vertical and consistent wall.

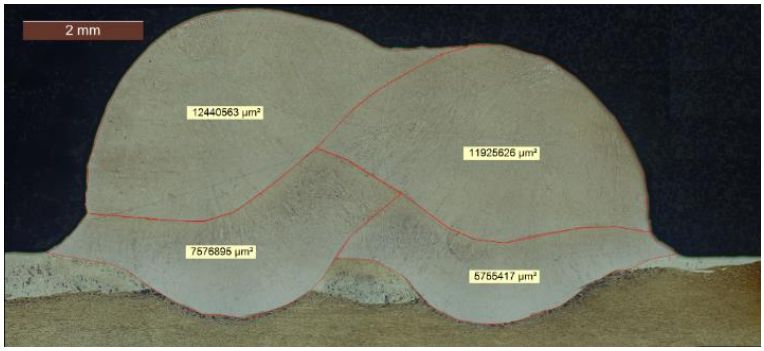

Figure 5.31 – Areas' measurements of the deposition 2.8 (middle cut)

5.5. Walls Try-out Experiment

5.5.1. Deposition Macroscopic Analysis

Figure 5.32 – Walls Try-out Experiment

The wall 3.0 (Figure 5.32) presented major flaws due to the robot's behaviour. It could be observed that the overlap is not the correct one and the layering is not correctly done. This problem seems to be due to the programming of the robot and probably to the understanding it makes regarding the transitions between the depositions direction. It is possible to identify lack of melting between cords of the same layer and it is also possible to see that the layering is not centred with each other and the process was very unstable. Due to these facts the process was stopped after only four layers.

The wall 3.1 shows lack of melting between cords of the same layer, possibly because of the small overlap. This type of flaws happens in almost every layer in different points and between different cords. It is also noticeable (Figure 5.32) a big difference of height between the starting point and the ending point of each cord.

The wall 3.2 shows the best congregation of parameters and overlap. There are no flaws macroscopically visible, the surface finishing between layers is not quite reasonable and the wall is straight on both sides. It still can be seen (Figure 5.32) big differences between the height of the starting point and the ending point of the deposition. This wall didn't present

any signs of lack of melting between cords or layers during the process, and the process of the layer by layer deposition seems consistent. The final result seems to be a solid wall.

The wall 3.3.A was produced with a zig-zag strategy (Figure 5.32) and doesn't show signs of consistency between cords of the same layer or even between layers. This strategy is clearly not suitable for this wall's construction as there is a lot of gaps between different points of the cords with lack of material.

The wall 3.3.B still doesn't show any improvement, comparing with the 3.3.A. The increment of speed just reduced even more the deposited material, leading to higher gaps between different points of the cords obtain trough this strategy (Figure 5.32).

5.5.2. Process Temperatures

The Table 5.18 present all the temperatures measured in this experiment.

Table 5.18 – Wall Try-out Process Temperatures

	Deposition		Medium Humidity (%)	Medium room's Temperature (ºC)	Initial substrate Temperature (ºC)	Final substrate Temperature (ºC)
6th substrate	3.0	3.0.1	35.9	21.4	20.7	59
		3.0.2			45	109
		3.0.3			95	127
		3.0.4			102	175
	3.1	3.1.1	37.5	21.6	22.9	41.1
		3.1.2			41.6	64.2
		3.1.3			52.1	74.6
		3.1.4			58.3	86
		3.1.5			58	84.9
		3.1.6			69.8	87.8
		3.1.7			83.9	105.8
		3.1.8			89	110
	3.2	3.2.1	38.7	21.5	46	70
		3.2.2			57.7	98.3
		3.2.3			84	125
		3.2.4			90.7	123.8
		3.2.5			107.1	142.3
		3.2.6			116.9	138.9
		3.2.7			120.1	152.5
		3.2.8			129.6	166
	3.3.A	3.3.A.1	35.8	21.5	46.9	96
		3.3.A.2			80.2	137
	3.3.B		35.6	21.7	50	65.2

5.5.3. Comparison between all walls

Table 5.19 – Wall Try-out Experiment macroscopic measurements

Sample	Type of trajectory	Overlap (%)	Length (mm)	Width min (mm)	Width max (mm)	Height min (mm)	Height max (mm)
3.0	Bi-directional	40	157	18.65	21.00	5.10	8.55
3.1	Uni-directional	40	150	18.30	19.70	15.25	20.1
3.2	Uni-directional	50	145	16.70	17.70	12.20	15.30
3.3.A	Transversal zig-zag	40	143	46	47.2	4.20	4.45
3.3.B						5.45	6.40

The wall 3.0 presented no consistency in its cords, with values of width and height that shouldn't be considered, as it can be seen in the Table 5.19 and Figure 5.33. It is full of flaws and would not be considered for a wall construction. The wall 3.3.A and 3.3.B are in the same conditions, with lack of consistency and full of flaws due to the use of this type of trajectory. This led to the discard of this type of approach for a wall construction.

As it can be seen in the Table 5.19 the only difference between the walls 3.1 and 3.2 is the overlap of 40% and 50%, respectively, with higher expected values of width in the 3.1 than in the 3.2. However, when analysing the wall height, the values measured are different from those expected, with the wall 3.1 (with the lower overlap value) presenting higher height values than the wall 3.2 (with the bigger overlap). The expected was a wider and lower wall with 40% overlap and a thinner and higher wall with the 50% overlap.

During the wall 3.1 deposition it was observed some flaws and lack of melting between cords of the same layer. This happened in several locations and in several layers. As it can be seen in figure 5.34, these flaws appeared in the cuts, leading to the appearance of empty holes inside the walls what is not admissible in a wall construction.

Figure 5.33 – Comparison between walls 3.0 to 3.2

5.5.4. Detailed Analysis of the wall

The wall 3.2 shown in Figure 5.34 demonstrates that the result of all the best parameters registered in all the previous experiments lead to the most reliable strategy to build it. The surface all around the wall has good quality, despite some spatter that can be seen due to the depositions made afterwards. It can be seen that there still is a big height difference between the starting point, on the left, and the ending point, on the right. The colour of the wall is

also good. This wall provides the information regarding how many cords, side by side and layers, are needed to make to build samples adequate for the flexural test.

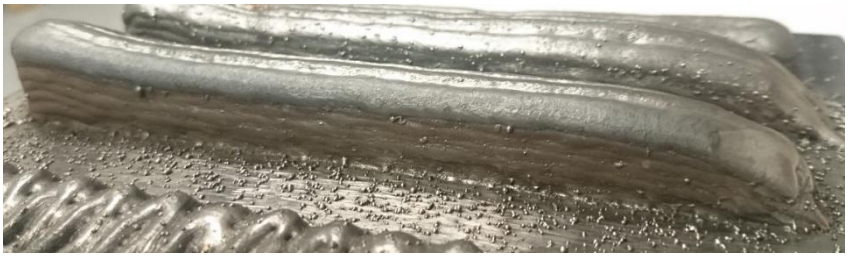

Figure 5.34 – Overview of the wall 3.2

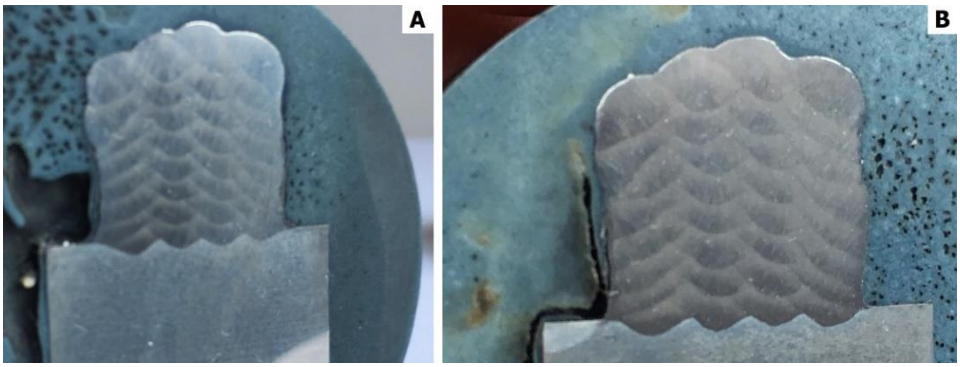

Figure 5.35 – Chosen wall after chemical attack. A-Beginning cut; B-Middle cut

In Figure 5.35 it is observable all the layers and cords made in this wall. It is clear the boundaries between them, which gives a perception of the material distribution from each cord during the wall construction.

5.6.Deposition Macroscopic Analysis in Wall Construction

Figure 5.36 – Wall's Construction

The wall 3.4 presented a consistent behaviour during all the deposition process. The wall on both sides is straight with perpendicular angle with the substrate but is possible to see (Figure 5.36) that not all cords of the same layer are at the same level. The surface has good quality but, at a certain point, during the deposition, a flaw due to the spatter hosted in the nozzle stopped the process which led to stop this wall with this height. With the alternated side of the starting points it managed to level a bit more the wall on both sides. It still has flaws on both tops but the wall height is much more levelled.

The wall 3.5 is straight on both sides, with good elevation, but is possible to see (Figure 5.36) that not all cords of the same layer are at the same level. The deposition, through all the process, presented a consistent behaviour resulting in a good quality surface and the process itself provided a high wall with lack of flaws mainly because of the removal of the spatter deposited on the nozzle between every three layers.

5.7.Microhardness Analysis

5.7.1. Laws Experiment

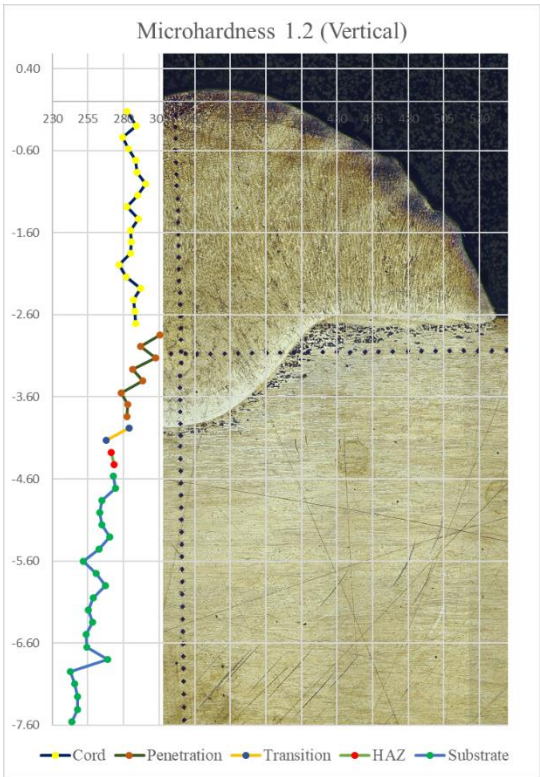

Figure 5.37 – Vertical Hardness of cord 1.2

In the microhardness test performed with a 500gf of charge on the chosen cord 1.2, it is possible to see that the Vickers hardness values in the cord are between 277.10 HV and 295.30 HV, with a difference between the maximum and the minimum values in the cord 18.2 HV, which seems to be consistent (Figure 5.37). The pattern that is understandable is that from the top of the cord in direction to the substrate, the microhardness values are decreasing. It can also be seen that there is a major difference between the microhardness values at the bottom of the penetration and the heat affected zone. In the cord 1.2 it was made 52 vertical measurements, looking for to understand if there was a pattern and what was the real reach of the heat affected zone.

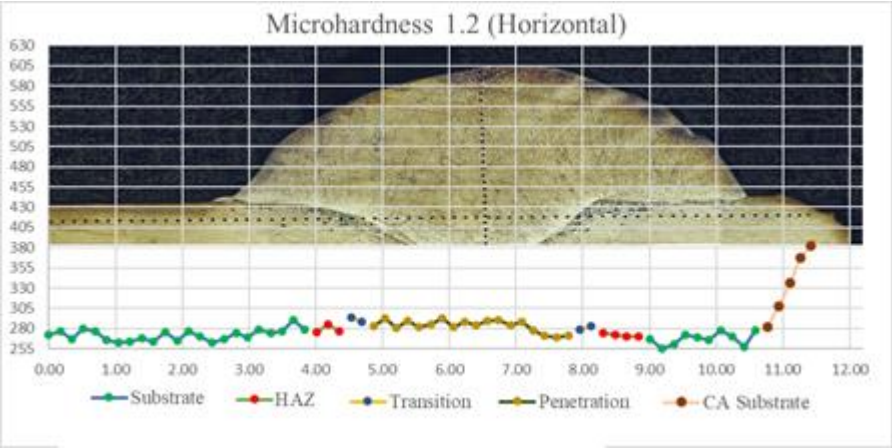

Figure 5.38 – Horizontal Hardness of cord 1.2

In the Figure 5.38 is possible to see that all microhardness measurements resulted on values between 255 HV and 293 HV, except the five indentations with the designation of the cut affected substrate (CA substrate), on the right side of the figure. These values are higher, possibly due to the material being affected by the cut made near these measurements.

The values of the substrate, the transition and the heat affected zone, on both sides of the cord, even being on separated sides have similar values between each other. The penetration measurements show consistent values until the four last measurements on the right side, where it revealed lower values, possibly due to a soft spot (less austenite percentage) or some defect on the deposition.

5.7.2. Robot Speed Experiment

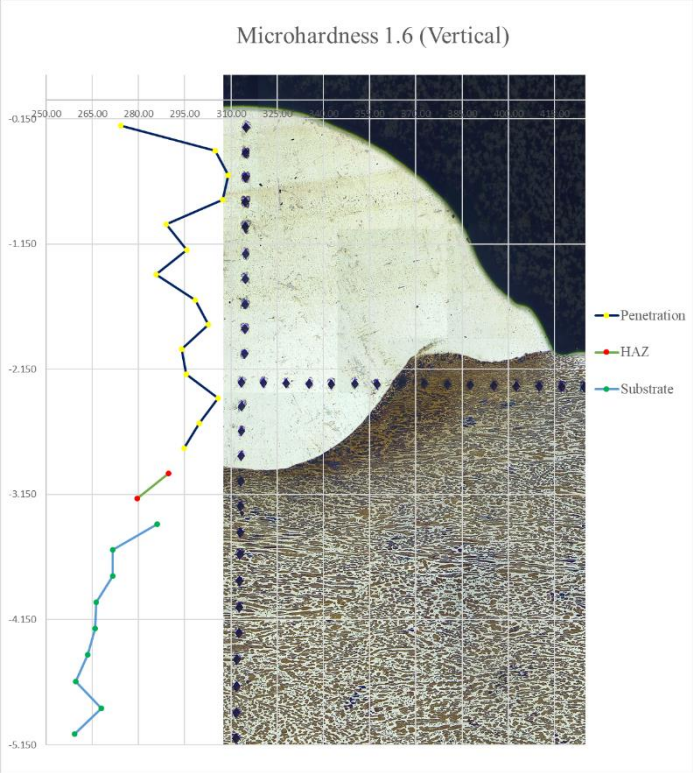

Figure 5.39 – Vertical Microhardness of cord 1.6

All the microhardness tests, from this experiment forward, was performed using a higher charge of 1000 gf with the aim of decrease the variability of the values achieved. On the chosen cord 1.6, it is possible to see three values near the top of the cord that are over the 300 HV. These high values of hardness, in this point of the cord, are not abnormal and are possibly connected to the microstructure reached. The first indentation of the cord, as the Figure 5.39 shows, is consistently a lower value than the following sequence of values. The consistency of the values from the second indentation to the fourteenth, put the cord with a gap between the best and worse values of 15.1 HV. This shows consistency and could mean that the microstructures achieved are very similar in all the cord and penetration. It is also possible to see in the figure a decreasing pattern (except the first indentation) in the values, which could mean that the cooling rate in this cord was slower in the higher part of the cord, having more austenitic structures and achieving harder material, according to the material supplier.

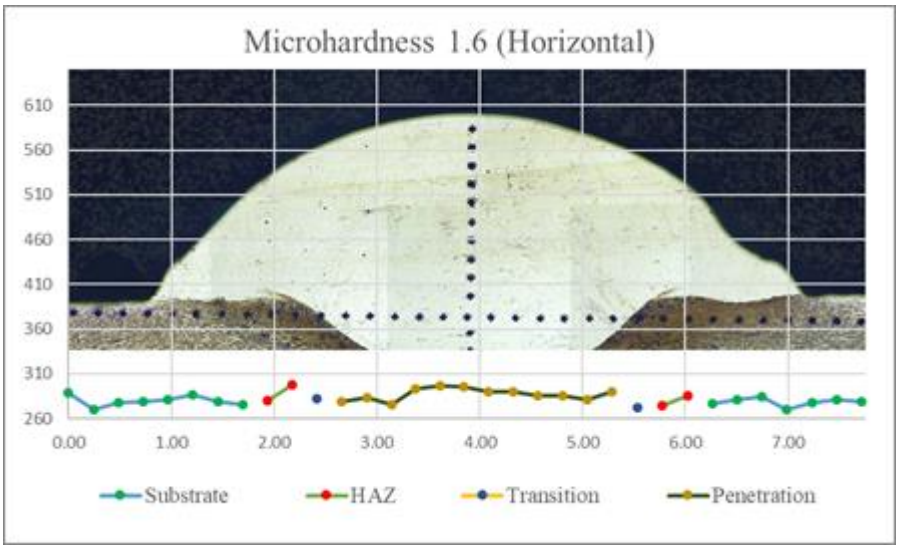

Figure 5.40 – Horizontal Microhardness of cord 1.6

In the microhardness test, done to the cord 1.6 with a horizontal orientation as it is possible to see in Figure 5.40, the substrate does not have much variability from the hardness's point of view once most of the values are all very similar. It is also noticeable that the indentation done in the transition from the substrate to the penetration, on both sides of the cord, have a difference of 10HV between the values. The cause of this difference is possibly linked to the position of each indentation: the left blue dot is more placed in the penetration zone and the right blue dot is placed in the transition zone but more in the HAZ.

It is understandable that the hardness values took in the penetration are very constant, possibly meaning that the microstructures, in this area, are very similar.

5.7.3. Wire Feed Speed Experiment

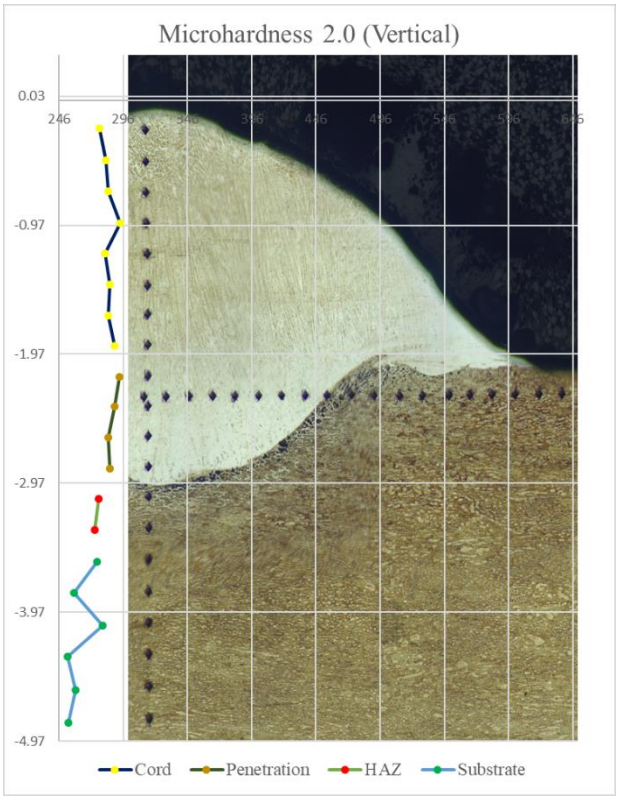

Figure 5.41 – Vertical Microhardness of cord 2.0

The hardness test made to the cord 2.0, with the vertical orientation shown in the Figure 5.41 displays a high variability in the substrate with a gap, between values, of 27.4 HV. This cord has the particularity of having groups of values that show a pattern. The first four indentations done from the top of the cord to the substrate, have an increasing pattern, stopping in the fourth indentation. The next four indentations also have an increasing pattern and with similar values to the group described before. It is also noticeable that beside the group of values, the cords Values from the top of the cord to the bottom of the penetration have a gap of 15.9 HV which show consistency.

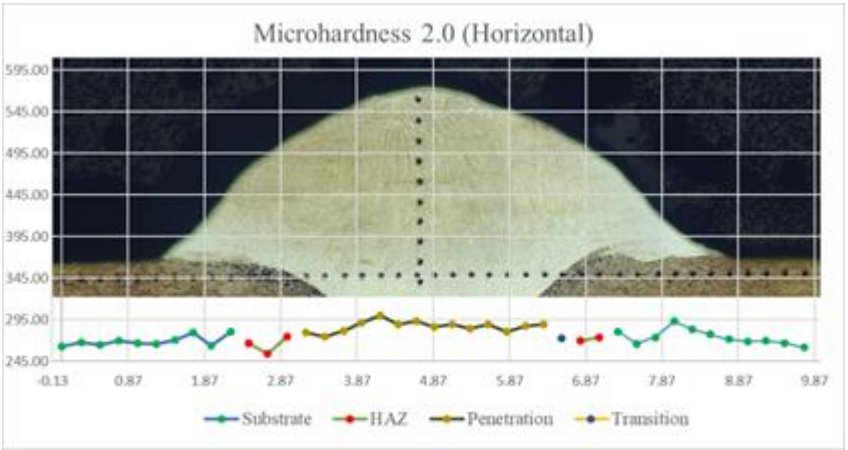

Figure 5.42 – Horizontal Microhardness of cord 2.0

In the microhardness test made to the cord 2.0, with a horizontal orientation as the Figure 5.42 shows, it is possible to see an inconsistent hardness values in the penetration zone, having a gap of 25.3HV between the higher value and the lower. Regarding the heat affected zone (HAZ), the indentations show discrepancies in values achieved, when comparing the right HAZ with the left HAZ, having this one higher variability. In the substrates, the indentations done under the cord deposition also show discrepancies between values, having a gap between the higher and the lower of 28.7HV.

5.7.4. Multi-cord Experiment

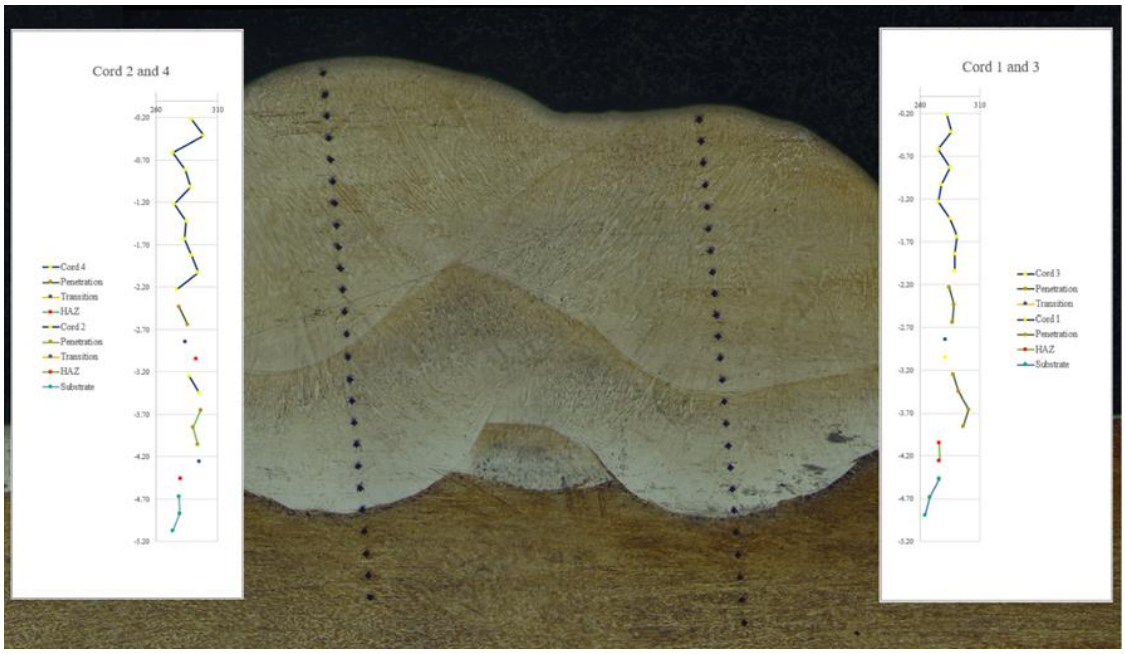

Figure 5.43 – Vertical Microhardness of wall 2.8

The microhardness measurements made in the wall 2.8 (Figure 5.43) shows that the microhardness values are all consistent and they are all between 270 HV and 300 HV, approximately. This shows that adding more layers or putting more cords side by side (re-melting material) are not going to change the achieved hardness values of this process. It can be presumed that adding layers, or cords, the values are going to remain similar.

5.7.5. Wall Try-out Experiment

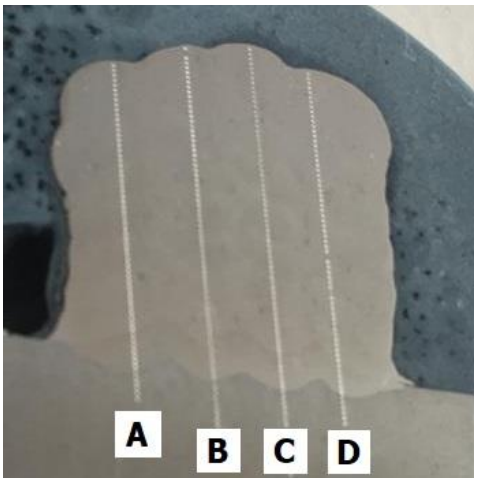

Figure 5.44 – Microhardness indentations of Wall 3.2 (middle cut)

The exhaustive measurements made in the wall 3.2 are shown in the Figure 5.44. More than sixty measurements for each column in the three cuts (Appendices C) were made to assure that the results were consistent with the ones obtained previously.

The Figure 5.45 shows the values obtained and the consistency of them being all, as expected, with values between 250 HV and 300 HV. This microhardness test shows that besides the variability of the values they are consistent in the range achieved, not only between columns but also between cuts (Appendices E). In the transition part of the cord from the penetration to the HAZ there are fluctuations in the values that do not allow to recognize a pattern.

Other observation that is coherent with the previous microhardness test made, is that the values of hardness in the deposited material is always higher than the substrate values. Despite the range of values is approximately 50 HV and the microstructure observation revealed a replication of the microstructures, which did not allow to establish a correlation between them.

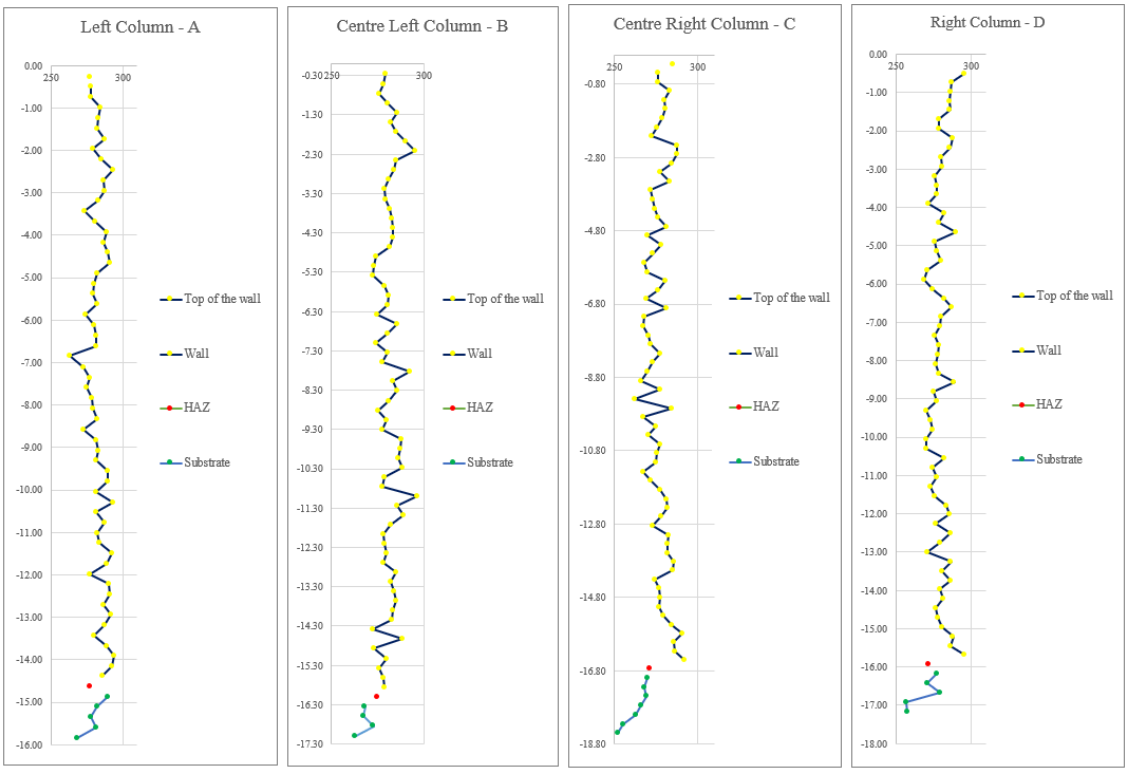

Figure 5.45 – Vertical Microhardness Values of Wall 3.2 (middle cut)

5.8. Three-point flexural Analysis

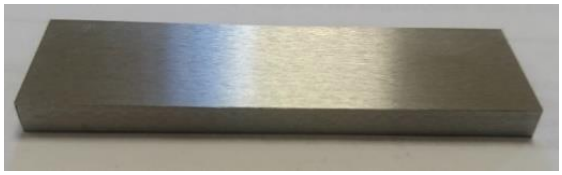

Figure 5.46 – Sample ready for Three-point Flexural test

The Figure 5.46 shows an example of the sample extracted from the walls after its cutting, milling and grinding. It was possible to extract three samples from the lower layers of each wall (3.4 and 3.5). These samples were machined together in order to have exactly the same geometry and surface quality so the results of the three-point flexural test could be comparable.

After the walls were done, there was the need to make some cuts with the right length to withdraw samples for this flexural test and for microscope analysis. In the cuts made, it was labelled all the samples of each wall and is due to this that the designation of the samples is 3.4.B, 3.4.D, 3.4.G. This designation also reveals the positioning of each sample in the wall, meaning that in the 3.4 wall, the B was the second cut, D was the fourth, and G was the sixth cut, in the 3.5 wall, it was used the same system.

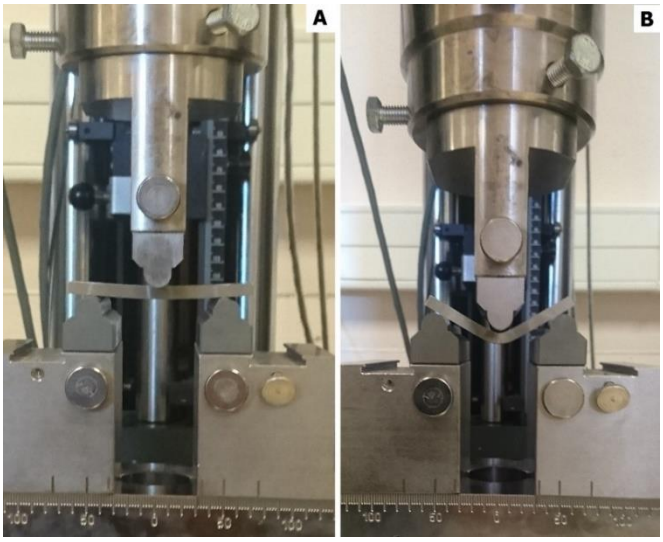

Figure 5.47 – Three-point flexural test. A-Initial; B-Final

The Figure 5.47A shows the three-point flexural test made to the samples with 70 mm of length, 20 mm of width and 5 mm of thickness, in the machine Roell Zwick Z100 ready for the start of flexural test. The distance used between the lower supports were 50 mm.

In the Figure 5.47B, it is possible to see the end of the three-point flexural test with the sample already bent after a stable test.

The Figure 5.48 is a graphic representation of the values achieved during the test of the 3.4.G sample. The values collected for the other experiments were similar and this graphic is representative of all of them.

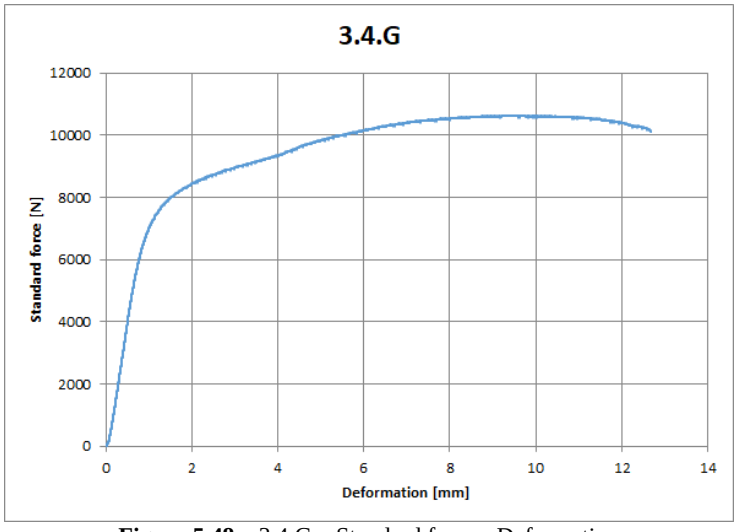

Figure 5.48 – 3.4.G – Standard force - Deformation

Conclusions

The analysis of the additive manufacturing cords produced by WAAM technology were performed concerning geometry and the aspect of the components built, the microstructure and the mechanical properties of the material.

Concerning the main objectives that were defined as key-points, some conclusions could be addressed to each point identified previously.

1. Main characteristics of the deposited material with the WAAM process and the correlation between input parameters and defects:

It was possible to observe some limitations on the control of the process. The result of these limitations usually was the wrong choice of the settled parameters. These wrong choices result naturally on flaws and defects. It was possible to identify wrong shape of the deposited cord, wrong size of the cord, low penetration, sharp contact angles and other flaws like spatter. It was possible to develop knowledge about single cord deposition but also on the dynamics with multiple cords deposition. In the case of multiple cords deposition, the decision of overlap is quite important, such as the strategy of deposition, that have a major contribution to assure a good melting and mixture on the material to avoid pores or lack of fusion between cords.

2. Optimization of the process parameters:

Some parameters are mixed together trying to achieve different combinations between them. The main conclusions to withdraw are that there is a big influence regarding the power input (amperage and voltage), the robot speed and the wire feed speed, in the shape of the cords or walls. An optimal cord geometry was achieved in the cord 2.0 due to a good combination of these parameters. It was also possible to understand that a combination of values for those three parameters could be achieved multiple times with good results.

The results obtained in the wall's try-out experiment provided a clear understanding of what is necessary regarding the programming and the intrinsic combination between the geometry and the defined parameters inputted in the CMT equipment and robot KUKA. It was also stated the big influence of geometry in the appearance of flaws and defects. It was possible to identify that the main challenge is on the first layers of the wall. After building

approximately four layers, occurs stabilization and there is no problem on flaws and defects of the process and remains the same despite the wall's height.

3. Development of a correlation between the obtained microstructures with the parameters used on the experiments:

It was not possible to establish a correlation between the microstructures obtained in the experiments and the inputted parameters in the CMT. It was only possible to verify that the microstructures are consistent with the literature regarding the welded stainless steel.

4. Find the microhardness pattern values inside the cords:

It was possible to understand that the values achieved were accordingly with the literature investigated in the state of the art. Despite the variations resulting of different aspects, it is possible to conclude that the hardness of the material deposited are always higher than the same material used in the substrate, produced by conventional techniques.

The conclusion from the three-point flexural test was that there is consistency in the values achieved, the process is replicable and does not occur changes on the maximum force achieve for each sample. Also, on multi layers deposition the same was possible to observe. This process has the advantages of using metallic materials often used in engineering, allowing not only the complete construction of a component but also the repair of a damaged component.

Future Work

For a future development there is a need to perform more extensive experiments with the same parameters in a wider spectrum that would help to create and develop production indicators. That will allow to predict the results obtained in the depositions or wall's construction, simply knowing the parameters and their values used, in each one of them.

Performing cuts and analysis of the bent samples to understand the behaviour in terms of microstructures. Developed tensile tests and other destructive and non-destructive tests, would help to complete the characterization and achieve an understanding of the material behaviour, regarding this production method, allowing to maximize the potential markets and applicability for it.

Bibliography

AGA. *Mison Shielding Gas*. Accessed in 21/07/2019. Available in https://www.aga.se/en/products_ren/cutting_welding_gases/shielding_gases/mison_shielding_gases/index.html.

Alcaraz, J. M. P. (2015). *Development and Automation of a Robotic Welding Cell Using Machine Vision in Halcon Programming Environment*. Universidad Politécnica de Cartagena - Escuela Técnica Superior de Ingeniería Industrial, Cartagena.

Almeida, P. & Williams, S. (2010). Innovative process model of Ti-6A1-4V additive layer manufacturing using cold metal transfer (CMT). *Proceedings of the Twenty-first Annual International Solid Freeform Fabrication Symposium*. University of Texas, Texas.

Anand, S (2017). *How to calculate heat input*. Accessed in 19/09/2019. Available in https://www.weldingandndt.com/how-to-calculate-heat-input/.

Bacelar, R. (2017). *Evaluation of WAAM Parts by NDT*. Instituto Superior Técnico, Universidade de Lisboa, Lisboa. Master Thesis.

Béranger, G., Henry, G., Sanz, G. (1996). *The book of steel*. France: Lavoisier Publishing.

Bigneat. *Clearview Fume Hood (BC 8004)*. Accessed in 06/07/2019. Available in https://www.safetyfumehoods.com/sfh-product/clearview-fume-hood-bc8004/.

Carou, D., Rubio, E. M., & Benedicto, B. (2017). Technical, Economic and Environmental Review of the Lubrication/Cooling Systems Used in Machining Processes. *Science Direct*. Elsevier.

Compositadour (2018). *Expertises & Équipements*. Accessed in 03/06/2019. Available in https://www.compositadour.com/expertises-equipements/expertises-fabrication-additive.html.

Drapinski, J. (1979). *Elementos de soldagem*. São Paulo: McGraw-Hill do Brasil.

ESAB. *Lesson 1 The Basics of Arc Welding*. Accessed in 18/09/2019. Available in https://www.esabna.com/euweb/awtc/lesson1_28.htm.

Fletcher, M. J. *WP-309 3-D Printing for the Marine Industry*. Accessed in 09/09/2019. Available in https://www.huntingdonfusion.com/index.php/de/technical-support/white-papers-40017/3156-3-d-printing-for-the-marine-industry.

Fronius. *RCU 5000 Operating Manual*. Accessed in 30/06/2019. Available in https://www.fronius.com.

Fronius (2014). *Cold Metal Transfer*.

FSH Welding Group. *Welding Product Programme Duplex and Super Duplex stainless steel*. Accessed in 16/06/2019. Available in https://www.fsh-welding.com/illicomag/pages/duplex-en-web.pdf.

Gu, J., Cong, B., Ding, J., Williams, *S. W., Zhai, Y. Wire+arc additive manufacturing of aluminium*. Accessed in 05/06/2019. Available in https://sffsymposium.engr.utexas.edu/sites/default/files/2014-038-Gu.pdf.

Hascoët, J-Y., Quérard, V., Rauch, M. (2018). Wire arc additive manufacturing of aluminium alloy structure on curved metal sheet using 5 axis tool paths and CMT welding process. *Soudage et Techniques Connexes*. Mars-Avril 2018, 37-45.

HESSE. *Surface grinding machine CHEVALIER FSG-3A818*. Accessed in 30/07/2019. Available in https://www.hesse-maschinen.com/en/products/datasheet/grinding-machines/2280-fsg-3a818/.

Holke F-10-V Ram-head Milling Machine. Accessed in 30/07/2019. Available in http://www.lathes.co.uk/holke/.

Honeycombe, R. W. K. (1981). *Aços microestrutura e propriedades*. Lisbon: Fundação Calouste Gulbenkian.

Hosseini, V. A. (2016). *Influence of multiple welding cycles on microstructure and corrosion resistance of a super duplex stainless steel*. University West, Trollhättan. Licenciate Thesis.

Hosseini, V. A., Karlsson, L., Engelberg, D., Wessman, S. (2018). Time-temperature-precipitation and property diagrams for super duplex stainless steel weld metals. *Welding in the world*. Springer.

Imoudu, N. E. (2017). *The Characteristic of Cold Metal Transfer (CMT) and its application For Cladding*. The Arctic University of Norway: Faculty of Technology, TromsØ. Master Thesis.

Ji, L., Lu, J., Jing, C., Fan, H., Ma, S. (2017). *Microstructure and mechanical properties of 340L steel fabricated by arc additive manufacturing*. School of Mechanical Engineering, Beijing Institute of Technology, Beijing.

Kobelco. Welding duplex stainless steels. *Technical Highlight*. Volume 18. Accessed in 09/07/2019. Available in https://www.kobelco-welding.jp/education-center/technical-highlight/vol18.html.

KUKA (2006). *Datasheet KR 100 HA*. Accessed in 26/09/2019. Available in https://www.kuka.com/

Lamb, S., Bringas, J. E. (2002). *CASTI Handbook of Stainless Steels & Nickel Alloys* (2nd edition). Alberta: CASTI Publishing.

Lopes, E. M. D., Miranda, R. M. (1993). *Metalurgia da soldadura*. Lisbon: Edições Técnicas do Instituto de Soldadura e Qualidade.

Harris, R. *The 7 Categories of Additive Manufacturing*. Loughborough University, Leicestershire. Accessed in 25/12/2019. Available in https://www.lboro.ac.uk/research/amrg/about/the7categoriesofadditivemanufacturing/.

Material District. *Waampeller is the world's first 3D printed ship's propeller*. Accessed in 29/06/2019. Available in https://materialdistrict.com/article/waampeller-3d-printed-propeller/.

Mendez, P. F. & Eagar, T. W. (2003). Penetration and defect formation in high-current arc welding. *Welding Journal*.

Nilsson, J.-O. (2016). 02. The role of nitrogen in duplex stainless steel. *Stainless Steel World Magazine*, July/August. Accessed in 21/07/2019. Available in https://www.materials.sandvik/en-ie/pod/season-1/02.-the-role-of-nitrogen-in-duplex-stainless-steels/.

Padilla, A. F., Plaut, R. L., Rios, P. R. (2007). *Steel Heat Treatment: Metallurgy and Technologies* (2nd edition). Boca Raton: CRC Press.

Posch, G., Chladil, K., Chladil H. (2017, April). Material properties of CMT - metal additive manufactured duplex stainless steel blade-like geometries. *Weld World*. Springer.

Presi. *Catalog 2020*. Accessed in 30/07/2019. Available in https://www.presi.com/en/catalogs/.

Research and Engineering Company. *WAAM – Wire Arc Additive Manufacturing*. Accessed in 19/09/2019. Available in http://www.avianik.com/en/articles/services/additive%20technology/waam/.

Select-Arc, Inc. *SelectAlloy 2209-AP*. Accessed in 16/06/2019. Available in http://www.select-arc.com/siteadmin/uploads/prod/prod-sheets/selectalloy-2209-ap.pdf.

Select-Arc, Inc. *SelectAlloy 2209C*. Accessed in 16/06/2019. Available in http://www.select-arc.com/siteadmin/uploads/prod/prod-sheets/selectalloy-2209c.pdf.

Select-Arc, Inc. (2017). *Select-Arc Premium Welding Products. Full line catalog*. Accessed in 16/06/2019. Available in http://select-arc.com/products/pdf/master_select-arc_catalog_2.17-updated.pdf.

Selvi, S., Vishvaksenan, A., Rajasekar, E. (2018). Cold metal transfer (CMT) technology – An overview. *Defence Technology*. Volume 14, 28-44. Accessed in 18/06/2019. Available in https://www.sciencedirect.com/science/article/pii/S2214914717301022.

Shen, C. (2016). *Application of wire-arc additive manufacturing (WAAM) process in in-situ fabrication of iron aluminide structures*. University of Wollongong Australia, Wollongong. PhD Thesis.

Smith, W. F. (1993). *Foundations of materials science and engineering* (2nd edition). Singapore: McGraw-Hill International Editions.

Smith, W. F. (1990). *Principles of materials science and engineering* (2nd edition). Singapore: McGraw-Hill International Editions.

Soares, P. (1992). *Aços características e tratamentos* (5th edition). Lisbon: Publindústria.

Struers. *Vickers Hardness Testing*. Accessed in 15/09/2019. Available in https://www.struers.com/en/Knowledge/Hardness-testing/Vickers#introduction.

Taban, E., Kaluç, E. (2013). Welding behaviour of Duplex and Superduplex Stainless Steels using Laser and Plasma ARC Welding processes. *Welding in the World, Le Soudage Dans Le Monde*. Springer Verlag. Accessed in 12/09/2019. Available in https://www.researchgate.net/publication/271817548_Welding_behaviour_of_Duplex_and_Superduplex_Stainless_Steels_using_Laser_and_Plasma_ARC_Welding_processes.

Tapiola, J. (2017). *Cold Metal Transfer cladding of wear and corrosion resistant coatings in engine applications*. Tampere University of Technology, Tampere. Master Thesis. Accessed in 18/06/2019. Available in https://www.researchgate.net/publication/313880652_Cold_Metal_Transfer_cladding_of_wear_and_corrosion_resistant_coatings_in_engine_applications.

TMR Stainless (2014). *Practical Guidelines for the Fabrication of Duplex Stainless Steels*. (3th edition). London: International Molybdenum Association (IMOA).

Vignesh, V. S. (2017). *3D Additive Manufacturing. WAAM Martensitic Stainless Steel: Process Optimization & Resulting Weld Geometrical Characterization*. TUDelft, Delft. Master Thesis.

Voort, G. F. V. (2004). *ASM Handbook Metallography and Microstructures* (Volume 9). Oklahoma: ASM International. Master Thesis.

Wainer, E., Brandi, S. D., Mello, F. D. H. de, (1995). *Soldagem processos e metalurgia*. São Paulo: Editora Edgard Blüchter.

Xu, X., Ganguly, S., Ding, J., Seow, C. E., Williams, S. (2018). Enhancing mechanical properties of wire + arc additively manufactured INCONEL 718 superalloy through in-process thermomechanical processing. *Materials & Design*. Volume 160, 1042-1051. Accessed in 18/06/2019. Available in https://www.sciencedirect.com/science/article/pii/S0264127518307937?via%3Dihub.

Zwick. *Zwick Z100/Z250 materials testing machine with central ball-lead screw*. Accessed in 30/07/2019. Available in https://www.zwickroell.com/-/media/files/sharepoint/vertriebsdoku_pi/08_437_single_screw_testing_machine_pi_en.pdf

Appendices

Appendices A - Protocols

A.1. Law's Experiment Protocol

1. Turn on all the equipment;
2. Insert all the data necessary for the deposition;
3. Fix the substrate in place;
4. Polish and clean the substrate after fixation;
5. Put the nozzle in place;
6. Simulate the deposition;
7. Measure the room temperature
8. Measure the room humidity;
9. Measure the substrate temperature;
10. Put the nozzle in place;
11. Do the Deposition;
12. Measure the substrate temperature, in the same place;
13. Measure the room temperature;
14. Measure the room humidity;
15. Take photos of the cord from all views;
16. Blow pressurized air to cool down the substrate;
17. Do the measurements of the cord's length, height and width;
18. Write what is identifiable (spatter, inclusions, oxidations, shape, colour, porosity and bead humping);
19. Put the nozzle in place for the next deposition;
20. Change the Law used;
21. Return to point 5.

A.2. Robot's Speed Experiment Protocol

1. Turn on all the equipment;
2. Insert all the data necessary for the deposition;
3. Fix the substrate in place;
4. Polish and clean the substrate after fixation;
5. Put the nozzle in place;

6. Simulate the deposition;
7. Measure the room temperature;
8. Measure the room humidity;
9. Measure the substrate temperature;
10. Put the nozzle in place;
11. Do the Deposition;
12. Measure the substrate temperature in the same place;
13. Measure the room temperature;
14. Measure the room humidity;
15. Take photos of the cord from all views;
16. While it cools down, do the measurements of the cord length, height, width;
17. Write what is identifiable (spatter, inclusions, oxidations, shape, colour, porosity and bead humping);
18. Put the nozzle in place for the next deposition;
19. Change the robot speed;
20. Return to point 5.

A.3. Wire's Speed Experiment Protocol

1. Turn on all the equipment;
2. Insert all the data necessary for the deposition;
3. Fix the substrate in place;
4. Polish and clean the substrate after fixation;
5. Put the nozzle in place;
6. Simulate the deposition;
7. Measure the room temperature;
8. Measure the room humidity;
9. Measure the substrate temperature;
10. Put the nozzle in place;
11. Do the deposition;
12. Measure the substrate temperature in the same place;
13. Measure the room temperature;
14. Measure the room humidity;
15. Take photos of the cord from all views;
16. While it cools down, do the measurements of the cord length, height, width;

17. Write what is identifiable (spatter, inclusions, oxidations, shape, colour, porosity and bead humping);
18. Put the nozzle in place for the next deposition;
19. Change the wire speed;
20. Return to point 5.

A.4. Multi-cord's Experiment Protocol (for 2.4)

1. Turn on all the equipment;
2. Insert all the data necessary for the deposition;
3. Fix the substrate in place;
4. Polish and clean the substrate after fixation;
5. Put the nozzle in place;
6. Simulate the deposition (four cords);
7. Measure the room temperature;
8. Measure the room humidity;
9. Measure the substrate temperature;
10. Put the nozzle in place;
11. Do the deposition;
12. Measure the substrate temperature in the same place;
13. Measure the room temperature;
14. Measure the room humidity;
15. Take photos of the four cords from all views;
16. Write what is identifiable (spatter, inclusions, oxidations, shape, colour, porosity and bead humping).

A.5. Multi-cord's Experimental Protocol (for 2.5 to 2.9)

1. Turn on all the equipment;
2. Insert all the data necessary for the deposition;
3. Fix the substrate in place;
4. Polish and clean the substrate after fixation;
5. Put the nozzle in place;
6. Simulate the deposition (two cords);
7. Measure the room temperature;
8. Measure the room humidity;

9. Measure the substrate temperature;
10. Put the nozzle in place;
11. Do the deposition;
12. Measure the substrate temperature in the same place;
13. Measure the room temperature;
14. Measure the room humidity;
15. Take photos of the two cords from all views;
16. Write what is identifiable (spatter, inclusions, oxidations, shape, colour, porosity and bead humping);
17. Put the nozzle in place for the second layer;
18. Return to point 6, and re-do the step 6 to 16).

A.6. Wall Try-out Experiment Protocol

1. Turn on all the equipment;
2. Insert all the data necessary for the deposition;
3. Fix the substrate in place;
4. Polish and clean the substrate after fixation;
5. Put the nozzle in place;
6. Simulate the deposition (four cords in sequence);
7. Measure the room temperature;
8. Measure the room humidity;
9. Measure the substrate temperature;
10. Put the nozzle in place;
11. Do the deposition;
12. Measure the substrate temperature in the same place;
13. Measure the room temperature;
14. Measure the room humidity;
15. Write what is identifiable (spatter, inclusions, oxidations, shape, colour, porosity and bead humping);
16. Put the nozzle in place for the second layer;
17. Return to point 6, and re-do the step 6 to 15).

A.7. Wall Construction Protocol

1. Turn on all the equipment;

2. Insert all the data necessary for the deposition;
3. Fix the substrate in place;
4. Polish and clean the substrate after fixation;
5. Put the nozzle in place in the first starting point;
6. Simulate the deposition (six cords in sequence);
7. Put the nozzle in place in the second starting point;
8. Simulate the deposition (six cords in sequence);
9. Measure the room temperature;
10. Measure the room humidity;
11. Measure the substrate temperature;
12. Put the nozzle in place in the first starting point;
13. Do the deposition;
14. Measure the substrate temperature in the same place;
15. Measure the room temperature;
16. Measure the room humidity;
17. Write what is identifiable (spatter, inclusions, oxidations, shape, colour, porosity and bead humping);
18. Put the nozzle in place in the second starting point;
19. Do the deposition;
20. Measure the substrate temperature in the same place;
21. Measure the room temperature;
22. Measure the room humidity;
23. Write what is identifiable (spatter, inclusions, oxidations, shape, colour, porosity and bead humping);
24. Return to point 12, and re-do the step 12 to 23).

Appendices B – Equipment preparation

In order to start the deposition, it is necessary to prepare all the equipment.

In the Fronius CMT tool bag you can find the tools to work with:

Figure B.1 – Necessary tools to prepare the machine

Step 1 – Turning on the equipment

- Turn on the power, on the circuit breaker (Robot 240)

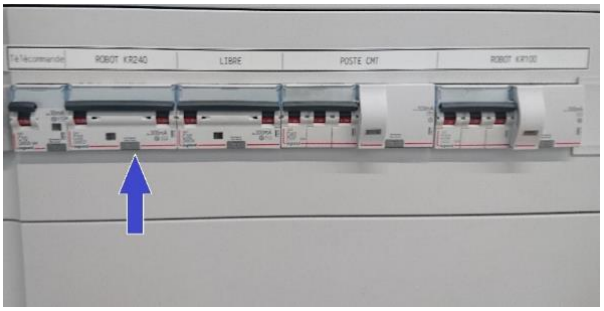

Figure B.2 – Circuit breaker of the Robot KUKA

- Turn on the Robot, turning the button to the right (inside the room)

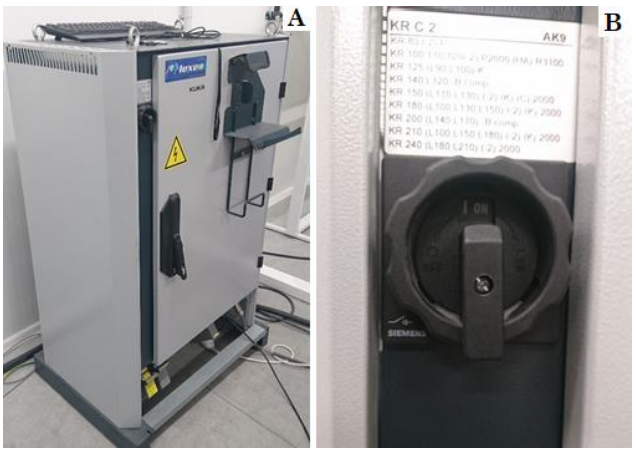

Figure B.3 – Robot KUKA's Controller

- On the robot Command (Grey one)

Figure B.4 – Robot KUKA's command

  - Press Configure (one of the Grey's buttons on top);
  - Press number 5 (on the bottom left side);
  - Press Expert;
  - Write the password;
  - Press Ok;
  - Press Accept.

- Turn on Fronius CMT (0 means turned off and 1 means turned on)

Figure B.5 – Fronius' controller

  - Back to the grey command
    - Turn the Key to manual (T);
    - Press Visualize
    - Press 0;
    - Press 1;
    - Check if the robot is ready (red light in dashboard must be on);
    - If it is turned off, configure by pressing 1 and then 2)

- Unlock red button;
- Press Accept;
- Press Blue button;
- Choose 12;
- At the same time, press the button on the back of the command, and the yellow button (Enter);
- Press Close;
- Lock the Red button.

- Go to the Fronius CMT command (Red one)

Figure B.6 – Fronius CMT's command

- It will appear a question. Press Yes;
- Press Menu;
- Press Machine pre-set;
- Select general parameters;
- Press Ok;
- Press Menu;
- Press Optimize parameters;
- Press Ok;
- Choose parameters.

Step 2 – Wire removal

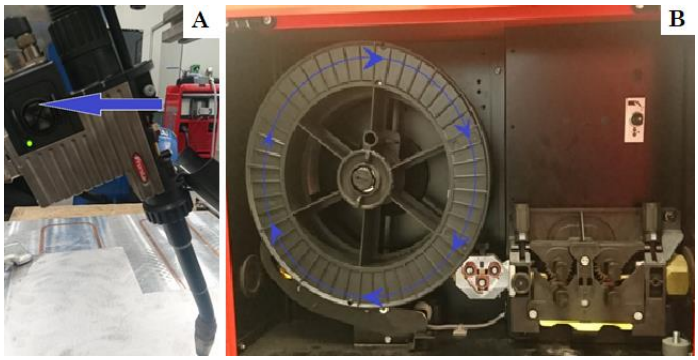

Figure B.7 –A-Press the button in the torch, to pull most of the wire back; B- Pull the wire back to the roller until the extremity of the wire is almost out of the rollers

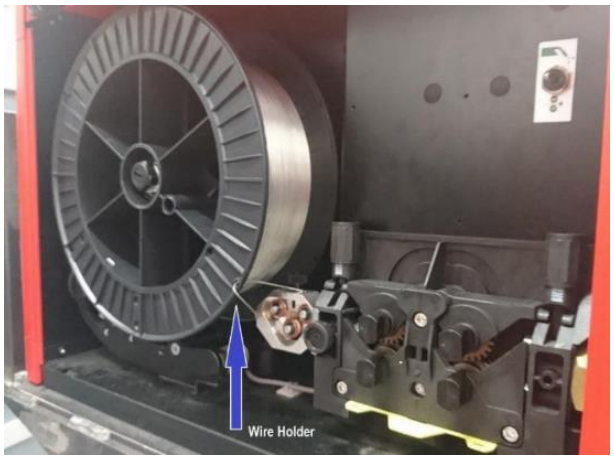

Figure B.8 - Take the end of the wire and put it enrolled on the plastic spool so it doesn't unroll, wasting material

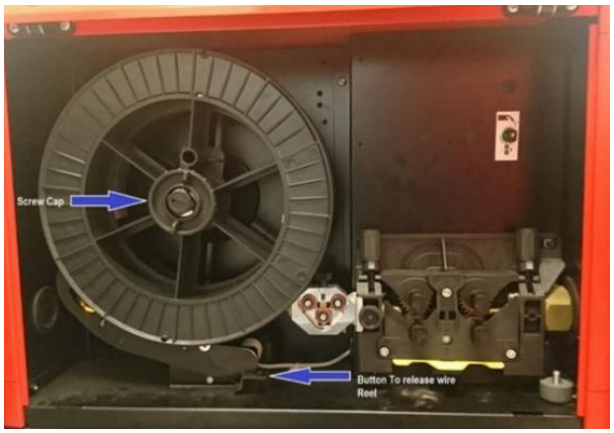

Figure B.9 – Press the button in the bottom and untighten the holder (plastic tight cap)

Step 3 – Choice of the material

Note: At this point the new material or the diameter of it requires a change of the tubes and tips.

Figure B.10 – Choose the right tube for the material and its diameter

Note: Check the specifications in the pack for each type of tube.

Figure B.11 – Different size tips to be attached in the black tubes according to each size of wire

Note: It must be done in the tubes, in the wire feeder and in the torch.

Procedure for changing the tubes for the wire

This procedure has to be done every time the materials' thickness of the wire changes.

Attention: If you are just changing the spool of the wire for the same material, with the same thickness, there is no need to do this!

Assuming that the wire has been previously removed, now it is time to remove the tubes and tips to change it.

Figure B.12 - Location of the tubes and tips

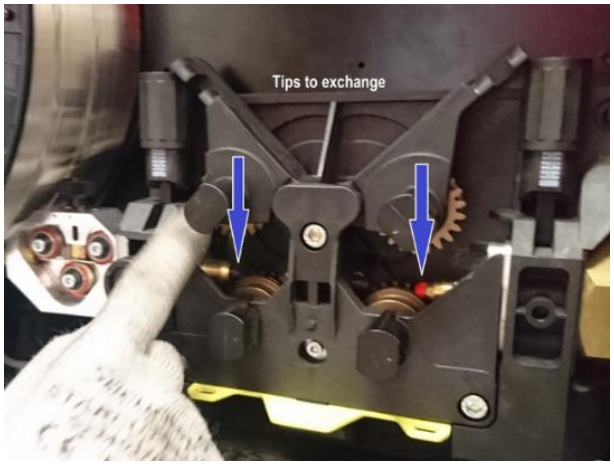

Figure B.13 – Tips to exchange in the feeder

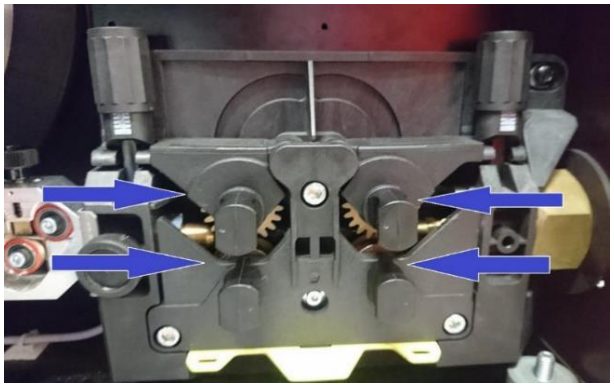

Figure B.14 – Roller that have to be changed every time the material is changed

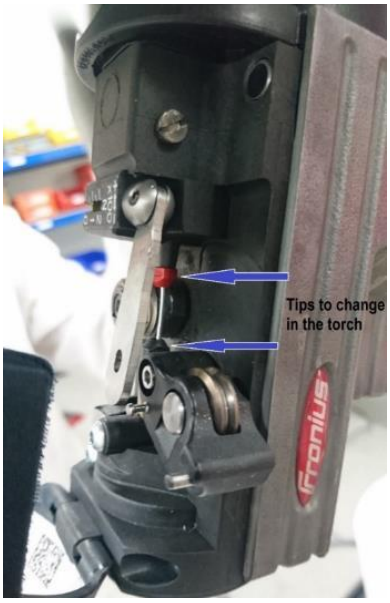

Figure B.15 – The tips to change in the torch

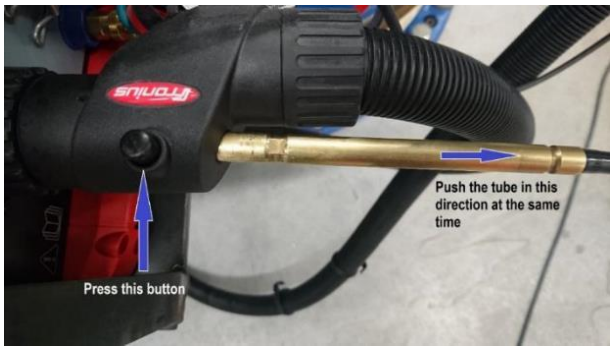

Figure B.16 – Detach the tube that is currently in use. Press the button and pull the tube in the exit of the feeder

Figure B.17 – Loose the tube from the main tube

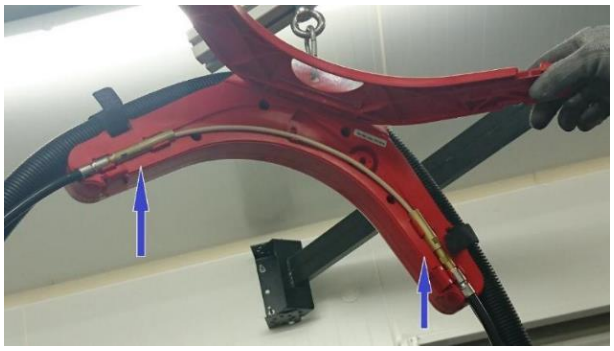

Figure B.18– In the buffer, detach both tubes and remove them

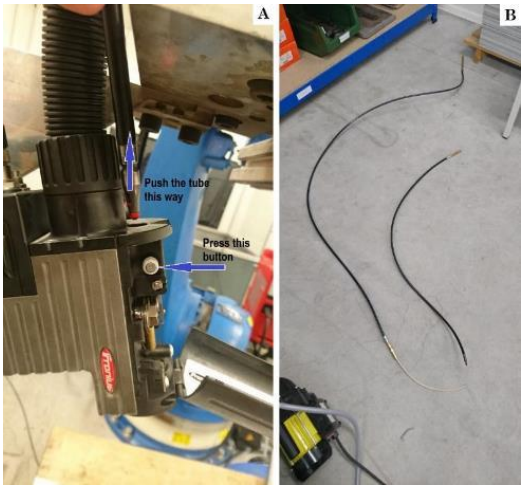

Figure B.19 – A-In the torch remove the tube, too; B- After the tubes are out

- Switch the interior of the one that is needed. Tools are needed.

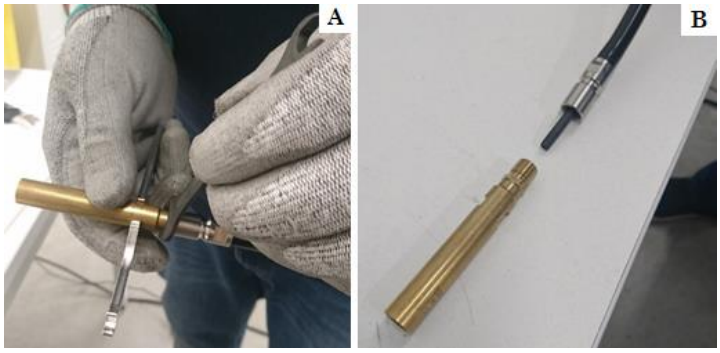

Figure B.20 – A-Detach the tubes end (yellow) from the tube (black); B-The interior has to be removed

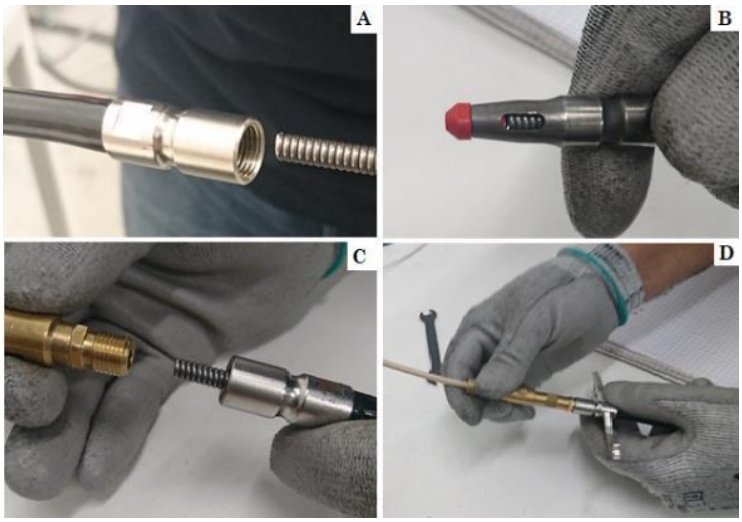

Figure B.21 – A-Put the new tube inside, according to the specifications of the wire that is going to be used; B-Check if it's placed in the other end; C-The new wire in place; D-Tighten it again

- Now it is time to change the other tube

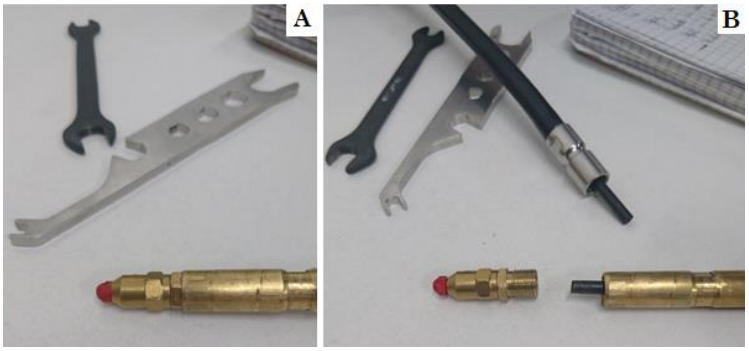

Figure B.22 – It is only needed to untighten one tip on this one (the shortest) to change it

Figure B.23 – After they are both changed, put the tubes back in place

- Change the rollers accordingly to the specification of the material.

Figure B.24 – This procedure consists in taking the spindle out. The roller pops off

Figure B.25 – It is important to change all the four rollers

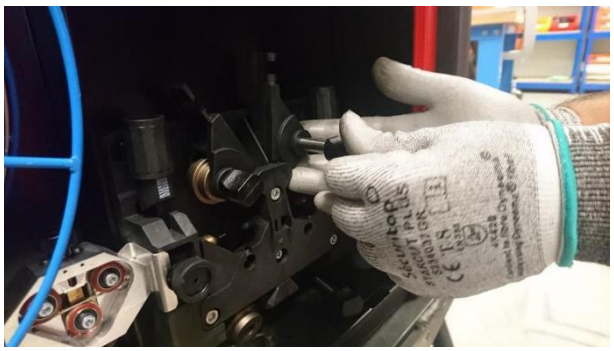

Figure B.26 – Put the upper rollers through the top

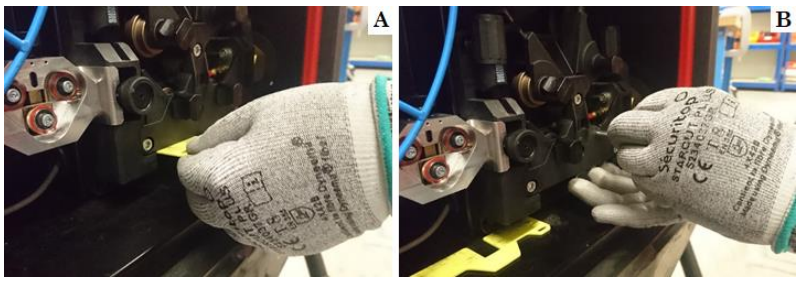

Figure B.27 – A- Remove the yellow security holder; B-Remove the spindle

Figure B.28 – Put the bottom rollers under the black plastic

Step 4 – Wire placement

Figure B.29 – Unpack a new wire from the box that comes in a spool

- Put the wire in the feeder, in the right position (Attention: the unroll direction is counter-clockwise).

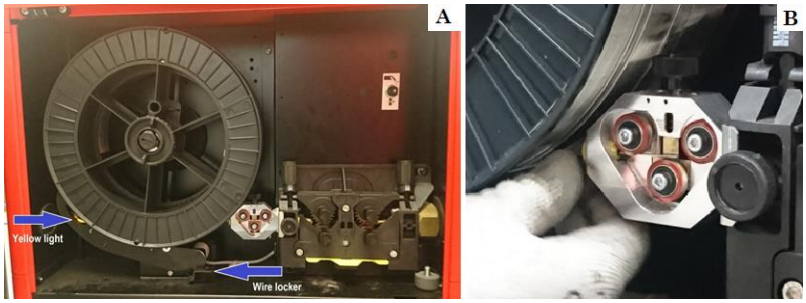

Figure B.30 – A-Tighten the plastic holder and unlock the wire holder (If the yellow light appears, it is ok); B-Put the wire through the guidance into the roller's, all the way, until it enters the tube.

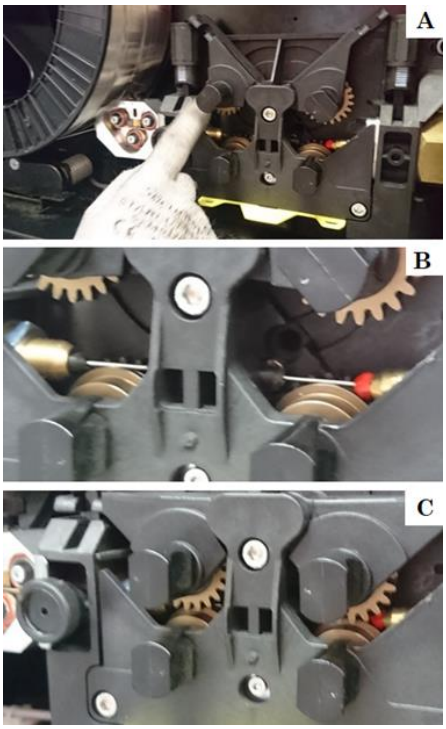

Figure B.31 – A-Open the roller holder's so the wire can be passed through; B- Through the tip into the tube; C-Close the roller's holders and adjust them if needed

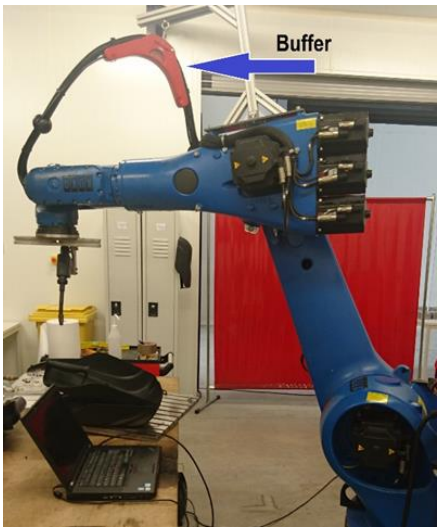

Figure B.32 – Buffer localization

Figure B.33 – Open the buffer so you can see if the wire reaches it

Figure B.34 – Press the button to unroll the wire until it gets to the buffer

.

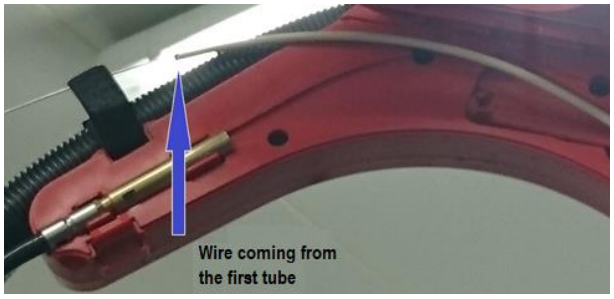

Figure B.35 – Open the buffer case (two plastic fasteners) and detach the tubes one of another

Figure B.36 – Pass the wire through the yellow tube and into the black one, which leads to the nozzle

Operations on the torch:

Figure B.37 – Open the torch's cover

Figure B.38 – Detach the tube in the torch

Figure B.39 – Detach the roller holder on the Torch, as seen in the photo below. The roller must be open to let the wire pass through

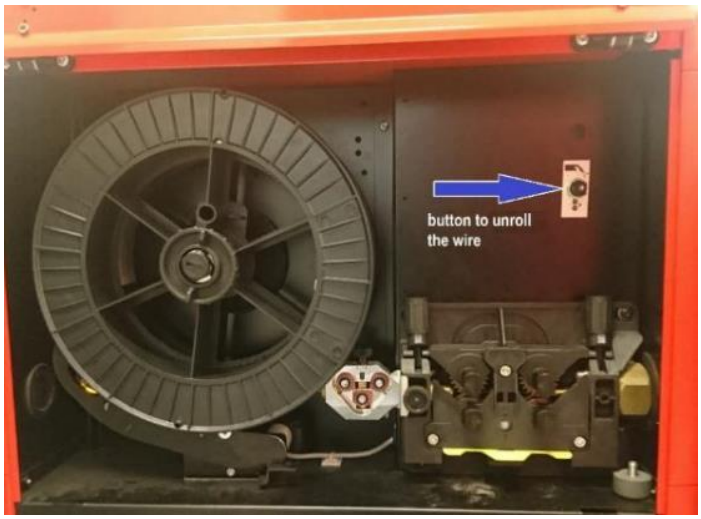

Figure B.40 – Press the button of the wire feeder until the wire gets to the end of that tube

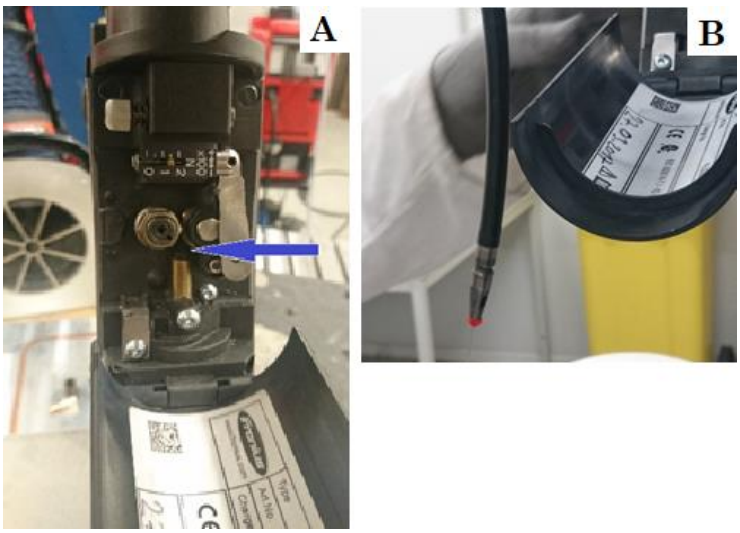

Figure B.41 – Pass the wire through the torch into the last tube. Press the button in the torch that feeds the wire

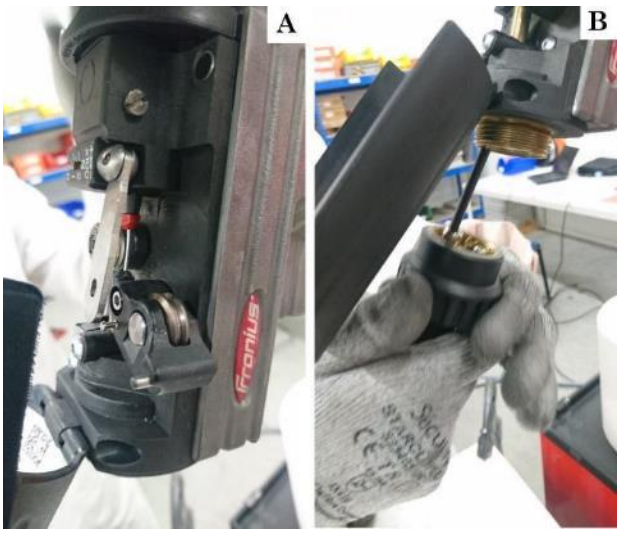

Figure B.42 – Put the wire inside the tube that goes to the nozzle, and tighten the roller again, push a little more wire and then close the cover

- Untighten the nozzle in the torch;

Figure B.43 – Untighten the nozzle in the torch

Figure B.44 – Untighten the nozzles cover

- Until everything is disassembled;

Figure B.45 – Parts that form the nozzle, and tools needed to disassemble them

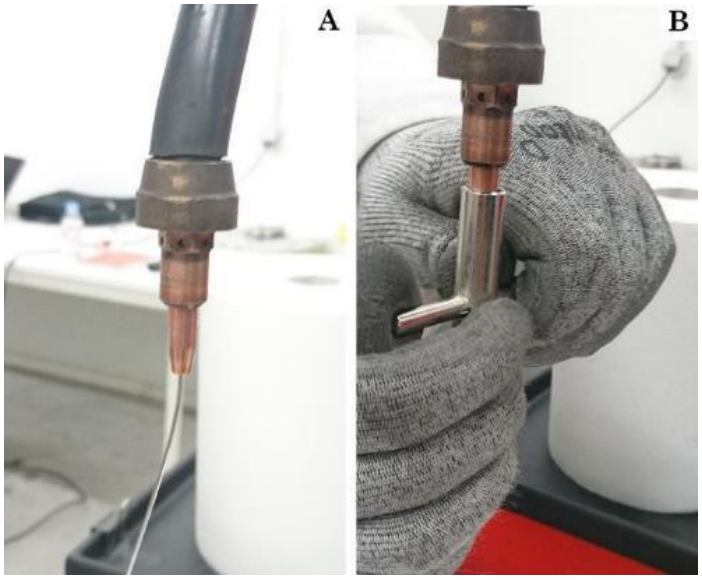

Figure B.46 – A-Push the wire through the torch; B-Tighten the nozzle's interior

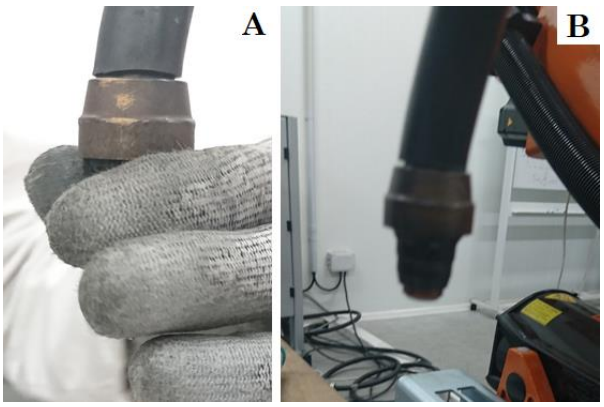

Figure B.47 – Tighten the booth nozzles covers

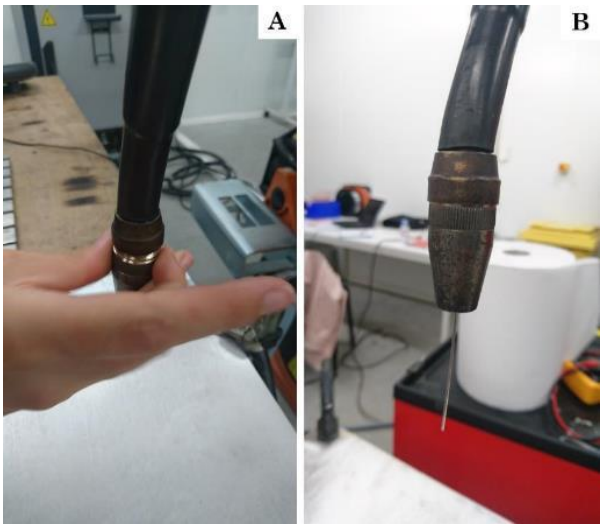

Figure B.47 – A-Tighten the booth nozzles covers; B-Cut the wire with 15 mm until it gets like this

Appendices C

Safety procedures

Safety measures and safety equipment are very important in every type of production.

The demanded safety equipment (Figure C.1) is the proper mask, because there are sparks that can damage directly the eyes and, indirectly, the light and fumes that this type of production produces, is very aggressive to the eyes. The hear protection is also very important as the electric arc makes very loud and consistently sounds. The breading mask is needed because of the toxic fumes that came out from the process.

Figure C.1 – Safety protections

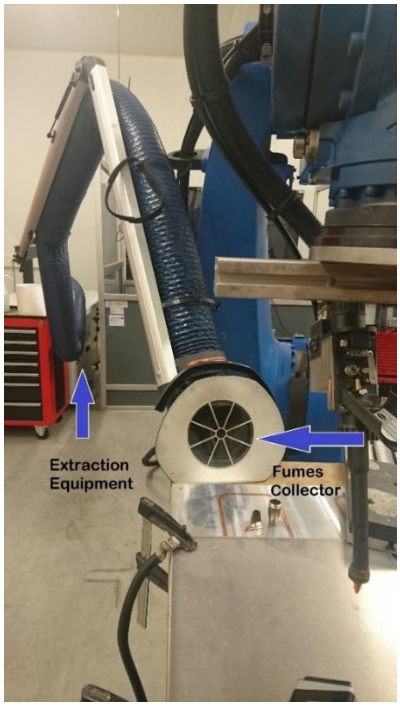

Figure C.2 - Fumes extraction systems (blue arrows)

Another safety measure is the air extraction that has a major importance. When the process is long, the fumes accumulate in closed environments without being noticed so, the extraction prevents it. The location of the extraction needs to be in a position where it does not affect the workability of the robot but, at the same time, allows it to collect all the fumes that is possible.

The dress code is also important. The use of safety shoes and a workshop coat to protect clothes are mandatory. Protective gloves for the heat, when handling the material, is important just after the process. The use of glasses is not user friendly once we already use the mask.

Figure C.3 – Safety shoes with stainless steel toe cap and midsole plate

Figure C.4 – Workshop Coat

Appendices D

Cooling System

The WAAM technology has the characteristic of starting with low temperatures (environmental temperature) and, as the process evolves, the temperature rises. This increment of the temperature of the part, and of the substrate (depending on the number of layers), could reach high temperatures, that can disturb the process, spoiling the material properties and, as a consequence, a poor quality of the final part produced, where there can appear some burns, lack of material properties and some geometry flaws.

To improve the evacuation of the heat from the substrate and the part, a cooling system was developed. With the ability to work without having a direct interaction on the chemical reaction, that is occurring between the torch and the substrate, to prevent the induction of impurities in the process.

The cooling system implemented has the objective of reducing the temperature in the substrate and in the part that is going to be built on top of it.

With that in mind, and due to limited resources and lack of development in this field, there is an aluminium plate with copper channels that are connected to two hoses. One of them is receiving water from a little water pump, which is connected to a 1000 litres tanks with water. The second hose is connected to the other end of the copper channels and returning the water to the tank.

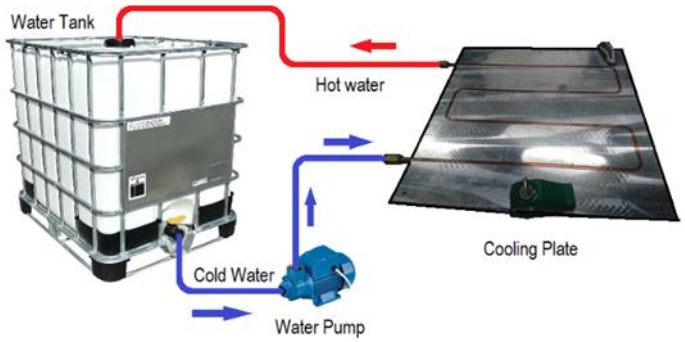

Figure D.1 – Cooling System scheme

With this system, it is possible to accomplish a significant reduction in the substrate plate's temperature and in the part that is being constructed.

Appendices E

Microhardness Analysis from all cords and depositions

Cord 1.0

Table E.1 – Cord 1.0 Vertical Microhardness Values

Cord	D used	Distance in YY	Incremental distance	HV	HRC	Place	Test nr
1.0	60.55	-0.15	-0.15	280.20	27.10	Cord	1
	57.90	-0.17	-0.32	289.70	28.40	Cord	2
	56.60	-0.17	-0.49	285.40	27.90	Cord	3
	57.30	-0.17	-0.67	284.50	27.70	Cord	4
	57.01	-0.17	-0.84	282.10	27.40	Cord	5
	56.84	-0.17	-1.01	289.60	28.40	Cord	6
	55.89	-0.17	-1.17	288.10	28.20	Cord	7
	56.01	-0.17	-1.34	285.90	27.90	Cord	8
	56.94	-0.17	-1.51	288.20	28.20	Cord	9
	56.84	-0.17	-1.68	295.70	29.20	Cord	10
	55.42	-0.17	-1.85	277.40	26.70	Cord	11
	57.56	-0.17	-2.02	279.10	27.00	Cord	12
	57.77	-0.17	-2.20	282.00	27.40	Cord	13
	57.61	-0.17	-2.37	288.90	28.30	Cord	14
	56.55	-0.17	-2.54	278.00	26.80	Cord	15
	58.34	-0.18	-2.71	262.50	24.40	Penetration	16
	60.43	-0.18	-2.90	293.00	28.80	Penetration	17
	56.97	-0.17	-3.07	290.20	28.50	Penetration	18
	57.66	-0.17	-3.24	285.30	27.90	Penetration	19
	57.17	-0.17	-3.41	302.60	30.00	HAZ	20
	54.47	-0.16	-3.57	299.30	29.60	HAZ	21
	54.75	-0.16	-3.74	272.00	26.00	Substrate	22
	57.09	-0.17	-3.91	253.50	22.90	Substrate	23
	60.59	-0.18	-4.09	272.80	26.10	Substrate	24
	58.94	-0.18	-4.27	269.40	25.50	Substrate	25
	59.65	-0.18	-4.45	276.40	26.60	Substrate	26
	58.99	-0.18	-4.62	284.70	27.80	Substrate	27
	56.48	-0.17	-4.79	272.80	26.10	Substrate	28
	59.13	-0.18	-4.97	241.50	20.70	Substrate	29
	61.20	-0.18	-5.15	270.90	25.80	Substrate	30
	57.38	-0.17	-5.33	265.50	24.90	Substrate	31
	57.86	-0.17	-5.50	270.80	25.80	Substrate	32
	58.38	-0.18	-5.68	254.10	23.00	Substrate	33
	58.87	-0.18	-5.85	256.70	23.40	Substrate	34
	60.47	-0.18	-6.03	261.10	24.10	Substrate	35
	59.05	-0.18	-6.21	257.20	23.50	Substrate	36
	60.82	-0.18	-6.40	260.30	24.00	Substrate	37
	58.30	-0.18	-6.58	261.40	24.20	Substrate	38

	60.30	-0.18	-6.76	263.80	24.60	Substrate	39

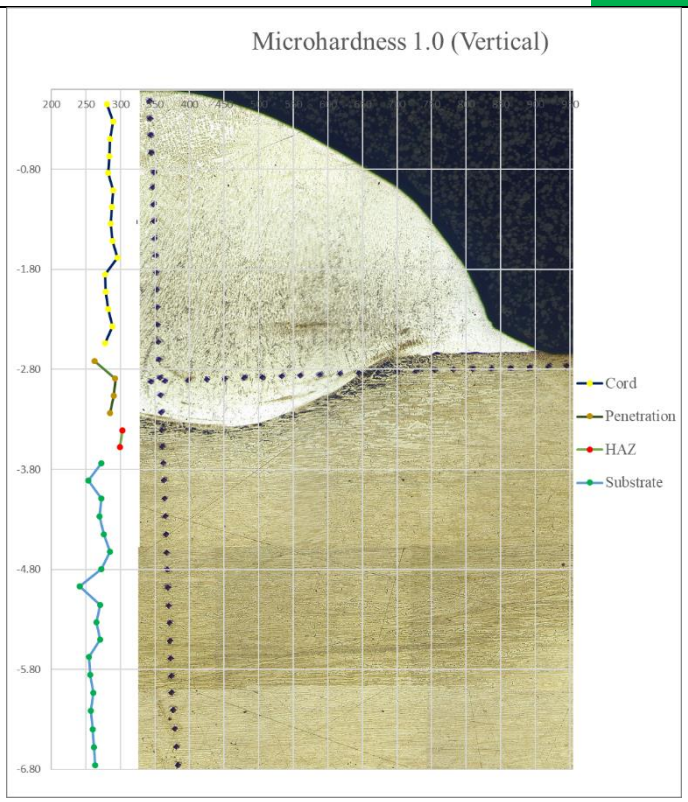

Figure E.1 – Cord 1.0 Vertical Microhardness

Table E.2 – Cord 1.0 Horizontal Microhardness Values

Cord	Distance in xx	D used	Incremental distance	HV	HRC	Place	Test nr
1.0	0.00	62.15	0.00	283.50	27.60	Substrate	1
	0.17	62.15	0.17	293.00	28.80	Substrate	2
	0.17	56.13	0.34	293.20	28.90	Substrate	3
	0.17	55.29	0.50	275.40	26.40	Substrate	4
	0.17	57.36	0.68	282.10	27.40	Substrate	5
	0.17	56.15	0.85	281.30	27.30	Substrate	6
	0.17	56.34	1.01	271.60	25.90	Substrate	7
	0.18	58.77	1.19	281.20	27.30	Substrate	8
	0.17	57.27	1.36	282.60	27.50	Substrate	9
	0.17	56.62	1.53	291.60	28.70	Substrate	10
	0.17	56.05	1.70	281.70	27.30	Substrate	11
	0.17	57.17	1.87	273.10	26.10	Substrate	12
	0.17	58.14	2.05	278.40	26.90	Substrate	13
	0.18	58.87	2.22	278.70	26.90	Substrate	14
	0.17	58.04	2.40	274.90	26.40	Substrate	15
	0.17	56.82	2.57	272.90	26.10	HAZ	16
	0.18	59.29	2.75	287.10	28.10	Transition	17
	0.17	57.62	2.92	292.80	28.80	Penetration	18

	0.17	55.79	3.09	274.90	26.40	Penetration	19
	0.17	58.18	3.26	289.20	28.40	Penetration	20
Cord	Distance in xx	D used	Incremental distance	HV	HRC	Place	Test nr
	0.17	57.69	3.43	300.40	29.80	Penetration	21
	0.17	55.50	3.60	304.60	30.30	Penetration	22
	0.16	54.43	3.76	287.40	28.10	Penetration	23
	0.17	56.63	3.93	298.30	29.50	Penetration	24
	0.17	55.57	4.10	292.10	28.70	Penetration	25
	0.17	56.45	4.27	298.40	29.50	Penetration	26
	0.17	55.20	4.43	289.30	28.40	Penetration	27
	0.17	56.06	4.60	291.80	28.70	Penetration	28
	0.17	56.31	4.77	283.20	27.60	Penetration	29
	0.17	57.52	4.94	294.90	29.10	Penetration	30
	0.17	56.83	5.11	295.30	29.10	Penetration	31
	0.17	56.04	5.28	278.50	26.90	Transition	32
	0.17	58.26	5.46	285.20	27.80	Transition	33
	0.17	56.51	5.63	294.20	29.00	HAZ	34
1.0	0.17	56.30	5.80	290.30	28.50	Substrate	35
	0.17	57.00	5.97	282.00	27.40	Substrate	36
	0.17	55.99	6.14	280.10	27.10	Substrate	37
	0.17	57.70	6.31	280.00	27.10	Substrate	38
	0.17	57.16	6.48	281.90	27.40	Substrate	39
	0.17	56.87	6.65	280.90	27.20	Substrate	40
	0.17	56.02	6.82	281.00	27.20	Substrate	41
	0.17	56.26	6.99	284.40	27.70	Substrate	42
	0.17	57.25	7.16	273.70	26.20	Substrate	43
	0.18	59.24	7.34	288.60	28.30	Substrate	44
	0.17	56.45	7.51	276.80	26.60	Substrate	45
	0.17	57.89	7.68	287.30	28.10	Substrate	46
	0.17	56.71	7.85	292.40	28.80	Substrate	47
	0.17	55.09	8.01	286.40	28.00	Substrate	48
	0.17	55.88	8.18	286.90	28.10	Substrate	49

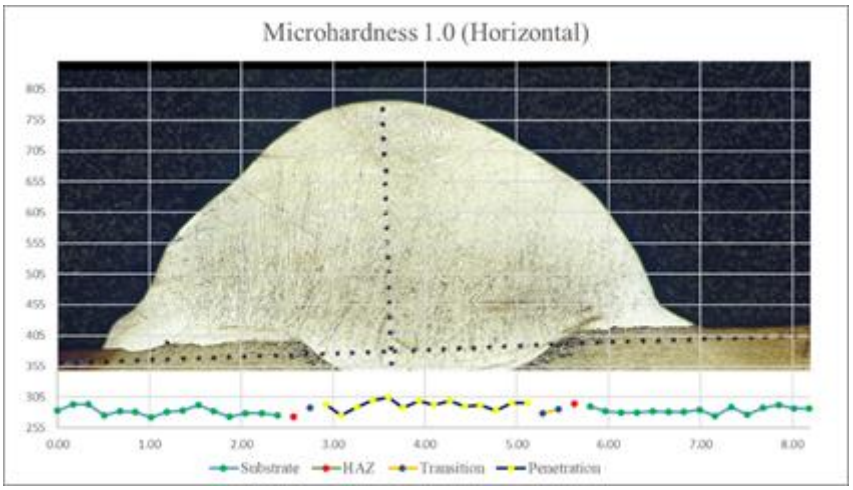

Figure E.2 – Cord 1.0 Horizontal Microhardness

Cord 1.1

Table E.3 – Cord 1.1 Vertical Microhardness Values

Cord	D used	Distance in yy	Incremental Distance	HV	HRC	Place	Test nr
1.1	62.15	-0.155	-0.155	277.60	26.80	Cord	1
	57.83	-0.173	-0.329	278.10	26.80	Cord	2
	58.40	-0.175	-0.504	272.30	26.00	Cord	3
	58.40	-0.175	-0.679	285.90	27.90	Cord	4
	56.01	-0.168	-0.847	279.80	27.10	Cord	5
	57.57	-0.173	-1.020	285.00	27.80	Cord	6
	56.73	-0.170	-1.190	286.90	28.10	Cord	7
	57.19	-0.172	-1.362	282.10	27.40	Cord	8
	57.58	-0.173	-1.535	285.20	27.80	Cord	9
	57.03	-0.171	-1.706	298.40	29.50	Cord	10
	56.86	-0.171	-1.876	283.30	27.60	Cord	11
	57.93	-0.174	-2.050	281.80	27.40	Cord	12
	58.22	-0.175	-2.225	286.30	28.00	Cord	13
	57.20	-0.172	-2.396	300.10	29.70	Cord	14
	55.34	-0.166	-2.562	289.20	28.40	Cord	15
	56.84	-0.171	-2.733	285.50	27.90	Penetration	16
	57.30	-0.172	-2.905	290.20	28.50	Penetration	17
	56.66	-0.170	-3.075	286.10	28.00	Penetration	18
	56.47	-0.169	-3.244	285.20	27.80	HAZ	19
	57.70	-0.173	-3.417	279.30	27.00	HAZ	20
	57.91	-0.174	-3.591	269.50	25.50	Substrate	21
	58.90	-0.177	-3.768	268.50	25.40	Substrate	22
	60.55	-0.182	-3.949	270.30	25.70	Substrate	23
	57.97	-0.174	-4.123	274.10	26.30	Substrate	24
	59.78	-0.179	-4.302	269.90	25.60	Substrate	25
	58.13	-0.174	-4.477	273.90	26.20	Substrate	26

	59.30	-0.178	-4.655	282.80	27.50	Substrate	27
Cord	D used	Distance in yy	Incremental Distance	HV	HRC	Place	Test nr
1.1	57.60	-0.173	-4.828	266.00	25.00	Substrate	28
	59.94	-0.180	-5.007	267.60	25.20	Substrate	29
	58.47	-0.175	-5.183	273.10	26.10	Substrate	30
	57.25	-0.172	-5.355	261.20	24.20	Substrate	31
	58.66	-0.176	-5.531	264.60	24.70	Substrate	32
	59.15	-0.177	-5.708	263.80	24.60	Substrate	33
	60.08	-0.180	-5.888	255.50	23.20	Substrate	34
	59.58	-0.179	-6.067	254.20	23.00	Substrate	35
	61.14	-0.183	-6.250	266.90	25.10	Substrate	36
	58.91	-0.177	-6.427	253.70	22.90	Substrate	37
	61.94	-0.186	-6.613	258.40	23.70	Substrate	38
	60.24	-0.181	-6.794	254.60	23.10	Substrate	39
	61.67	-0.185	-6.979	261.10	24.10	Substrate	40
	59.68	-0.179	-7.158	261.10	24.10	Substrate	41
	59.06	-0.177	-7.335	248.50	22.00	Substrate	42
	61.74	-0.185	-7.520	237.50	19.80	Substrate	43
	63.44	-0.190	-7.710	243.90	21.10	Substrate	44
	61.88	-0.186	-7.896	245.30	21.40	Substrate	45

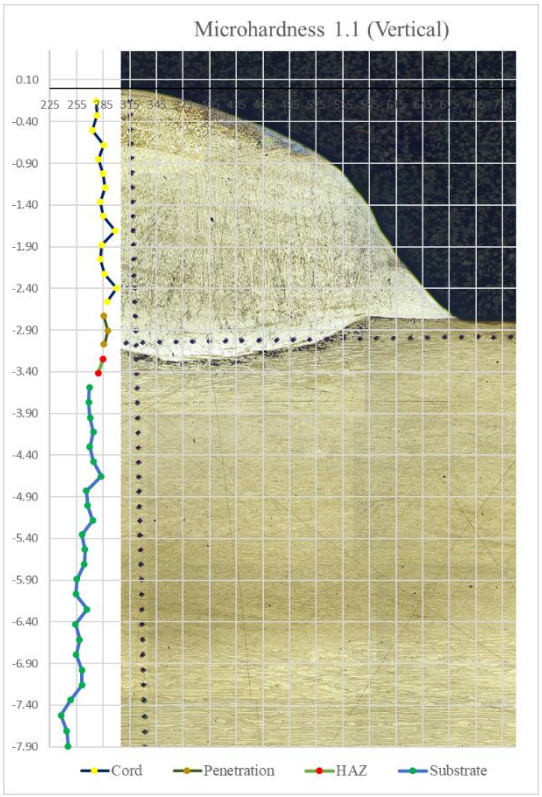

Figure E.3 – Cord 1.1 Vertical Microhardness

Table E.4 – Cord 1.1 Horizontal Microhardness Values

Cord	Distance in xx	D used	Incremental distance	HV	HRC	Place	Test nr
	0.000	62.15	0.000	276.10	26.50	Substrate	1
	0.174	57.95	0.174	276.30	26.60	Substrate	2
	0.174	58.05	0.348	273.30	26.10	Substrate	3
	0.174	57.99	0.522	281.60	27.30	Substrate	4
	0.177	59.02	0.699	283.00	27.50	Substrate	5
	0.172	57.37	0.871	267.80	25.30	Substrate	6
	0.181	60.17	1.052	275.50	26.50	Substrate	7
	0.174	58.05	1.226	288.90	28.30	Substrate	8
	0.168	56.09	1.394	279.50	27.00	Substrate	9
	0.172	57.27	1.566	290.40	28.50	Substrate	10
	0.172	57.24	1.738	286.60	28.00	Substrate	11
	0.170	56.64	1.908	290.60	28.50	Substrate	12
	0.166	55.44	2.074	311.90	31.20	Substrate	13
	0.163	54.40	2.237	296.60	29.30	Substrate	14
	0.168	55.91	2.405	295.50	29.10	Substrate	15
	0.167	55.60	2.572	287.00	28.10	Substrate	16
	0.167	55.81	2.739	279.00	27.00	Substrate	17
	0.169	56.21	2.908	275.20	26.40	Substrate	18
	0.174	57.86	3.081	273.60	26.20	Substrate	19
	0.172	57.23	3.253	279.90	27.10	Substrate	20
1.1	0.173	57.65	3.426	278.90	26.90	Substrate	21
	0.174	58.05	3.600	285.50	27.90	Substrate	22
	0.174	57.88	3.774	281.30	27.30	Substrate	23
	0.172	57.30	3.946	282.60	27.50	Substrate	24
	0.174	58.01	4.120	274.20	26.30	Substrate	25
	0.179	59.69	4.299	281.70	27.30	Substrate	26
	0.174	58.16	4.473	290.40	28.50	Substrate	27
	0.170	56.79	4.643	273.90	26.20	Substrate	28
	0.171	56.94	4.814	284.10	27.70	Substrate	29
	0.171	57.12	4.986	294.00	29.00	Substrate	30
	0.169	56.17	5.154	283.30	27.60	Substrate	31
	0.173	57.73	5.327	291.80	28.70	Substrate	32
	0.171	56.96	5.498	285.80	27.90	Substrate	33
	0.169	56.17	5.667	287.80	28.20	Substrate	34
	0.167	55.72	5.834	278.50	26.90	HAZ	35
	0.170	56.78	6.004	295.90	29.20	HAZ	36
	0.169	56.21	6.173	280.80	27.20	Transition	37
	0.169	56.32	6.342	285.30	27.90	Transition	38
	0.171	57.02	6.513	284.50	27.70	Penetration	39
	0.169	56.42	6.682	290.50	28.50	Penetration	40
	0.169	56.31	6.851	298.90	29.60	Penetration	41

	0.168	56.16	7.020	297.70	29.40	Penetration	42
Cord	Distance in xx	D used	Incremental distance	HV	HRC	Place	Test nr
1.1	0.167	55.55	7.186	289.90	28.40	Penetration	43
	0.165	55.00	7.351	277.60	26.80	Penetration	44
	0.174	58.09	7.526	270.10	25.60	Penetration	45
	0.173	57.82	7.699	289.40	28.40	Penetration	46
	0.170	56.72	7.869	276.60	26.60	Penetration	47
	0.173	57.61	8.042	273.10	26.10	Penetration	48
	0.175	58.18	8.216	276.50	26.60	Penetration	49
	0.171	57.15	8.388	277.00	26.70	Transition	50
	0.169	56.24	8.557	271.90	25.90	Transition	51
	0.173	57.63	8.730	275.20	26.40	HAZ	52
	0.174	57.94	8.903	283.70	27.60	Substrate	53
	0.171	56.99	9.074	277.50	26.70	Substrate	54
	0.169	56.35	9.243	275.80	26.50	Substrate	55
	0.179	59.51	9.422	264.20	24.70	Substrate	56
	0.174	57.92	9.596	274.90	26.40	Substrate	57
	0.173	57.64	9.769	276.30	26.60	Substrate	58
	0.171	56.94	9.939	270.70	25.70	Substrate	59
	0.175	58.28	10.114	269.20	25.50	Substrate	60
	0.178	59.20	10.292	275.10	26.40	Substrate	61
	0.171	57.15	10.463	274.90	26.40	Substrate	62
	0.172	57.25	10.635	266.60	25.10	Substrate	63
	0.176	58.64	10.811	271.30	25.80	Substrate	64
	0.174	57.92	10.985	272.30	26.00	Substrate	65
	0.173	57.58	11.157	266.10	25.00	Substrate	66
	0.176	58.66	11.333	271.30	25.80	Substrate	67
	0.176	58.83	11.510	275.60	26.50	Substrate	68
	0.175	58.39	11.685	272.00	26.00	Substrate	69
	0.172	57.21	11.857	276.10	26.50	Substrate	70
	0.175	58.21	12.031	261.90	24.30	Substrate	71
	0.177	58.85	12.208	262.40	24.40	Substrate	72
	0.181	60.31	12.389	259.40	23.90	Substrate	73
	0.176	58.56	12.565	270.30	25.70	Substrate	74
	0.175	58.32	12.740	277.00	26.70	Substrate	75
	0.174	57.96	12.913	270.50	25.70	Substrate	76

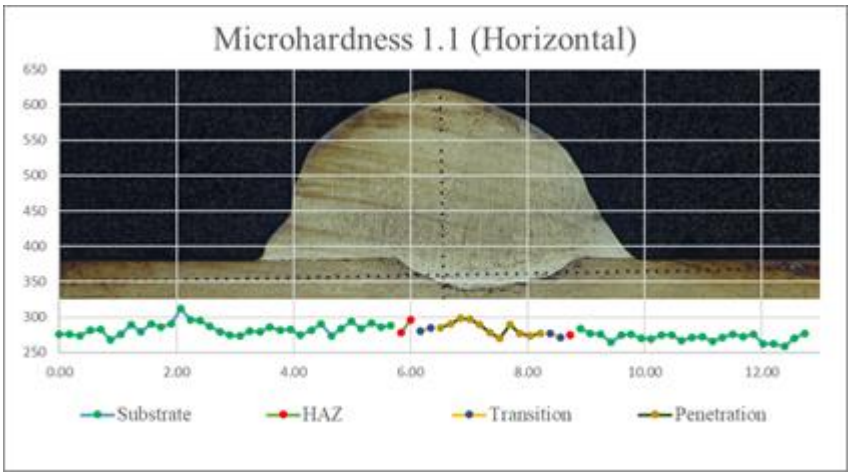

Figure E.4 – Cord 1.1 Horizontal Microhardness

Cord 1.2

Table E.5 – Cord 1.2 Vertical Microhardness Values

Cord	D used	Distance in yy	Incremental distance	HV	HRC	Place	Test nr
	50.29	-0.126	-0.126	282.60	27.50	Cord	1
	56.89	-0.171	-0.296	288.80	28.30	Cord	2
	56.04	-0.140	-0.436	279.40	27.00	Cord	3
	56.69	-0.142	-0.578	283.20	27.60	Cord	4
	56.95	-0.142	-0.721	288.70	28.30	Cord	5
	57.10	-0.143	-0.863	289.40	28.40	Cord	6
	56.30	-0.141	-1.004	295.30	29.10	Cord	7
	55.88	-0.140	-1.144	290.20	28.50	Cord	8
	56.39	-0.141	-1.285	282.30	27.40	Cord	9
	58.14	-0.145	-1.430	290.70	28.50	Cord	10
	56.85	-0.142	-1.572	284.90	27.80	Cord	11
	56.13	-0.140	-1.713	285.30	27.90	Cord	12
1.2	56.03	-0.140	-1.853	285.00	27.80	Cord	13
	56.39	-0.141	-1.994	277.10	26.70	Cord	14
	56.88	-0.142	-2.136	281.70	27.30	Cord	15
	56.78	-0.142	-2.278	292.20	28.70	Cord	16
	56.65	-0.142	-2.419	287.20	28.10	Cord	17
	56.81	-0.142	-2.561	287.80	28.20	Cord	18
	57.29	-0.143	-2.705	288.50	28.30	Cord	19
	56.85	-0.142	-2.847	305.60	30.40	Penetration	20
	55.10	-0.138	-2.985	292.20	28.70	Penetration	21
	56.66	-0.142	-3.126	302.80	30.10	Penetration	22
	56.05	-0.140	-3.266	286.70	28.00	Penetration	23
	56.05	-0.140	-3.406	293.40	28.90	Penetration	24
	57.14	-0.143	-3.549	278.50	26.90	Penetration	25

	57.52	-0.144	-3.693	283.00	27.50	Penetration	26
Cord	D used	Distance in yy	Incremental distance	HV	HRC	Place	Test nr
1.2	58.37	-0.146	-3.839	282.20	27.40	Penetration	27
	57.87	-0.145	-3.984	284.10	27.70	Transition	28
	57.33	-0.143	-4.127	267.80	25.30	Transition	29
	58.22	-0.146	-4.273	271.30	25.80	HAZ	30
	60.40	-0.151	-4.424	273.40	26.10	HAZ	31
	58.08	-0.145	-4.569	272.90	26.10	Substrate	32
	58.07	-0.145	-4.714	274.30	26.30	Substrate	33
	58.08	-0.145	-4.859	265.00	24.80	Substrate	34
	59.81	-0.150	-5.009	263.20	24.50	Substrate	35
	58.81	-0.147	-5.156	264.80	24.80	Substrate	36
	59.42	-0.149	-5.304	270.50	25.70	Substrate	37
	59.90	-0.150	-5.454	262.90	24.40	Substrate	38
	58.77	-0.147	-5.601	251.90	22.60	Substrate	39
	60.26	-0.151	-5.752	260.80	24.10	Substrate	40
	59.39	-0.148	-5.900	267.10	25.10	Substrate	41
	59.55	-0.149	-6.049	259.00	23.80	Substrate	42
	60.32	-0.151	-6.200	255.20	23.20	Substrate	43
	59.54	-0.149	-6.349	258.20	23.70	Substrate	44
	58.92	-0.147	-6.496	253.70	22.90	Substrate	45
	59.88	-0.150	-6.646	254.40	23.00	Substrate	46
	60.25	-0.151	-6.796	269.00	25.50	Substrate	47
	59.03	-0.148	-6.944	242.60	20.90	Substrate	48
	61.41	-0.154	-7.097	245.90	21.50	Substrate	49
	61.70	-0.154	-7.252	247.50	21.90	Substrate	50
	61.78	-0.154	-7.406	247.50	21.90	Substrate	51
	59.80	-0.150	-7.555	243.90	21.10	Substrate	52

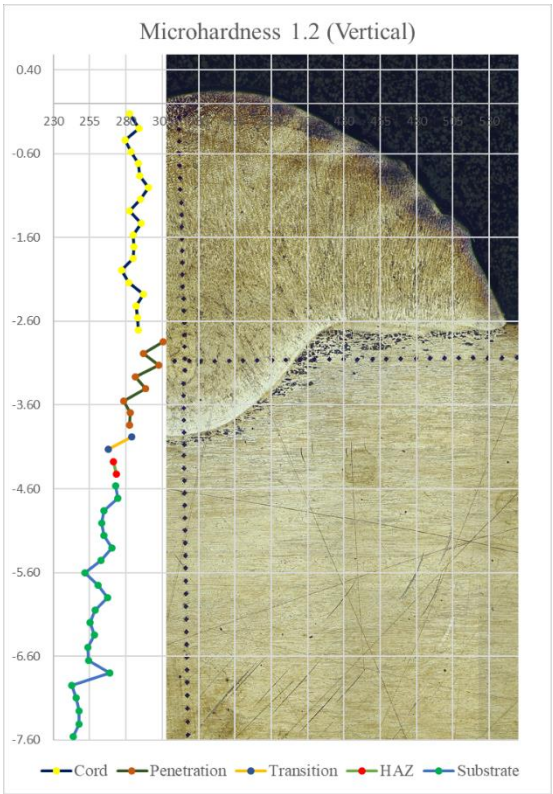

Figure E.5 – Cord 1.2 Vertical's Microhardness

Table E.6 – Cord 1.2 Horizontal Microhardness Values

Cord	Distance in xx	D used	Incremental distance	HV	HRC	Place	Test nr
	0.00	57.07	0.00	272.30	26.00	Substrate	1
	0.18	58.34	0.18	276.60	26.60	Substrate	2
	0.17	56.83	0.35	267.20	25.20	Substrate	3
	0.17	56.65	0.52	280.00	27.10	Substrate	4
	0.17	58.22	0.69	276.70	26.60	Substrate	5
	0.17	58.16	0.86	266.40	25.00	Substrate	6
	0.18	58.55	1.04	263.00	24.50	Substrate	7
	0.17	57.75	1.21	263.80	24.60	Substrate	8
	0.18	60.00	1.39	268.40	25.40	Substrate	9
1.2	0.17	57.17	1.57	264.10	24.60	Substrate	10
	0.18	59.82	1.74	275.70	26.50	Substrate	11
	0.18	58.57	1.92	264.50	24.70	Substrate	12
	0.18	58.88	2.10	276.80	26.60	Substrate	13
	0.17	57.50	2.27	270.10	25.60	Substrate	14
	0.18	58.48	2.44	262.20	24.30	Substrate	15
	0.18	60.25	2.63	267.00	25.10	Substrate	16
	0.18	59.42	2.80	274.40	26.30	Substrate	17
	0.17	56.74	2.97	269.00	25.50	Substrate	18
	0.17	57.83	3.15	278.40	26.90	Substrate	19

	0.17	57.61	3.32	274.50	26.30	Substrate	20
Cord	Distance in xx	D used	Incremental distance	HV	HRC	Place	Test nr
	0.17	57.81	3.49	276.40	26.60	Substrate	21
	0.17	58.23	3.67	290.00	28.50	Substrate	22
	0.17	56.55	3.84	278.70	26.90	Substrate	23
	0.17	57.77	4.01	276.00	26.50	HAZ	24
	0.17	57.99	4.19	284.70	27.80	HAZ	25
	0.17	57.09	4.36	276.10	26.50	HAZ	26
	0.17	56.92	4.53	293.40	28.90	Transition	27
	0.17	55.43	4.69	288.20	28.20	Transition	28
	0.17	56.63	4.86	282.60	27.50	Penetration	29
	0.17	57.38	5.04	292.10	28.70	Penetration	30
	0.17	56.27	5.20	280.60	27.20	Penetration	31
	0.17	57.39	5.38	289.20	28.40	Penetration	32
	0.17	56.37	5.55	282.30	27.40	Penetration	33
	0.18	58.50	5.72	285.60	27.90	Penetration	34
	0.17	57.40	5.89	292.20	28.70	Penetration	35
	0.17	55.74	6.06	282.00	27.40	Penetration	36
	0.17	56.66	6.23	288.10	28.20	Penetration	37
	0.17	56.62	6.40	284.50	27.70	Penetration	38
	0.17	57.43	6.57	289.90	28.40	Penetration	39
	0.17	56.49	6.74	290.70	28.50	Penetration	40
1.2	0.17	56.86	6.91	284.40	27.70	Penetration	41
	0.17	57.00	7.08	288.30	28.20	Penetration	42
	0.17	57.39	7.26	277.60	26.80	Penetration	43
	0.17	57.61	7.43	271.60	25.90	Penetration	44
	0.18	59.30	7.61	269.50	25.50	Penetration	45
	0.17	58.30	7.78	271.20	25.80	Penetration	46
	0.18	58.92	7.96	279.20	27.00	Transition	47
	0.17	57.19	8.13	283.20	27.60	Transition	48
	0.18	58.86	8.31	274.70	26.30	HAZ	49
	0.18	58.36	8.48	272.20	26.00	HAZ	50
	0.17	58.24	8.66	270.10	25.60	HAZ	51
	0.18	59.27	8.83	270.70	25.70	HAZ	52
	0.17	56.98	9.01	267.10	25.10	Substrate	53
	0.18	59.58	9.18	255.00	23.10	Substrate	54
	0.18	61.30	9.37	260.90	24.10	Substrate	55
	0.18	58.47	9.54	272.70	26.10	Substrate	56
	0.18	59.16	9.72	268.80	25.40	Substrate	57
	0.17	57.53	9.89	265.70	24.90	Substrate	58
	0.18	58.64	10.07	277.20	26.70	Substrate	59
	0.17	58.33	10.24	270.00	25.60	Substrate	60

	0.18	58.83	10.42	257.80	23.60	Substrate	61
Cord	Distance in xx	D used	Incremental distance	HV	HRC	Place	Test nr
1.2	0.17	57.69	10.59	277.30	26.70	Substrate	62
	0.18	59.29	10.77	281.70	27.30	CA Substrate	63
	0.17	56.31	10.94	307.90	30.70	CA Substrate	64
	0.16	54.87	11.11	336.20	34.00	CA Substrate	65
	0.16	52.56	11.26	367.30	37.40	CA Substrate	66
	0.15	50.29	11.41	382.40	39.00	CA Substrate	67

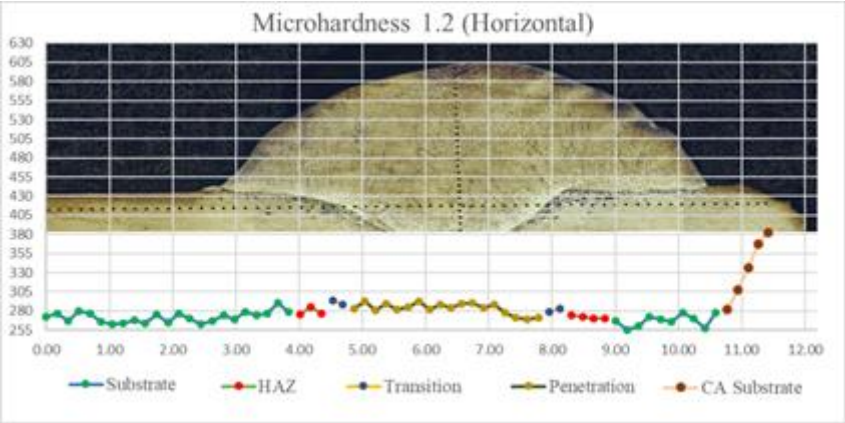

Figure E.6 – Cord 1.2 Horizontal Microhardness

Cord 1.3

Table E.7 – Cord 1.3 Vertical Microhardness Values

Cord	D used	Distance in YY	Incremental distance	HV	HRC	Place	Test nr
	59.25	-0.15	-0.15	288.30	28.20	Cord	1
	55.86	-0.17	-0.32	288.80	28.30	Cord	2
	56.61	-0.17	-0.49	305.80	30.40	Cord	3
	54.12	-0.16	-0.65	289.60	28.40	Cord	4
	55.98	-0.17	-0.82	301.60	29.90	Cord	5
	54.41	-0.16	-0.98	287.20	28.10	Cord	6
	57.42	-0.17	-1.15	296.90	29.30	Cord	7
	56.40	-0.17	-1.32	290.60	28.50	Cord	8
	56.35	-0.17	-1.49	285.50	27.90	Cord	9
	56.24	-0.17	-1.66	297.60	29.40	Cord	10
	55.89	-0.17	-1.83	293.30	28.90	Penetration	11
	56.76	-0.17	-2.00	297.60	29.40	Transition	12
1.3	54.40	-0.16	-2.16	308.80	30.80	HAZ	13
	57.19	-0.17	-2.33	295.90	29.20	Substrate	14
	55.55	-0.17	-2.50	279.40	27.00	Substrate	15
	57.64	-0.17	-2.67	284.80	27.80	Substrate	16
	57.36	-0.17	-2.84	276.50	26.60	Substrate	17
	56.69	-0.17	-3.01	276.30	26.60	Substrate	18
	56.98	-0.17	-3.18	275.80	26.50	Substrate	19
	58.66	-0.18	-3.36	268.90	25.40	Substrate	20
	58.51	-0.18	-3.54	285.20	27.80	Substrate	21
	56.49	-0.17	-3.70	286.90	28.10	Substrate	22
	56.72	-0.17	-3.87	273.90	26.20	Substrate	23
	56.32	-0.17	-4.04	276.70	26.20	Substrate	24
	59.20	-0.18	-4.22	266.40	25.00	Substrate	25

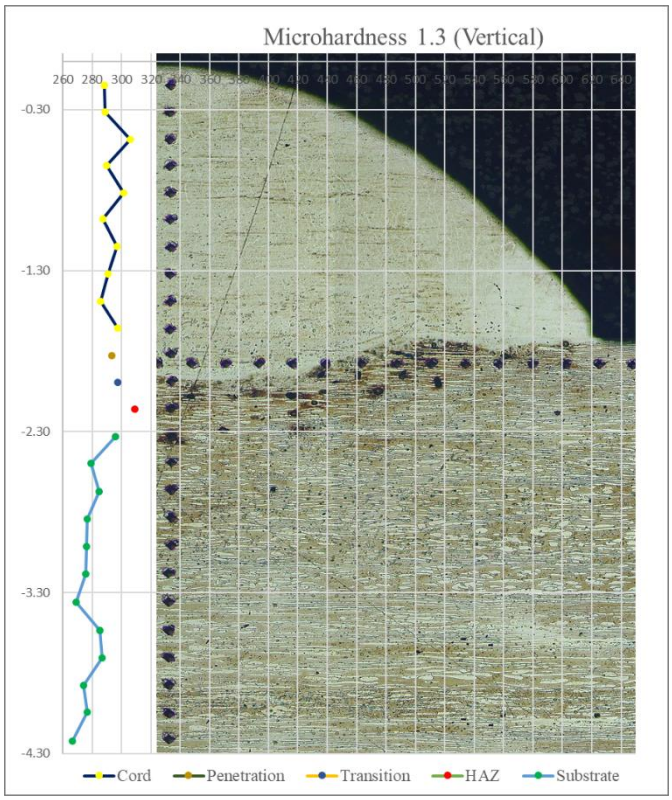

Figure E.7 – Cord 1.3 Vertical Microhardness

Table E.8 – Cord 1.3 Horizontal Microhardness Values

Cord	Distance in xx	D used	Incremental distance	HV	HRC	Place	Test nr
	0.00	59.25	0.00	291.30	28.60	Substrate	1
	0.17	55.34	0.17	281.20	27.30	Substrate	2
	0.17	56.32	0.33	279.30	27.00	Substrate	3
	0.17	56.30	0.50	290.20	28.50	Substrate	4
	0.17	56.29	0.67	293.50	28.90	Substrate	5
	0.17	55.44	0.84	288.30	28.20	Substrate	6
	0.17	55.46	1.01	304.50	30.30	Substrate	7
	0.17	55.06	1.17	282.30	27.40	Substrate	8
	0.17	56.91	1.34	278.40	26.90	Substrate	9
1.3	0.17	57.03	1.51	294.10	29.00	Substrate	10
	0.17	55.96	1.68	287.40	28.10	Substrate	11
	0.17	58.28	1.86	293.80	28.90	Transition	12
	0.17	56.29	2.02	304.40	30.30	Transition	13
	0.16	54.42	2.19	297.20	29.40	Transition	14
	0.17	55.83	2.35	300.20	29.70	Penetration	15
	0.17	55.06	2.52	302.80	30.10	Penetration	16
	0.17	56.01	2.69	291.30	28.60	Penetration	17
	0.17	56.61	2.86	304.30	30.20	Penetration	18
	0.16	54.41	3.02	285.40	27.90	Transition	19

	0.17	57.33	3.19	301.60	29.90	Transition	20
Cord	Distance in xx	D used	Incremental distance	HV	HRC	Place	Test nr
1.3	0.17	55.98	3.36	283.40	27.60	HAZ	21
	0.17	56.18	3.53	293.10	28.80	HAZ	22
	0.16	54.93	3.69	286.60	28.00	HAZ	23
	0.17	55.76	3.86	293.90	28.90	HAZ	24
	0.16	53.42	4.02	287.20	28.10	HAZ	25
	0.17	56.09	4.19	286.10	28.00	HAZ	26
	0.17	57.29	4.36	273.20	26.10	HAZ	27
	0.17	57.77	4.54	281.50	27.30	Substrate	28
	0.17	56.12	4.70	287.40	28.10	Substrate	29
	0.17	56.20	4.87	290.30	28.50	Substrate	30
	0.17	57.53	5.04	277.40	26.70	Substrate	31
	0.17	56.26	5.21	281.10	27.30	Substrate	32
	0.17	58.10	5.39	282.10	27.40	Substrate	33
	0.17	57.18	5.56	290.50	28.50	Substrate	34
	0.17	56.75	5.73	303.30	30.10	Substrate	35
	0.17	55.35	5.90	292.00	28.70	Substrate	36
	0.17	55.00	6.06	303.10	30.10	Substrate	37
	0.17	55.06	6.23	308.70	30.80	Substrate	38
	0.17	55.28	6.39	307.90	30.70	Substrate	39
	0.16	54.01	6.55	298.10	29.50	Substrate	40

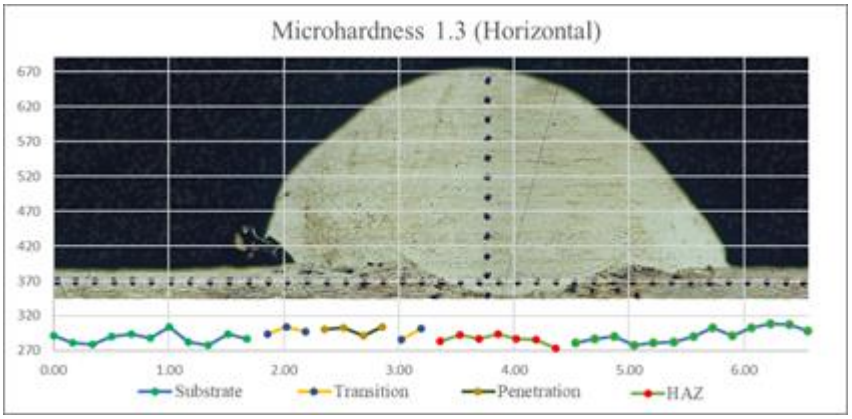

Figure E.8 – Cord 1.3 Horizontal Microhardness

Cord 1.4

Table E.9 – Cord 1.4 Vertical Microhardness Values

Cord	D used	Distance in YY	Incremental distance	HV	HRC	Place	Test nr
	56.25	-0.14	-0.14	274.90	26.40	Cord	1
	57.44	-0.14	-0.28	281.80	27.40	Cord	2
	59.44	-0.15	-0.43	293.20	28.90	Cord	3
	56.60	-0.14	-0.57	288.60	28.30	Cord	4
	57.03	-0.14	-0.72	303.10	30.10	Cord	5
	54.95	-0.14	-0.85	291.50	28.60	Cord	6
	56.34	-0.14	-1.00	297.30	29.40	Cord	7
	56.72	-0.14	-1.14	305.00	30.30	Cord	8
	55.94	-0.14	-1.28	292.50	28.80	Cord	9
	57.28	-0.14	-1.42	293.60	28.90	Cord	10
	55.89	-0.14	-1.56	291.50	28.60	Cord	11
	56.66	-0.14	-1.70	292.20	28.70	Cord	12
	56.86	-0.14	-1.84	292.50	28.80	Cord	13
	56.78	-0.14	-1.99	294.10	29.00	Cord	14
	57.29	-0.14	-2.13	291.20	28.60	Cord	15
	57.24	-0.14	-2.27	286.30	28.00	Cord	16
	58.23	-0.15	-2.42	292.90	28.80	Cord	17
	57.09	-0.14	-2.56	282.20	27.40	Cord	18
	58.17	-0.15	-2.71	295.80	29.20	Penetration	19
1.4	55.54	-0.14	-2.84	294.20	29.00	Penetration	20
	56.51	-0.14	-2.99	292.90	28.80	Penetration	21
	56.92	-0.14	-3.13	296.90	29.30	Transition	22
	55.86	-0.14	-3.27	299.70	29.70	HAZ	23
	55.65	-0.14	-3.41	262.50	24.40	HAZ	24
	58.32	-0.15	-3.55	278.40	26.90	HAZ	25
	56.86	-0.14	-3.69	283.00	27.50	Substrate	26
	57.72	-0.14	-3.84	277.30	26.70	Substrate	27
	57.18	-0.14	-3.98	288.60	28.30	Substrate	28
	55.96	-0.14	-4.12	272.10	26.00	Substrate	29
	59.66	-0.15	-4.27	290.20	28.50	Substrate	30
	55.70	-0.14	-4.41	275.70	26.50	Substrate	31
	58.01	-0.15	-4.56	272.50	26.00	Substrate	32
	58.13	-0.15	-4.70	255.90	23.30	Substrate	33
	62.04	-0.16	-4.86	262.50	24.40	Substrate	34
	59.00	-0.15	-5.00	282.60	27.50	Substrate	35
	57.83	-0.14	-5.15	260.00	24.00	Substrate	36
	58.68	-0.15	-5.29	270.90	25.80	Substrate	37
	59.25	-0.15	-5.44	280.20	27.10	Substrate	38
	58.87	-0.15	-5.59	271.90	25.90	Substrate	39

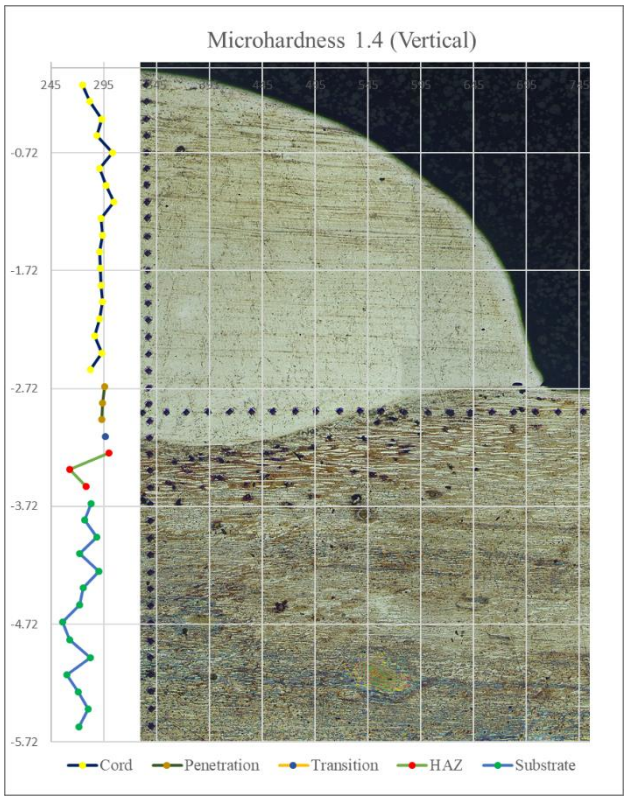

Figure E.9 – Cord 1.4 Vertical Microhardness

Table E.10 – Cord 1.4 Horizontal Microhardness Values

Cord	Distance em xx	D used	Incremental distance	HV	HRC	Place	Test nr
1.4	0.00	60.00	0.00	284.20	27.70	Substrate	1
	0.17	55.94	0.17	277.30	26.70	Substrate	2
	0.17	55.94	0.34	283.50	27.60	Substrate	3
	0.17	57.12	0.51	283.90	27.70	Substrate	4
	0.17	57.75	0.68	301.50	29.90	Substrate	5
	0.17	55.23	0.85	282.10	27.40	Substrate	6
	0.17	58.26	1.02	285.70	27.90	Substrate	7
	0.17	56.63	1.19	297.90	29.40	Substrate	8
	0.17	56.09	1.36	295.80	29.20	Substrate	9
	0.17	55.64	1.53	293.00	28.80	Substrate	10
	0.17	56.22	1.69	296.20	29.20	Substrate	11
	0.17	56.00	1.86	281.40	27.30	Substrate	12
	0.17	57.85	2.04	268.50	25.40	Substrate	13
	0.17	57.00	2.21	281.10	27.30	Substrate	14
	0.17	56.19	2.38	279.00	27.00	Substrate	15
	0.17	56.64	2.55	268.60	25.40	Substrate	16
	0.17	57.62	2.72	337.40	34.10	Substrate	17
	0.16	52.34	2.88	287.50	28.10	Substrate	18
	0.17	56.70	3.05	289.90	28.40	Substrate	19
	0.17	56.97	3.22	295.20	29.10	Transition	20

Cord	Distance em xx	D used	Incremental distance	HV	HRC	Place	Test nr
1.4	0.17	55.20	3.38	298.60	29.50	Transition	21
	0.16	54.84	3.55	278.50	26.90	Transition	22
	0.17	56.85	3.72	292.70	28.80	Penetration	23
	0.16	54.89	3.88	283.30	27.60	Penetration	24
	0.17	56.83	4.05	283.40	27.60	Penetration	25
	0.17	57.52	4.22	299.30	29.60	Penetration	26
	0.16	53.78	4.39	293.50	28.90	Penetration	27
	0.17	56.33	4.56	297.70	29.40	Penetration	28
	0.17	55.03	4.72	299.90	29.70	Penetration	29
	0.17	55.86	4.89	288.80	28.30	Penetration	30
	0.17	56.08	5.06	288.80	28.30	Penetration	31
	0.17	56.40	5.23	289.10	28.30	Penetration	32
	0.17	55.52	5.39	291.90	28.70	Penetration	33
	0.17	57.47	5.56	299.90	29.70	Transition	34
	0.17	55.42	5.73	294.60	29.00	Transition	35
	0.17	55.43	5.90	303.30	30.10	Transition	36
	0.17	55.28	6.06	288.10	28.20	Transition	37
	0.17	57.32	6.23	287.00	28.10	Substrate	38
	0.17	55.55	6.40	299.50	29.60	Substrate	39
	0.16	54.56	6.56	290.60	28.50	Substrate	40
	0.16	54.75	6.73	287.60	28.20	Substrate	41
	0.17	57.15	6.90	283.10	27.50	Substrate	42
	0.17	56.36	7.07	278.60	26.90	Substrate	43
	0.17	56.99	7.24	278.80	26.90	Substrate	44
	0.17	56.86	7.41	279.40	27.00	Substrate	45
	0.17	56.48	7.58	290.00	28.50	Substrate	46
	0.17	55.94	7.75	298.90	29.60	Substrate	47
	0.16	54.84	7.91	273.70	26.20	Substrate	48
	0.17	56.35	8.08	275.10	26.40	Substrate	49
	0.17	58.13	8.26	286.80	28.10	Substrate	50

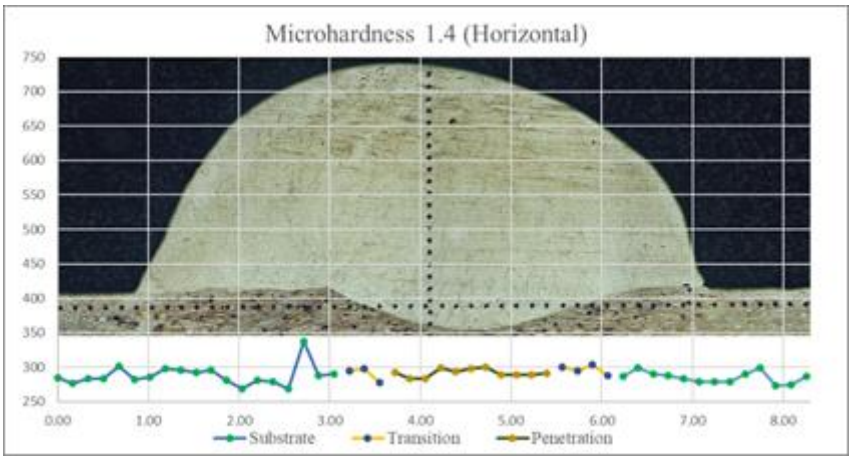

Figure E.10 – Cord 1.4 Horizontal Microhardness

Cord 1.5

Table E.11 – Cord 1.5 Vertical Microhardness Values

Cord	D used	Distance in YY	Incremental distance	HV	HRC	Place	Test nr
1.5	85.25	-0.21	-0.21	277.50	26.70	Cord	1
	80.41	-0.20	-0.41	284.20	27.70	Cord	2
	81.26	-0.20	-0.62	278.80	26.90	Cord	3
	81.93	-0.20	-0.82	290.40	28.50	Cord	4
	80.68	-0.20	-1.02	295.10	29.10	Cord	5
	79.61	-0.20	-1.22	288.10	28.20	Cord	6
	80.35	-0.20	-1.42	283.20	27.60	Cord	7
	79.98	-0.20	-1.62	288.80	28.30	Cord	8
	79.29	-0.20	-1.82	300.20	29.70	Cord	9
	78.30	-0.20	-2.02	292.00	28.70	Cord	10
	80.29	-0.20	-2.22	278.50	26.90	Cord	11
	81.55	-0.20	-2.42	288.90	28.30	Penetration	12
	81.52	-0.20	-2.63	291.20	28.60	Penetration	13
	79.84	-0.20	-2.83	299.40	29.60	Penetration	14
	78.14	-0.20	-3.02	299.70	29.70	Penetration	15
	78.29	-0.20	-3.22	290.10	28.50	Penetration	16
	79.22	-0.20	-3.41	276.40	26.60	HAZ	17
	80.59	-0.20	-3.62	262.80	24.40	HAZ	18
	86.55	-0.22	-3.83	272.40	26.00	Substrate	19
	83.89	-0.21	-4.04	269.30	25.50	Substrate	20
	84.53	-0.21	-4.25	279.10	27.00	Substrate	21
	82.53	-0.21	-4.46	261.50	24.20	Substrate	22
	84.20	-0.21	-4.67	267.60	25.20	Substrate	23
	83.71	-0.21	-4.88	271.80	25.90	Substrate	24
	83.53	-0.21	-5.09	268.50	25.40	Substrate	25
	83.53	-0.21	-5.30	255.70	23.20	Substrate	26

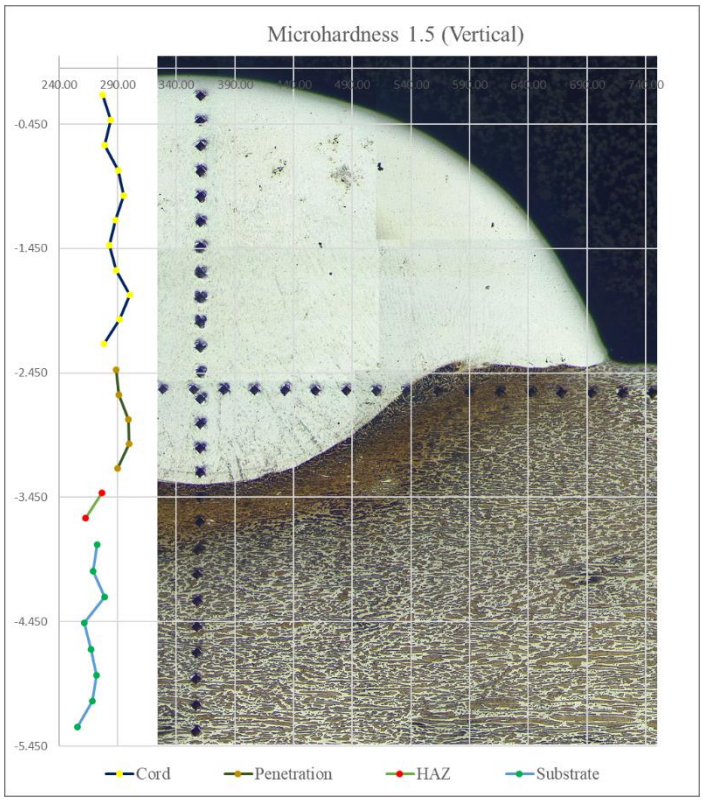

Figure E.11 – Cord 1.5 Vertical Microhardness

Table E.12 – Cord 1.5 Horizontal Microhardness Values

Cord	Distance in XX	D used	Incremental distance	HV	HRC	Place	Test nr
	0.00	82.39	0.00	265.20	24.80	Substrate	1
	0.24	81.62	0.24	264.90	24.80	Substrate	2
	0.25	83.53	0.50	279.60	27.00	Substrate	3
	0.24	80.75	0.74	278.10	26.80	Substrate	4
	0.24	80.89	0.98	282.50	27.50	Substrate	5
	0.24	79.46	1.22	281.30	27.30	Substrate	6
	0.24	79.60	1.46	274.40	26.30	Substrate	7
	0.25	82.20	1.70	274.70	26.30	Substrate	8
	0.24	79.50	1.94	276.50	26.60	Substrate	9
	0.25	81.78	2.19	279.30	27.00	Substrate	10
	0.25	82.78	2.44	289.20	28.40	Substrate	11
	0.24	79.00	2.67	281.50	27.30	HAZ	12
	0.24	80.85	2.92	281.70	27.30	Penetration	13
	0.24	80.59	3.16	281.20	27.30	Penetration	14
	0.24	80.40	3.40	287.30	28.10	Penetration	15
	0.24	79.56	3.64	282.80	27.50	Penetration	16
1.5	0.24	80.98	3.88	294.00	29.00	Penetration	17
	0.24	78.87	4.12	277.60	26.80	Penetration	18
	0.24	81.50	4.36	291.60	28.70	Penetration	19
	0.24	79.85	4.60	288.50	28.30	Penetration	20
	0.24	80.66	4.84	283.30	27.60	Penetration	21
	0.24	80.92	5.09	269.40	25.50	Penetration	22
	0.25	82.65	5.33	273.00	26.10	Penetration	23
	0.24	81.37	5.58	295.60	29.20	Penetration	24
	0.23	77.01	5.81	274.20	26.30	HAZ	25
	0.24	79.21	6.05	296.10	29.20	Substrate	26
	0.24	79.89	6.29	280.70	27.20	Substrate	27
	0.24	78.49	6.52	266.80	25.10	Substrate	28
	0.24	81.64	6.77	273.50	26.20	Substrate	29
	0.24	79.69	7.01	280.70	27.20	Substrate	30
	0.24	80.01	7.25	271.40	25.80	Substrate	31
	0.25	82.87	7.49	283.10	27.50	Substrate	32
	0.24	79.47	7.73	273.60	26.20	Substrate	33

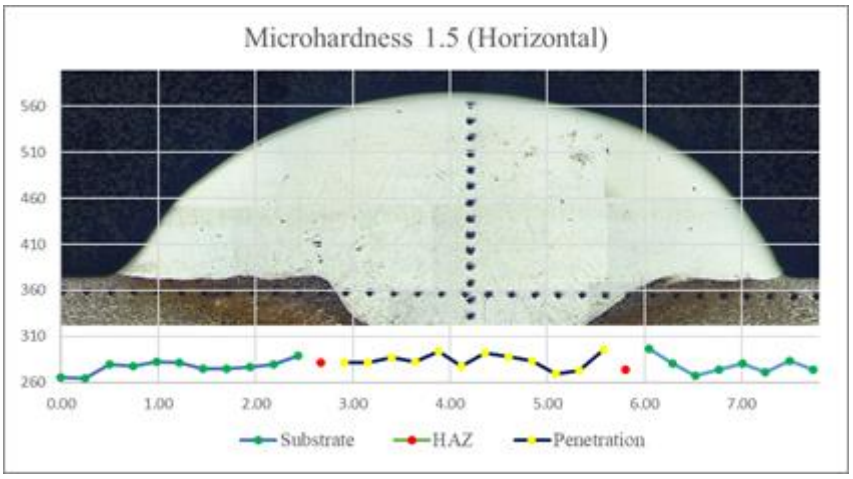

Figure E.12 – Cord 1.5 Horizontal Microhardness

Cord 1.6

Table E.13 – Cord 1.6 Vertical Microhardness Values

Cord	D used	Distance in YY	Incremental distance	HV	HRC	Place	Test nr
	81.33	-0.20	-0.20	274.20	26.30	Cord	1
	81.35	-0.20	-0.41	304.90	30.30	Cord	2
	77.86	-0.19	-0.60	309.10	30.80	Cord	3
	77.77	-0.19	-0.80	307.30	30.60	Cord	4
	78.12	-0.20	-0.99	289.00	28.30	Cord	5
	81.50	-0.20	-1.19	295.60	29.20	Cord	6
	79.79	-0.20	-1.39	285.70	27.90	Cord	7
	81.59	-0.20	-1.60	298.50	29.50	Cord	8
	78.38	-0.20	-1.79	302.60	30.00	Cord	9
	78.75	-0.20	-1.99	294.00	29.00	Cord	10
	78.81	-0.20	-2.19	295.40	29.10	Penetration	11
	77.87	-0.19	-2.38	305.80	30.40	Penetration	12
1.6	79.17	-0.20	-2.58	299.70	29.70	Penetration	13
	79.92	-0.20	-2.78	294.80	29.10	Penetration	14
	80.21	-0.20	-2.98	289.70	28.40	HAZ	15
	81.00	-0.20	-3.18	279.60	27.00	Substrate	16
	82.45	-0.21	-3.39	286.10	28.00	Substrate	17
	80.41	-0.20	-3.59	271.70	25.90	Substrate	18
	84.36	-0.21	-3.80	271.60	25.90	Substrate	19
	84.26	-0.21	-4.01	266.30	25.00	Substrate	20
	83.09	-0.21	-4.22	266.00	25.00	Substrate	21
	84.78	-0.21	-4.43	263.50	24.50	Substrate	22
	85.38	-0.21	-4.65	259.60	23.90	Substrate	23
	85.69	-0.21	-4.86	268.00	25.30	Substrate	24
	81.19	-0.20	-5.06	259.20	23.80	Substrate	25

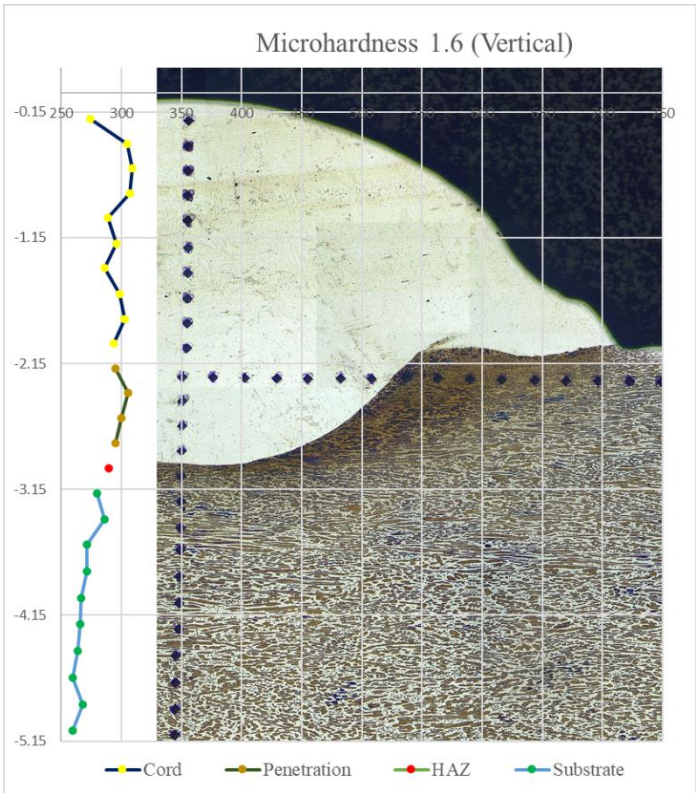

Figure E.13 – Cord 1.6 Vertical Microhardness

Table E.14 – Cord 1.6 Horizontal Microhardness Values

Cord	Distance em XX	D used	Incremental distance	HV	HRC	Place	Test nr
	0.00	85.00	0.00	288.20	28.20	Substrate	1
	0.24	81.64	0.24	270.00	25.60	Substrate	2
	0.24	79.64	0.48	277.30	26.70	Substrate	3
	0.24	80.14	0.72	278.70	26.90	Substrate	4
	0.24	78.76	0.96	281.50	27.30	Substrate	5
	0.25	82.29	1.21	286.10	28.00	Substrate	6
	0.24	81.17	1.45	278.40	26.90	Substrate	7
	0.24	80.18	1.69	275.00	26.40	Substrate	8
	0.24	80.26	1.93	280.00	27.10	HAZ	9
	0.24	80.68	2.17	297.20	29.40	HAZ	10
	0.24	81.57	2.42	282.00	27.40	Transition	11
	0.24	80.03	2.66	278.60	26.90	Penetration	12
	0.25	82.32	2.91	283.40	27.60	Penetration	13
	0.24	79.11	3.14	275.30	26.40	Penetration	14
	0.24	78.38	3.38	292.70	28.80	Penetration	15
	0.23	77.57	3.61	296.00	29.20	Penetration	16
1.6	0.23	77.83	3.84	295.40	29.10	Penetration	17
	0.24	81.10	4.09	289.70	28.40	Penetration	18
	0.24	80.57	4.33	290.20	28.50	Penetration	19
	0.24	79.54	4.57	285.00	27.80	Penetration	20
	0.24	79.31	4.81	285.60	27.90	Penetration	21
	0.24	78.52	5.04	281.00	27.30	Penetration	22
	0.25	82.61	5.29	290.30	28.50	Penetration	23
	0.24	80.99	5.53	272.60	26.00	Transition	24
	0.24	80.80	5.78	274.90	26.40	HAZ	25
	0.25	81.82	6.02	285.40	27.90	HAZ	26
	0.24	80.94	6.26	277.00	26.70	Substrate	27
	0.24	79.79	6.50	281.10	27.30	Substrate	28
	0.24	80.77	6.74	284.70	27.80	Substrate	29
	0.24	79.94	6.98	269.60	25.60	Substrate	30
	0.25	81.84	7.23	277.70	26.80	Substrate	31
	0.24	80.78	7.47	281.50	27.30	Substrate	32
	0.24	81.33	7.72	279.30	27.00	Substrate	33

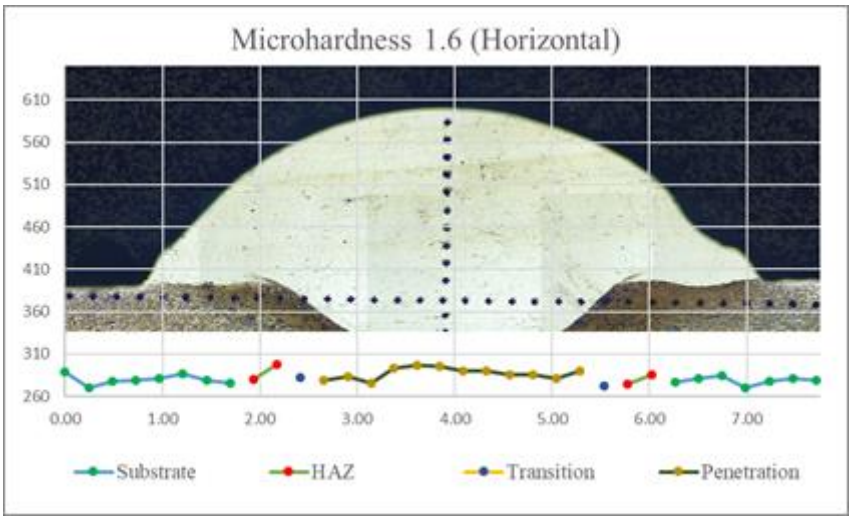

Figure E.14 – Cord 1.6 Horizontal Microhardness

Cord 1.7

Table E.15 – Cord 1.7 Vertical Microhardness Values

Cord	D used	Distance in YY	Incremental distance	HV	HRC	Place	Test nr
1.7	85.23	-0.21	-0.21	275.20	26.40	Cord	1
	82.55	-0.25	-0.46	294.90	29.10	Cord	2
	80.93	-0.24	-0.70	298.40	29.50	Cord	3
	80.20	-0.24	-0.94	298.60	29.50	Cord	4
	80.09	-0.24	-1.18	295.80	29.20	Cord	5
	80.11	-0.24	-1.42	302.10	30.00	Cord	6
	78.40	-0.24	-1.66	292.90	28.80	Cord	7
	79.97	-0.24	-1.90	301.20	29.90	Penetration	8
	79.10	-0.24	-2.14	304.00	30.20	Penetration	9
	77.63	-0.23	-2.37	283.60	27.60	Transition	10
	80.95	-0.24	-2.61	267.70	25.20	HAZ	11
	83.02	-0.25	-2.86	281.10	27.30	HAZ	12
	83.12	-0.25	-3.11	279.40	27.00	Substrate	13
	81.68	-0.25	-3.36	265.80	24.90	Substrate	14
	83.80	-0.25	-3.61	261.10	24.10	Substrate	15
	85.53	-0.26	-3.86	260.50	24.00	Substrate	16
	85.04	-0.26	-4.12	258.30	23.70	Substrate	17
	84.98	-0.25	-4.37	259.30	23.80	Substrate	18
	84.46	-0.25	-4.63	258.30	23.70	Substrate	19
	84.26	-0.25	-4.88	265.90	24.90	Substrate	20
	82.25	-0.25	-5.13	255.20	23.20	Substrate	21
	85.31	-0.26	-5.38	260.60	24.10	Substrate	22

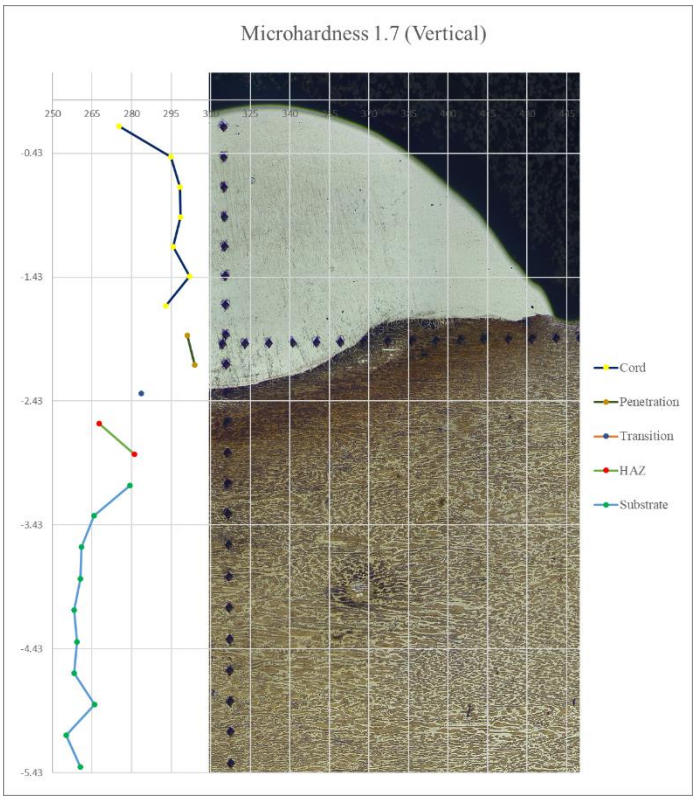

Figure E.15 – Cord 1.7 Vertical Microhardness

Table E.16 – Cord 1.7 Horizontal Microhardness Values

Cord	Distance in XX	D used	Incremental distance	HV	HRC	Place	Test nr
1.7	0.00	0.00	0.00	275.10	26.40	Substrate	1
	0.24	79.51	0.24	269.10	25.50	Substrate	2
	0.24	80.63	0.48	275.80	26.50	Substrate	3
	0.25	82.52	0.73	274.80	26.40	Substrate	4
	0.25	82.33	0.97	297.30	29.40	Substrate	5
	0.24	78.47	1.21	292.80	28.80	Substrate	6
	0.24	79.14	1.45	292.90	28.80	Substrate	7
	0.24	80.31	1.69	277.00	26.70	HAZ	8
	0.24	80.42	1.93	312.40	31.30	Transition	9
	0.23	76.64	2.16	289.00	28.30	Penetration	10
	0.24	80.30	2.40	280.70	27.20	Penetration	11
	0.24	81.00	2.64	305.20	30.40	Penetration	12
	0.23	77.00	2.87	295.20	29.10	Penetration	13
	0.23	78.24	3.11	312.00	31.20	Penetration	14
	0.23	75.73	3.34	294.10	29.00	Penetration	15
	0.24	80.06	3.58	288.30	28.20	Penetration	16
	0.24	79.15	3.81	289.90	28.40	Penetration	17
	0.24	79.25	4.05	287.20	28.10	Penetration	18
	0.24	80.77	4.29	288.20	28.20	Penetration	19
	0.24	79.04	4.53	278.70	26.90	Transition	20
	0.24	81.28	4.78	273.30	26.10	HAZ	21
	0.24	81.07	5.02	278.90	26.90	Substrate	22
	0.24	80.34	5.26	280.30	27.10	Substrate	23
	0.24	80.54	5.50	280.90	27.20	Substrate	24
	0.24	79.18	5.74	278.90	26.90	Substrate	25
	0.24	81.55	5.98	286.30	28.00	Substrate	26
	0.24	78.57	6.22	287.60	28.20	Substrate	27
	0.25	82.48	6.47	280.00	27.10	Substrate	28
	0.24	80.95	6.71	279.50	27.00	Substrate	29
	0.25	81.82	6.95	295.50	29.10	Substrate	30

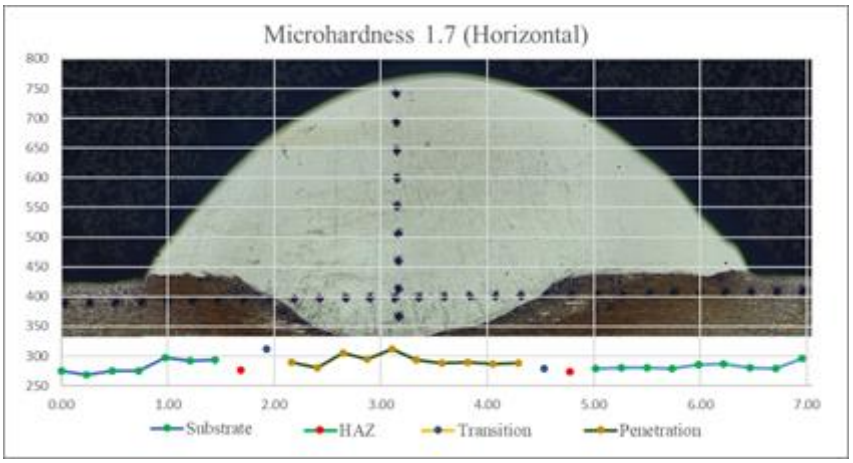

Figure E.16 – Cord 1.7 Horizontal Microhardness

Cord 1.8

Table E.17 – Cord 1.8 Vertical Microhardness Values

Cord	D used	Distance in YY	Incremental distance	HV	HRC	Place	Test nr
1.8	88.35	-0.22	-0.22	288.00	28.20	Cord	1
	80.42	-0.20	-0.42	289.80	28.40	Cord	2
	78.88	-0.20	-0.62	291.70	28.70	Cord	3
	78.86	-0.20	-0.82	301.00	29.80	Cord	4
	79.98	-0.20	-1.02	293.40	28.90	Cord	5
	81.40	-0.20	-1.22	301.90	29.90	Cord	6
	78.24	-0.20	-1.42	299.80	29.70	Cord	7
	78.39	-0.20	-1.61	287.50	28.10	Cord	8
	81.39	-0.20	-1.81	296.40	29.30	Penetration	9
	79.79	-0.20	-2.01	302.90	30.10	Penetration	10
	78.20	-0.20	-2.21	274.90	26.40	Transition	11
	82.66	-0.21	-2.42	273.10	26.10	HAZ	12
	83.48	-0.21	-2.63	277.50	26.70	Substrate	13
	82.74	-0.21	-2.83	283.80	27.60	Substrate	14
	80.90	-0.20	-3.03	268.00	25.30	Substrate	15
	84.29	-0.21	-3.24	277.00	26.70	Substrate	16
	83.04	-0.21	-3.45	267.60	25.20	Substrate	17
	81.97	-0.20	-3.66	260.50	24.00	Substrate	18
	84.18	-0.21	-3.87	276.10	26.50	Substrate	19
	81.47	-0.20	-4.07	259.10	23.80	Substrate	20

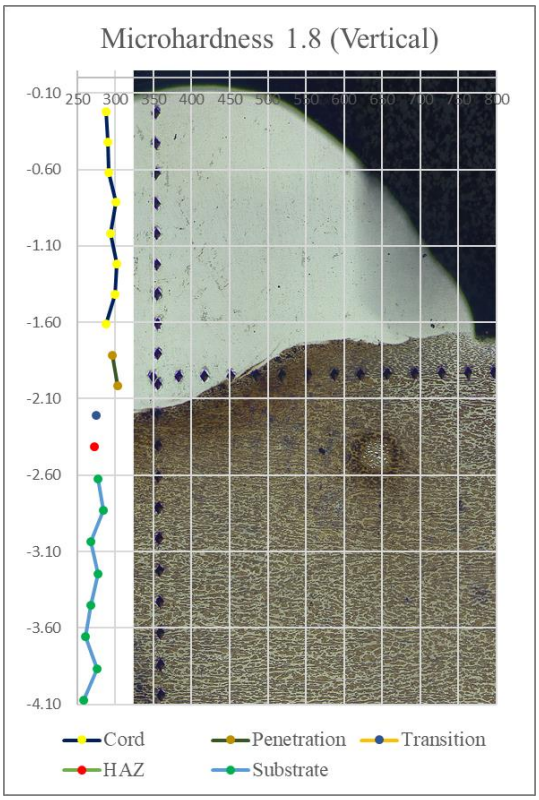

Figure E.17 – Cord 1.8 Vertical Microhardness

Table E.18 – Cord 1.8 Horizontal's Microhardness Values

Cord	Distance in XX	D used	Incremental distance	HV	HRC	Place	Test nr
1.8	0.00	88.35	0.00	265.30	24.80	Substrate	1
	0.26	85.38	0.26	271.70	25.90	Substrate	2
	0.24	79.43	0.49	266.10	25.00	Substrate	3
	0.25	81.90	0.74	278.40	26.90	Substrate	4
	0.24	81.23	0.98	268.10	25.30	Substrate	5
	0.24	80.42	1.23	294.10	29.00	Substrate	6
	0.24	79.73	1.46	288.20	28.20	HAZ	7
	0.24	81.14	1.71	288.20	28.20	Transition	8
	0.24	79.37	1.95	298.10	29.50	Transition	9
	0.24	79.08	2.18	287.70	28.20	Penetration	10
	0.24	79.56	2.42	294.60	29.00	Penetration	11
	0.24	78.62	2.66	294.40	29.00	Penetration	12
	0.24	79.08	2.89	293.00	28.80	Penetration	13
	0.24	79.37	3.13	299.80	29.70	Penetration	14
	0.24	78.89	3.37	280.70	27.20	Penetration	15
	0.24	80.47	3.61	291.20	28.60	Transition	16
	0.24	79.98	3.85	285.00	27.80	Transition	17
	0.24	79.23	4.09	280.70	27.20	HAZ	18
	0.24	81.14	4.33	264.60	24.70	Substrate	19
	0.25	81.71	4.58	282.80	27.50	Substrate	20
	0.24	81.00	4.82	270.50	25.70	Substrate	21
	0.25	82.29	5.07	277.90	26.80	Substrate	22
	0.25	84.15	5.32	270.50	25.70	Substrate	23
	0.25	82.82	5.57	274.00	26.20	Substrate	24
	0.24	80.68	5.81	278.80	26.90	Substrate	25
	0.24	80.72	6.05	271.10	25.80	Substrate	26
	0.24	80.87	6.29	278.80	26.90	Substrate	27
	0.24	81.07	6.538	268.50	25.40	Substrate	28

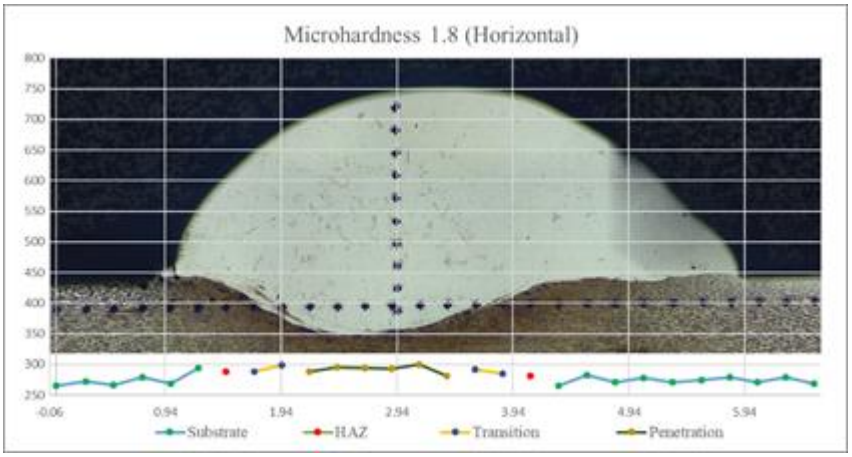

Figure E.1 – Cord 1.8 Horizontal Microhardness

Cord 1.9

Table E.19 – Cord 1.9 Vertical Microhardness Values

Cord	D used	Distance in YY	Incremental Distance	HV	HRC	Place	Test nr
	87.46	-0.22	-0.22	281.90	27.40	Cord	1
	81.89	-0.25	-0.46	291.20	28.60	Cord	2
	80.34	-0.24	-0.71	296.20	29.20	Cord	3
	80.28	-0.24	-0.95	301.20	29.90	Cord	4
	79.50	-0.24	-1.18	306.80	30.60	Cord	5
	78.20	-0.23	-1.42	290.50	28.50	Cord	6
	80.95	-0.24	-1.66	296.90	29.30	Cord	7
1.9	78.58	-0.24	-1.90	287.50	28.10	Cord	8
	80.66	-0.24	-2.14	282.10	27.40	HAZ	9
	80.53	-0.24	-2.38	277.80	26.80	HAZ	10
	83.23	-0.25	-2.63	285.30	27.90	Substrate	11
	79.80	-0.24	-2.87	267.00	25.10	Substrate	12
	82.14	-0.25	-3.12	259.40	23.90	Substrate	13
	85.32	-0.26	-3.37	272.90	26.10	Substrate	14
	81.44	-0.24	-3.62	262.60	24.40	Substrate	15

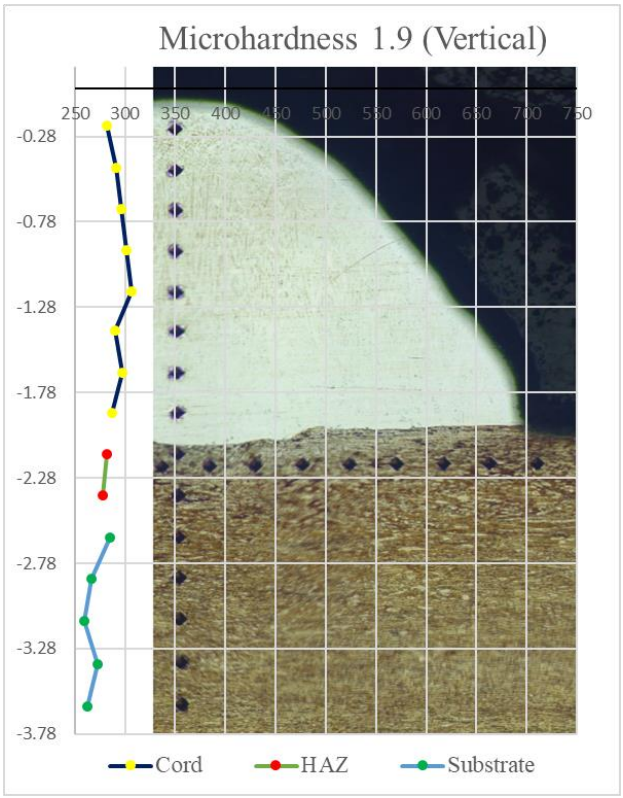

Figure E.19 – Cord 1.9 Vertical's Microhardness

Table E.20 – Cord 1.9 Horizontal's Microhardness Values

Cord	Distance in XX	D used	Incremental distance	HV	HRC	Place	Test nr
	0.00	87.46	0.000	264.20	24.70	Substrate	1
	0.25	83.11	0.249	264.30	24.70	Substrate	2
	0.25	82.85	0.498	274.00	26.20	Substrate	3
	0.24	79.96	0.738	285.30	27.90	Substrate	4
	0.24	81.36	0.982	283.70	27.60	Substrate	5
	0.24	79.65	1.221	291.40	28.60	Substrate	6
	0.23	78.11	1.455	277.90	26.80	Substrate	7
	0.24	81.57	1.700	279.10	27.00	Substrate	8
	0.24	80.02	1.940	275.10	26.40	Substrate	9
	0.24	80.91	2.183	283.10	27.50	HAZ	10
	0.24	80.40	2.424	268.30	25.30	HAZ	11
1.9	0.25	82.74	2.672	279.70	27.10	HAZ	12
	0.24	80.49	2.914	280.40	27.20	HAZ	13
	0.24	79.32	3.151	276.70	26.60	HAZ	14
	0.24	79.21	3.389	275.70	26.50	HAZ	15
	0.25	82.25	3.636	276.50	26.60	Substrate	16
	0.24	80.59	3.878	266.70	25.10	Substrate	17
	0.25	82.99	4.127	293.60	28.90	Substrate	18
	0.24	78.93	4.363	286.20	28.00	Substrate	19
	0.24	79.81	4.603	280.50	27.20	Substrate	20
	0.25	81.77	4.848	276.70	26.60	Substrate	21
	0.24	80.48	5.090	276.20	26.60	Substrate	22
	0.25	82.13	5.336	270.60	25.70	Substrate	23

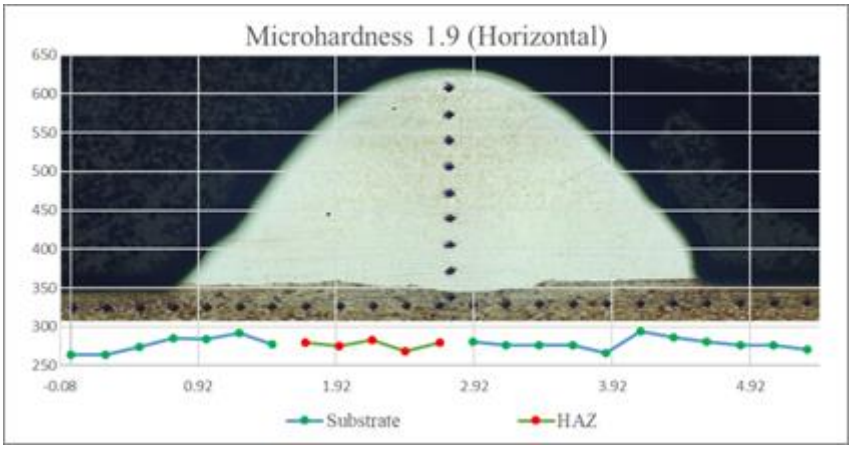

Figure E.20 – Cord 1.9 Horizontal Microhardness

Cord 2.0

Table E.21 – Cord 2.0 Vertical Microhardness Values

Cord	D used	Distance in YY	Incremental distance	HV	HRC	Place	Test
2.0	87.46	-0.22	-0.22	277.90	26.80	Cord	1
	83.04	-0.25	-0.47	282.50	27.50	Cord	2
	80.62	-0.24	-0.71	284.40	27.70	Cord	3
	80.86	-0.24	-0.95	293.80	28.90	Cord	4
	79.79	-0.24	-1.19	282.10	27.40	Cord	5
	80.45	-0.24	-1.43	285.40	27.90	Cord	6
	78.77	-0.24	-1.67	284.40	27.70	Cord	7
	79.55	-0.24	-1.91	289.40	28.40	Cord	8
	79.19	-0.24	-2.15	293.20	28.90	Penetration	9
	77.42	-0.23	-2.38	289.60	28.40	Penetration	10
	79.05	-0.24	-2.61	284.20	27.70	Penetration	11
	80.09	-0.24	-2.86	285.80	27.90	Penetration	12
	79.78	-0.24	-3.09	276.70	26.60	HAZ	13
	80.20	-0.24	-3.34	273.60	26.20	HAZ	14
	81.46	-0.24	-3.58	275.60	26.50	Substrate	15
	81.42	-0.24	-3.82	257.80	23.60	Substrate	16
	82.93	-0.25	-4.07	280.40	27.20	Substrate	17
	80.77	-0.24	-4.31	253.00	22.80	Substrate	18
	85.57	-0.26	-4.57	258.80	23.80	Substrate	19
	85.32	-0.26	-4.83	253.40	22.90	Substrate	20

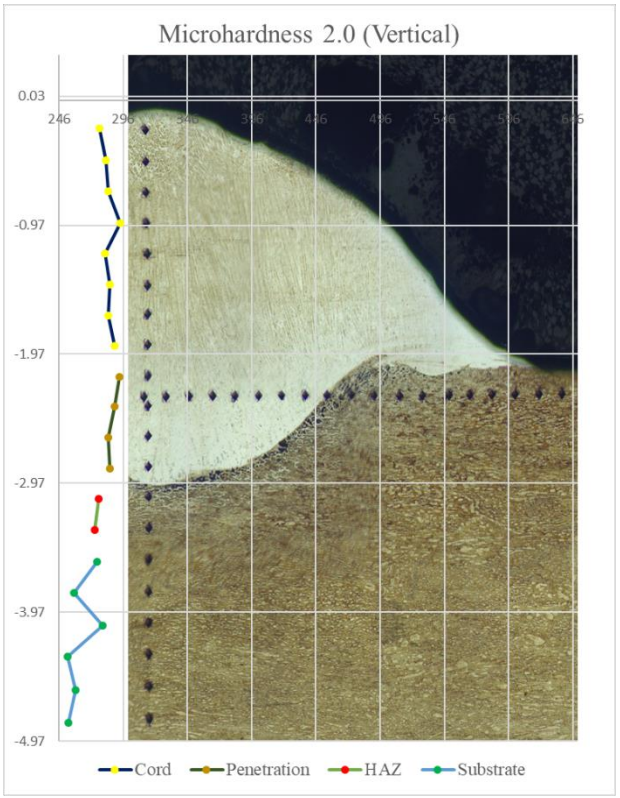

Figure E.21 – Cord 2.0 Vertical's Microhardness

Table E.22 – Cord 2.0 Horizontal's Microhardness Values

Cord	Distance in XX	D used	Incremental distance	HV	HRC	Place	Test nr
	0.00	87.46	0.00	262.70	24.40	Substrate	1
	0.25	83.98	0.25	268.00	25.30	Substrate	2
	0.24	81.63	0.50	264.20	24.70	Substrate	3
	0.25	82.87	0.75	269.90	25.60	Substrate	4
	0.25	82.35	0.99	266.30	25.00	Substrate	5
	0.25	81.87	1.24	265.70	24.90	Substrate	6
	0.25	81.84	1.48	270.40	25.70	Substrate	7
	0.24	80.33	1.72	279.60	27.00	Substrate	8
	0.24	79.16	1.96	264.10	24.60	Substrate	9
	0.25	83.76	2.21	280.60	27.20	Substrate	10
	0.24	81.03	2.46	266.70	25.10	HAZ	11
	0.25	82.08	2.70	253.80	22.90	HAZ	12
	0.25	84.69	2.96	274.60	26.30	HAZ	13
	0.24	81.20	3.20	279.40	27.00	Penetration	14
	0.25	81.82	3.45	274.90	26.40	Penetration	15
	0.25	82.34	3.69	281.10	27.30	Penetration	16
	0.24	80.61	3.93	291.00	28.60	Penetration	17
	0.24	78.79	4.17	300.20	29.70	Penetration	18
	0.24	78.80	4.41	289.60	28.40	Penetration	19
	0.24	78.71	4.64	293.00	28.80	Penetration	20
2.0	0.24	78.66	4.88	286.30	28.00	Penetration	21
	0.24	78.83	5.12	288.90	28.30	Penetration	22
	0.24	79.79	5.36	284.50	27.70	Penetration	23
	0.24	79.70	5.59	289.00	28.30	Penetration	24
	0.24	80.80	5.84	280.40	27.20	Penetration	25
	0.24	80.34	6.08	287.50	28.10	Penetration	26
	0.24	80.30	6.32	288.90	28.30	Penetration	27
	0.23	78.21	6.55	272.50	26.00	Transition	28
	0.25	82.00	6.80	269.70	25.60	HAZ	29
	0.24	81.56	7.04	273.30	26.10	HAZ	30
	0.25	84.48	7.30	280.80	27.20	Substrate	31
	0.24	79.89	7.54	266.10	25.00	Substrate	32
	0.25	81.70	7.78	273.70	26.20	Substrate	33
	0.25	81.88	8.03	292.80	28.80	Substrate	34
	0.24	78.60	8.26	283.40	27.60	Substrate	35
	0.24	79.46	8.50	277.10	26.70	Substrate	36
	0.25	81.94	8.75	271.40	25.90	Substrate	37
	0.24	81.33	8.99	268.90	25.40	Substrate	38
	0.24	81.51	9.24	269.50	25.50	Substrate	39
	0.24	81.53	9.48	267.00	25.10	Substrate	40
	0.25	83.69	9.73	261.30	24.20	Substrate	41

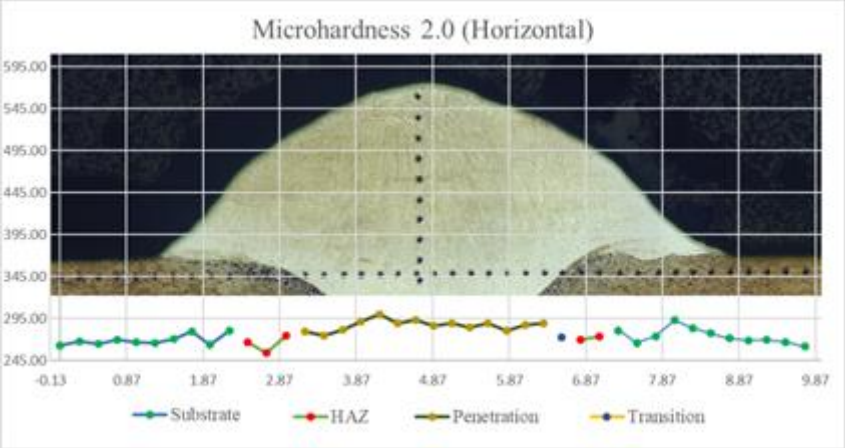

Figure E.22 – Cord 2.0 Horizontal Microhardness

Cord 2.1

Table E.23– Cord 2.1 Vertical Microhardness Values

Cord	D used	Distance in YY	Incremental distance	HV	HRC	Place	Test nr
2.1	87.46	-0.22	-0.22	279.70	27.10	Cord	1
	81.13	-0.24	-0.46	278.70	26.90	Cord	2
	82.32	-0.25	-0.71	291.50	28.60	Cord	3
	79.34	-0.24	-0.95	292.00	28.70	Cord	4
	79.38	-0.24	-1.19	277.20	26.70	Cord	5
	81.67	-0.25	-1.43	292.30	28.70	Cord	6
	78.57	-0.24	-1.67	285.10	27.80	Cord	7
	79.64	-0.24	-1.90	283.00	27.50	Cord	8
	81.67	-0.25	-2.15	283.80	27.60	Penetration	9
	81.78	-0.25	-2.40	286.80	28.10	Penetration	10
	81.06	-0.24	-2.64	287.90	28.20	Penetration	11
	80.09	-0.24	-2.88	286.00	28.00	Penetration	12
	80.98	-0.24	-3.12	279.10	27.00	Penetration	13
	82.41	-0.25	-3.37	286.50	28.00	Penetration	14
	80.30	-0.24	-3.61	275.50	26.50	HAZ	15
	81.40	-0.24	-3.85	258.40	23.70	Substrate	16
	84.92	-0.25	-4.11	269.60	25.60	Substrate	17
	83.93	-0.25	-4.36	267.00	25.10	Substrate	18
	84.06	-0.25	-4.61	261.30	24.20	Substrate	19
	85.48	-0.26	-4.87	259.10	23.80	Substrate	20
	85.90	-0.26	-5.13	253.30	22.80	Substrate	21
	85.61	-0.26	-5.38	257.90	23.60	Substrate	22

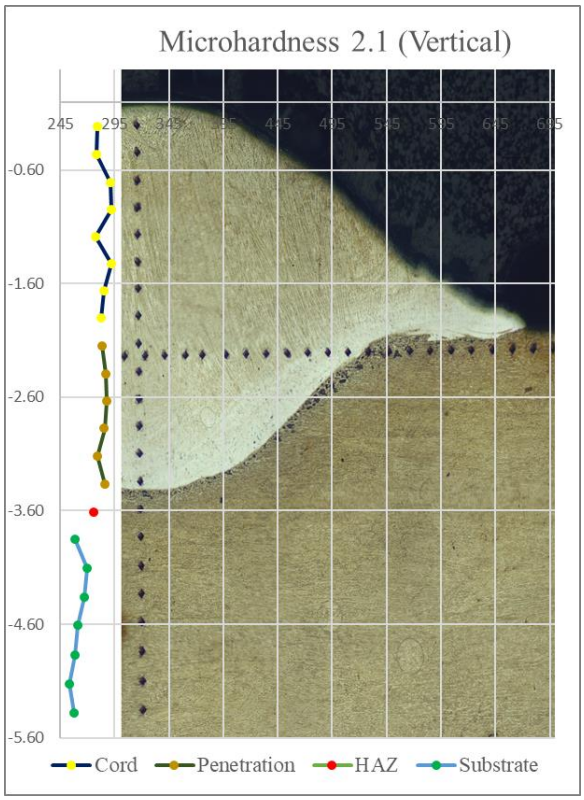

Figure E.23 – Cord 2.1 Vertical Microhardness

Table E.24 – Cord 2.1 Horizontal Microhardness Values

Cord	Distance in xx	D used	Incremental distance	HV	HRC	Place	Test nr
2.1	0.00	87.46	0.00	255.10	23.10	Substrate	1
	0.25	84.17	0.25	257.40	23.50	Substrate	2
	0.25	84.76	0.51	256.90	23.40	Substrate	3
	0.26	86.10	0.77	261.50	24.20	Substrate	4
	0.25	84.85	1.02	252.50	22.70	Substrate	5
	0.26	86.31	1.28	258.90	23.80	HAZ	6
	0.25	84.05	1.53	264.60	24.70	Transition	7
	0.25	83.77	1.78	280.40	27.20	Penetration	8
	0.24	80.68	2.02	292.60	28.80	Penetration	9
	0.24	79.50	2.26	278.70	26.90	Penetration	10
	0.25	82.10	2.51	290.10	28.50	Penetration	11
	0.24	79.94	2.75	279.10	27.00	Penetration	12
	0.25	82.40	3.00	287.70	28.20	Penetration	13
	0.25	81.70	3.24	283.60	27.60	Penetration	14
	0.24	79.19	3.48	285.00	27.80	Penetration	15
	0.24	79.48	3.72	283.30	27.60	Penetration	16
	0.24	79.43	3.96	286.70	28.00	Penetration	17
	0.23	78.29	4.19	289.70	28.40	Penetration	18
	0.23	77.77	4.42	290.20	28.50	Penetration	19
	0.24	79.87	4.66	286.40	28.00	Penetration	20

Cord	Distance in xx	D used	Incremental distance	HV	HRC	Place	Test nr
2.1	0.24	78.59	4.90	290.30	28.50	Penetration	21
	0.24	78.49	5.13	274.10	26.30	Penetration	22
	0.24	81.00	5.38	273.70	26.20	Penetration	23
	0.25	82.26	5.62	287.10	28.10	Penetration	24
	0.24	81.00	5.87	284.00	27.70	Penetration	25
	0.24	78.96	6.10	271.00	25.80	Penetration	26
	0.25	83.84	6.36	290.90	28.60	Penetration	27
	0.24	79.67	6.59	282.80	27.50	Penetration	28
	0.24	79.64	6.83	280.50	27.20	Penetration	29
	0.24	81.03	7.08	277.70	26.80	Penetration	30
	0.24	80.81	7.32	271.90	25.90	Transition	31
	0.25	83.19	7.57	275.70	26.50	HAZ	32
	0.24	81.50	7.81	281.40	27.30	HAZ	33
	0.24	80.07	8.05	275.20	26.40	Substrate	34
	0.24	81.44	8.30	275.60	26.50	Substrate	35
	0.25	81.70	8.54	273.20	26.10	Substrate	36
	0.25	81.90	8.79	279.10	27.00	Substrate	37
	0.24	79.81	9.03	260.90	24.10	Substrate	38
	0.25	83.29	9.28	284.10	27.70	Substrate	39
	0.24	79.72	9.52	271.90	25.90	Substrate	40
	0.24	81.00	9.76	253.30	22.80	Substrate	41
	0.26	85.31	10.02	258.80	23.80	Substrate	42

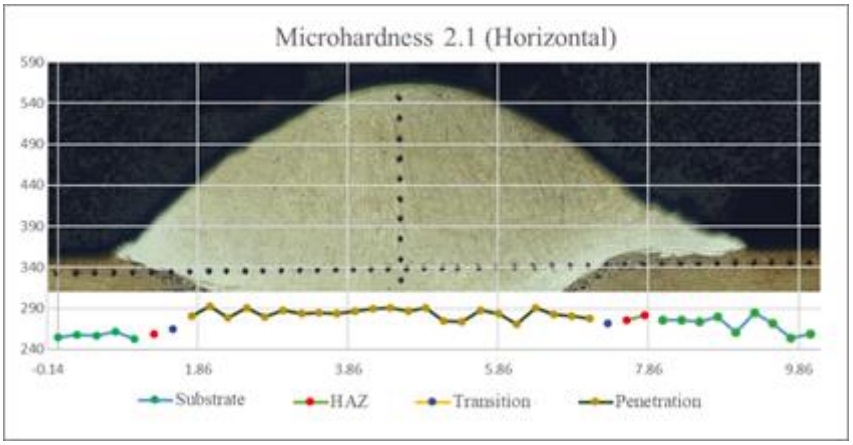

Figure E.24 – Cord 2.1 Horizontal Microhardness

Cord 2.2

Table E.25 – Cord 2.2 Vertical Microhardness Values

Cord	D used	Distance in YY	Incremental distance	HV	HRC	Place	Test nr
	87.46	-0.22	-0.22	278.70	26.90	Cord	1
	81.14	-0.24	-0.46	284.90	27.80	Cord	2
	80.35	-0.24	-0.70	287.30	28.10	Cord	3
	79.75	-0.24	-0.94	281.40	27.30	Cord	4
	80.94	-0.24	-1.19	276.50	26.60	Cord	5
	82.16	-0.25	-1.43	275.90	26.50	Cord	6
	82.38	-0.25	-1.68	276.50	26.60	Cord	7
	82.77	-0.25	-1.93	275.20	26.40	Cord	8
	82.11	-0.25	-2.17	284.00	27.70	Cord	9
	81.37	-0.24	-2.42	269.10	25.50	Penetration	10
	82.67	-0.25	-2.67	281.80	27.40	Penetration	11
2.2	81.75	-0.25	-2.91	275.60	26.50	Penetration	12
	83.10	-0.25	-3.16	277.10	26.70	Penetration	13
	82.41	-0.25	-3.41	286.10	28.00	Penetration	14
	80.39	-0.24	-3.65	285.40	27.90	Penetration	15
	81.65	-0.24	-3.89	287.30	28.10	Penetration	16
	81.09	-0.24	-4.14	277.40	26.70	Transition	17
	83.06	-0.25	-4.39	264.80	24.80	HAZ	18
	85.00	-0.26	-4.64	262.80	24.40	Substrate	19
	84.63	-0.25	-4.89	262.00	24.30	Substrate	20
	84.24	-0.25	-5.15	260.90	24.10	Substrate	21
	84.61	-0.25	-5.40	261.00	24.10	Substrate	22
	86.03	-0.26	-5.66	263.30	24.50	Substrate	23

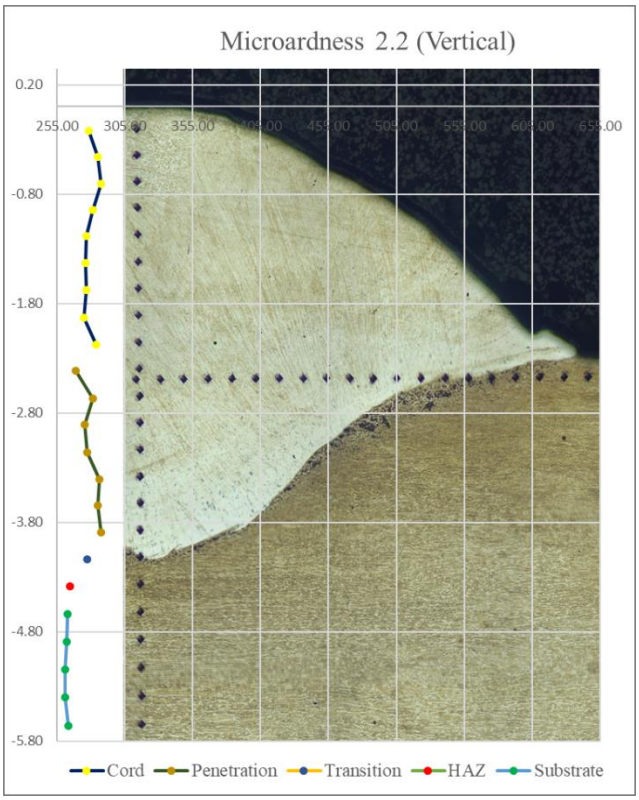

Figure E.25 – Cord 2.2 Vertical Microhardness

Table E.26 – Cord 2.2 Horizontal's Microhardness Values

Cord	Distance in XX	D used	Incremental distance	HV	HRC	Place	Test nr
2.2	0.00	87.46	0.00	260.00	24.00	Substrate	1
	0.25	84.35	0.25	260.30	24.00	Substrate	2
	0.26	86.91	0.51	272.70	26.10	Substrate	3
	0.25	82.93	0.76	254.20	23.00	Substrate	4
	0.26	87.27	1.02	276.90	26.60	Transition	5
	0.24	80.08	1.26	277.40	26.70	Penetration	6
	0.25	81.91	1.51	273.20	26.10	Penetration	7
	0.25	82.72	1.76	277.80	26.80	Penetration	8
	0.25	81.73	2.00	267.70	25.20	Penetration	9
	0.25	82.64	2.25	282.80	27.50	Penetration	10
	0.24	80.66	2.49	286.90	28.10	Penetration	11
	0.24	79.25	2.73	286.70	28.00	Penetration	12
	0.24	80.11	2.97	285.00	27.80	Penetration	13
	0.24	79.57	3.21	285.80	27.90	Penetration	14
	0.24	79.00	3.45	287.60	28.20	Penetration	15
	0.24	80.35	3.69	284.20	27.70	Penetration	16
	0.24	79.02	3.93	268.40	25.40	Penetration	17
	0.25	84.79	4.18	277.90	26.80	Penetration	18
	0.24	81.52	4.42	279.30	27.00	Penetration	19
	0.24	80.33	4.67	273.00	26.10	Penetration	20
	0.24	81.39	4.91	267.00	25.10	Penetration	21
	0.25	83.50	5.16	275.10	26.40	Penetration	22
	0.24	81.65	5.41	267.40	25.20	Penetration	23
	0.25	82.54	5.65	273.10	26.10	Penetration	24
	0.24	81.11	5.90	287.20	28.10	Penetration	25
	0.24	78.63	6.13	284.30	27.70	Penetration	26
	0.24	79.62	6.37	278.80	26.90	Penetration	27
	0.24	79.94	6.61	281.70	27.30	Penetration	28
	0.24	80.29	6.85	274.40	26.30	Penetration	29
	0.25	82.70	7.10	280.60	27.20	Penetration	30
	0.24	81.17	7.34	283.20	27.60	Transition	31
	0.24	80.76	7.59	278.60	26.90	Transition	32
	0.24	81.60	7.83	276.20	26.60	HAZ	33
	0.24	80.39	8.07	265.60	24.90	HAZ	34
	0.25	83.28	8.32	267.60	25.20	Substrate	35
	0.25	83.52	8.57	265.30	24.80	Substrate	36
	0.25	83.51	8.82	262.10	24.30	Substrate	37
	0.25	83.01	9.07	269.70	25.60	Substrate	38
	0.25	82.16	9.32	270.90	25.80	Substrate	39
	0.25	82.58	9.57	256.90	23.40	Substrate	40
	0.26	85.16	9.82	255.40	23.20	Substrate	41
	0.25	83.66	10.07	262.70	24.40	Substrate	42

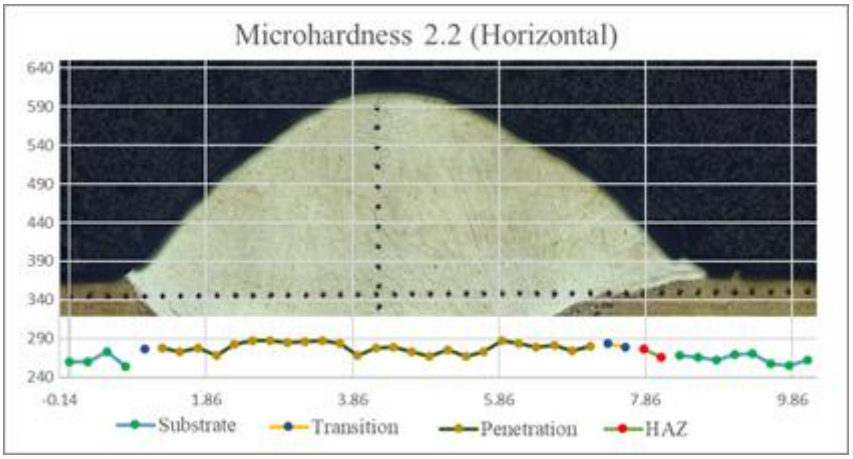

Figure E.26 – Cord 2.2 Horizontal Microhardness

Cord 2.3

Table E.27 – Cord 2.3 Vertical Microhardness Values

Cord	D used	Distance in YY	Incremental distance	HV	HRC	Place	Test nr
2.3	87.46	-0.22	-0.22	292.70	28.80	Cord	1
	80.95	-0.24	-0.46	283.50	27.60	Cord	2
	80.69	-0.24	-0.70	292.80	28.80	Cord	3
	81.78	-0.25	-0.95	296.30	29.20	Cord	4
	79.61	-0.24	-1.19	296.10	29.20	Cord	5
	81.22	-0.24	-1.43	295.70	29.20	Cord	6
	80.34	-0.24	-1.67	291.80	28.70	Cord	7
	80.50	-0.24	-1.91	297.20	29.40	Cord	8
	79.32	-0.24	-2.15	285.40	27.90	Penetration	9
	80.96	-0.24	-2.39	266.50	25.00	HAZ	10
	83.30	-0.25	-2.64	270.80	25.80	Substrate	11
	85.32	-0.26	-2.90	263.20	24.50	Substrate	12
	82.53	-0.25	-3.15	257.90	23.60	Substrate	13
	84.46	-0.25	-3.40	258.30	23.70	Substrate	14
	84.83	-0.25	-3.66	261.30	24.20	Substrate	15
	84.15	-0.25	-3.91	251.00	22.50	Substrate	16

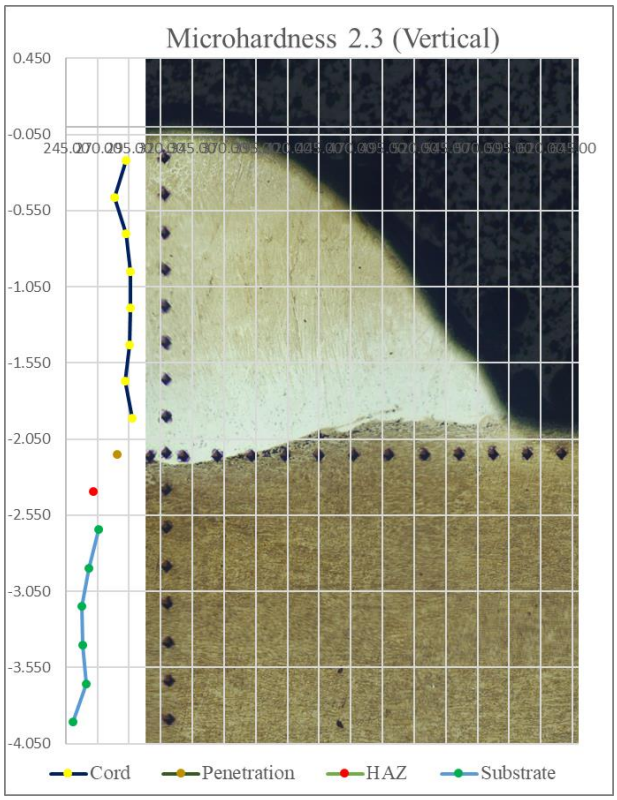

Figure E.27 – Cord 2.3 Vertical Microhardness

Table E.28 – Cord 2.3 Horizontal Microhardness Values

Cord	Distance in XX	D used	Incremental distance	HV	HRC	Place	Test nr
2.3	0.00	87.46	0.00	258.90	23.80	Substrate	1
	0.26	85.56	0.26	277.70	26.80	Substrate	2
	0.25	81.73	0.50	270.00	25.60	Substrate	3
	0.25	82.47	0.75	269.40	25.50	Substrate	4
	0.24	81.45	0.99	276.90	26.60	Substrate	5
	0.24	80.80	1.24	283.60	27.60	Substrate	6
	0.24	79.82	1.48	281.90	27.40	Substrate	7
	0.24	79.31	1.71	275.30	26.40	HAZ	8
	0.24	81.19	1.96	267.50	25.20	HAZ	9
	0.24	81.48	2.20	279.80	27.10	HAZ	10
	0.25	81.67	2.45	293.80	28.90	HAZ	11
	0.23	77.94	2.68	289.10	28.30	Transition	12
	0.24	78.79	2.92	299.60	29.70	Penetration	13
	0.23	78.28	3.15	278.80	26.90	Transition	14
	0.24	81.46	3.40	284.30	27.70	Transition	15
	0.24	79.80	3.64	284.20	27.70	HAZ	16
	0.24	79.43	3.87	285.00	27.80	HAZ	17
	0.24	80.99	4.12	272.50	26.00	Substrate	18
	0.25	82.28	4.36	275.10	26.40	Substrate	19
	0.25	83.34	4.61	289.30	28.40	Substrate	20
	0.24	79.67	4.85	277.10	26.70	Substrate	21
	0.24	80.53	5.09	278.50	26.90	Substrate	22
	0.24	79.82	5.33	279.80	27.10	Substrate	23
	0.24	80.69	5.58	266.60	25.10	Substrate	24
	0.25	83.89	5.83	272.00	26.00	Substrate	25
	0.24	80.52	6.07	260.70	24.10	Substrate	26

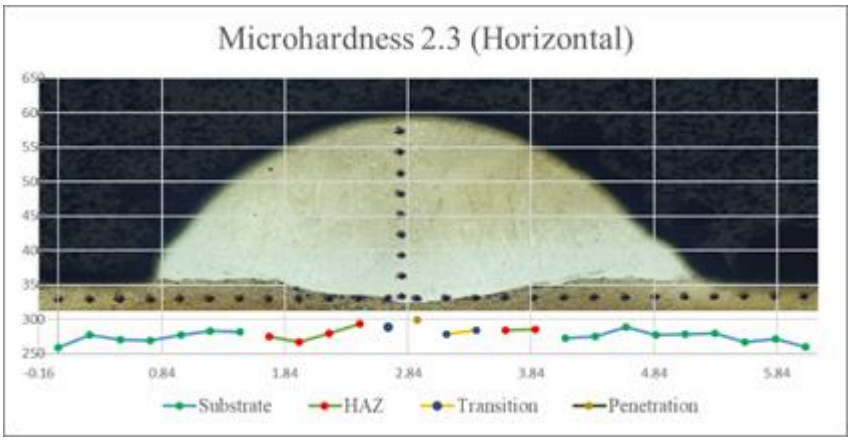

Figure E.28 – Cord 2.3 Horizontal Microhardness

Appendices F

Three-point flexural test

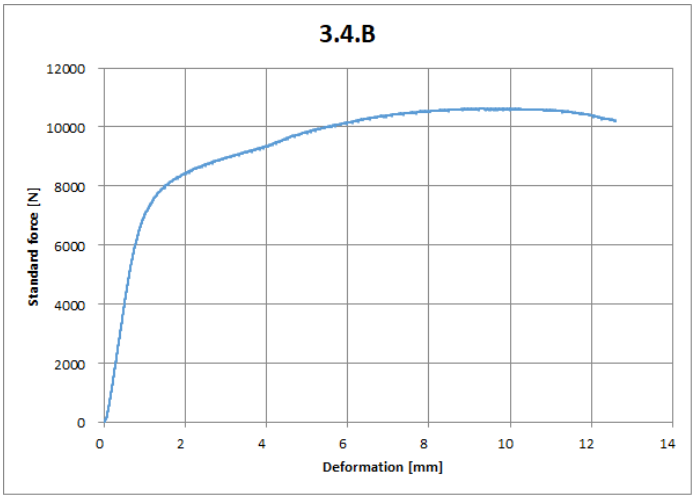

Figure F.1 – 3.4.B Standard force - Deformation

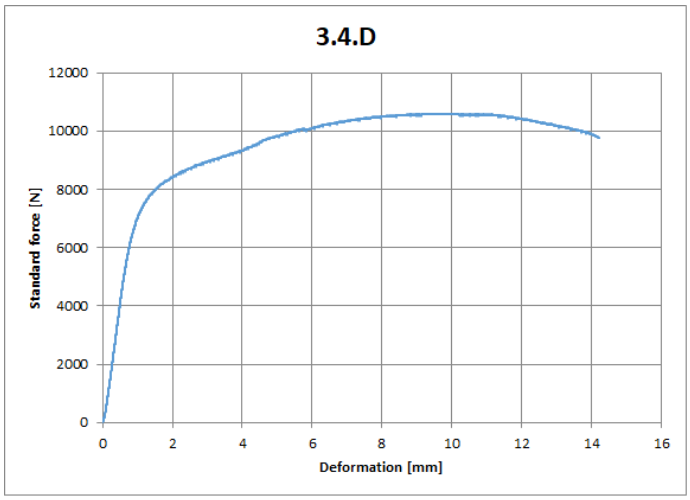

Figure F.2 – 3.4.D Standard force - Deformation

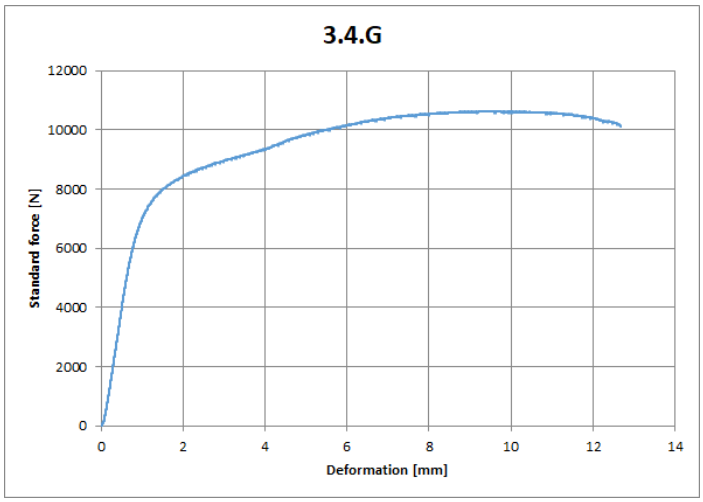

Figure F.3 – 3.4.G Standard force - Deformation

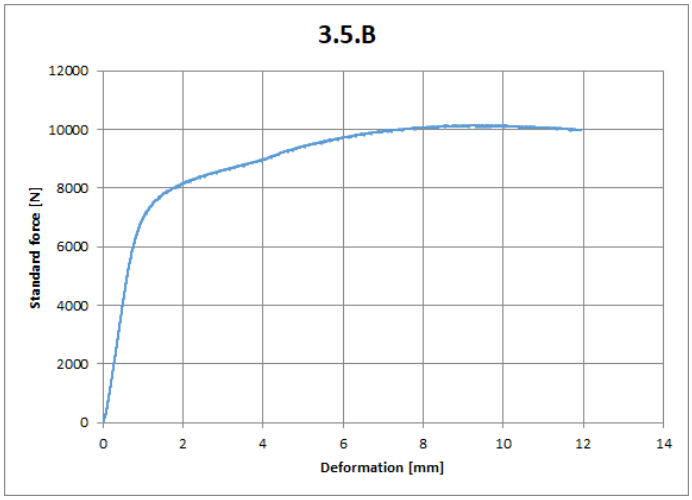

Figure F.4 – 3.5.B Standard force - Deformation

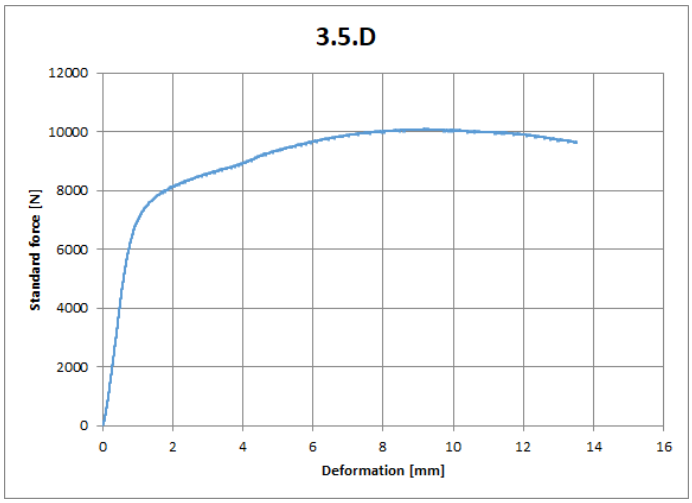

Figure F.5 – 3.5.D Standard force - Deformation

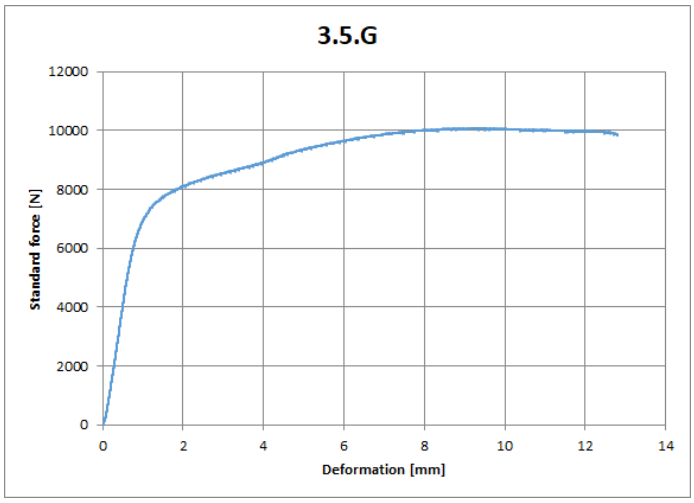

Figure F.6 – 3.5.G Standard force - Deformation